FATIGUE PRECRACKING OF A TITANIUM ALLOY

by

Mohammed Naeem

M. Phil. Thesis

A Master's Thesis submitted in partial fulfilment of the requirements for the award of Master of Philosophy at the Loughborough University of Technology, England.

December 1982.

Supervisor: Dr. T.E. Chung,
Department of Materials Engineering and Design.

ABSTRACT

The extensive use of Ti-6Al-4V forgings in aircraft gas engine compressor discs and blades has generated considerable interest in its crack growth behaviour at elevated temperatures.

Before crack growth studies can be performed on test specimens it is necessary to precrack the specimen to provide consistently sharp fatigue cracks of adequate size and straightness.

Initially the stress intensity amplitude used to grow a precrack is considerably higher than that used in the actual crack growth studies but it is progressively reduced as the required length of precrack is achieved. The reductions in stress intensity amplitude are usually made manually by observing the crack length as stress cycling proceeds and decreasing the stress amplitude on the test machine as the crack length grows.

In this study, a method of performing this precracking operation automatically by the use of computer control of the test machine was developed, and tested. The results confirm the method used to be successful.

ACKNOWLEDGEMENTS

I would like to express my thanks to Professor I.A. Menzies, the Head of Department and Director of Research, for the use of the Department's laboratory facilities.

My sincere thanks and gratitude to Dr. T.E. Chung, my Supervisor, for his invaluable help, advice and guidance throughout the course of my research.

I would also like to thank all the technicians for their assistance during this piece of research, and to Mrs. Bartrop, who transformed a very untidy draft into most attractive type-script.

And last but not least, I would like to thank Rolls Royce Ltd. (Derby) for providing the test specimens.

CONTENTS

Page:

continued

CONTENTS

continued

CONTENTS

continued

CONTENTS

1. INTRODUCTION

The phenomenon of metal fatigue has been studied for over 100 years and now has a voluminous literature. Despite this, fatigue continues to be a major problem and is the most common cause of failures in engineering structures. The traditional approach to design against fatigue is to base allowable fatigue stresses on the results of tests on carefully-made plain or notched laboratory specimens, or on representative structures. The results of such tests are presented as S/N curves, which relate cyclic stress to number of cycles to failure. The use of a traditional approach based on S/N curves leads to difficulties because a conventional fatigue test does not give any information on the relative contribution of crack initiation and crack growth to total fatigue life. This can lead to difficulties in the understanding of the behaviour of sharply notched or cracked structures. Also, the effect of size on the fatigue life of a structure or component is not accounted for. As a result, testing to determine fatigue crack growth data is now widespread. The concept of stress intensity factor has proved to be a particularly convenient applied mechanics framework for the description and analysis of fatigue crack growth behaviour and for the solution of particular engineering problems involving fatigue crack growth; consequently its use is now virtually universal. The fracture mechanics concept of stress intensity factor has proved particularly convenient for the analysis of fatigue crack growth data in a form which can be applied directly to engineering problems, and its use had led to a much better understanding of the fatigue behaviour of structures.

Fatigue testing has profited greatly from recent changes in equipment technology. The development of closed-loop concepts, for example, has resulted in extremely versatile test systems with capabilities to meet more complex experimental requirements. With the advent of the minicomputer and the increased accessibility of time-sharing facilities, it has become apparent that the integration of computers with such test systems provides a useful and logical extension to testing capability. In addition to data analysis and reduction functions, computers are also well suited for real time programming and process control.

The advent of closed-loop servohydraulic materials testing system in the late 1950's (1) and development of minicomputers in the 1960's and 70's (2) have made it possible to construct extremely versatile fatigue testing machines with combined speed and accuracy. The amount and variety of data acquired and stored during testing can also be remarkably increased. One of the most significant advantages of computer control in fatigue testing systems is the ability to work out very complex functions derived from easily measureable load and strain on control quantities, and make on-line decisions on how to continue the test in the light of its current state. There are still some problems on the hardware side, e.g. inertia forces at high frequencies, but most shortcomings are evidently on the software side. Computer-controlled fatigue testing systems are already commercially available (3) but they are not, so far, very useful for fatigue laboratories with complex, wide and varying testing programs.

The material used in this project is a titanium alloy, i.e. Ti-6Al-4v alloy. This alloy is used for compressor disc applications (4) in Rolls Royce RB 211 gas turbine engines. The properties which have made titanium an accepted material of construction are its high strength-to-weight ratio and its exceptional resistance to corrosion. The specific strength of titanium, with a density just over half that of steel, is superior to most other structural metals; and it is this high strength-low density characteristic, maintained at elevated temperatures, which has resulted in the rapid growth in its use in aero engines over the last 30 years. For equal strength, savings in weight of up to 40% are possible by replacing steel and nickel base alloys with titanium. The use of titanium alloys in gas turbine engines has grown to the point where they account for about 25 per cent of the weight of the latest large fan engines. Titanium alloys have lower thermal conductivity and thermal expansion than steel or nickel base alloys. The lower thermal expansion is advantageous for components where there is a considerable temperature gradient between one part and another because it reduces the thermal stress in the component.

CHAPTER 2

2.0 LITERATURE REVIEW

2.1 The Fracture Mechanics of Fatigue Behaviour

2.1.1 The Stress Intensity Factor

The stress intensity factor proposed [5] characterises the level of the stress distribution close to a crack tip in a stressed body. The attainment of a critical stress intensity factor is the criterion for the onset of fracture in fracture mechanics. A stress intensity factor is not a stress concentration factor since the latter is concerned only with stress at some point. The attainment of a critical stress concentration factor is not a useful criterion for fracture in the case of purely elastic behaviour at the crack tip, or in the case of local plasticity at the crack tip. In the case of very sharp crack tips, behaving in a purely elastic manner, the stress distribution rises to an infinite value at the tip itself. In the case of local plasticity preceding crack growth from the tip, the stress immediately ahead of the tip is simply the yield stress under the prevailing stress distribution. This second case is by far the most important since crack advance in most materials, including brittle ceramics [6] and glasses [7] is known to be preceded by limited plastic behaviour.

Irwin pointed out that the local concentrated tensile stress,(σ_y) at the tip of through crack in a body stressed in tension (as illustrated in Figure 1), [8] is given by

$$\sigma_y = \frac{K_I}{(2\pi r)^{\frac{1}{2}}} \cos\frac{\theta}{2}\left[1 + \sin\frac{\theta}{2}\sin\frac{3\theta}{2}\right]$$

in the region $\rho \ll r \ll a$, where ρ is the radius of a curvature of the crack tip and a the length of an edge crack or half the length of a central crack.

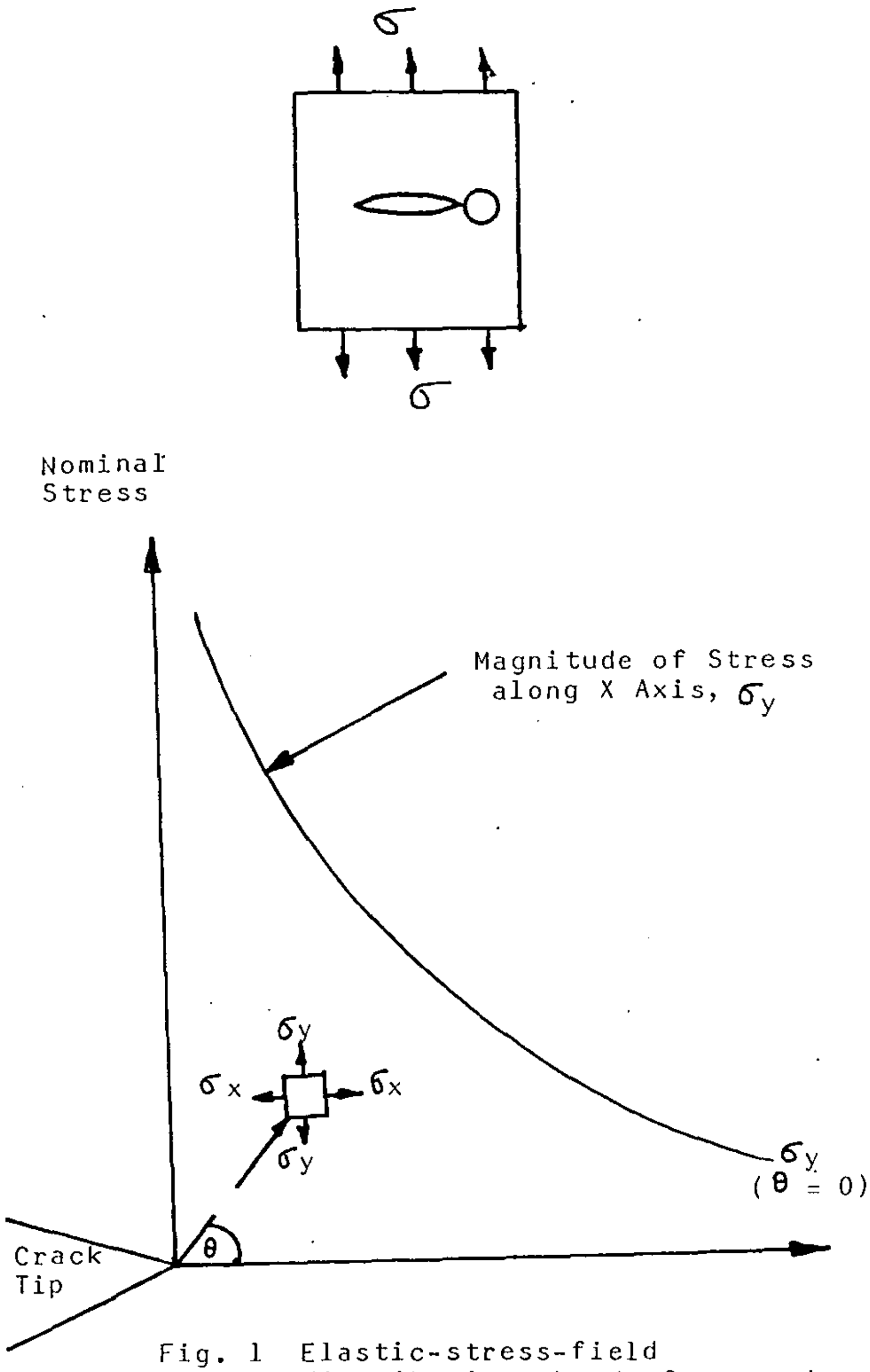

Fig. 1 Elastic-stress-field distribution ahead of a crack.

Under plane-strain conditions, at an arbitrary point (r,θ) ahead of the crack tip there are also present the direct stresses, σx and the shear stress, τxy, given by:

$$\sigma x = \frac{K_I}{(2\pi r)^{\frac{1}{2}}} \cos\frac{\theta}{2}\left[1 - \sin\frac{\theta}{2}\sin\frac{3\theta}{2}\right]$$

$$\tau xy = \frac{K_I}{(2\pi r)^{\frac{1}{2}}} \sin\frac{\theta}{2}\cos\frac{\theta}{2}\cos\frac{3\theta}{2}$$

These expressions show that the stress distribution is characterised by its dependence on the inverse square root of distance, r, from the crack tip, and the constant K_I designated the stress intensity factor. This stress intensity factor is a function of the applied stress, the crack shape, size and orientation, and the structural configuration associated with structural components. Thus it is possible to translate laboratory results into practical design information without the use of extensive service or correlations.

Equations relating the stress intensity factor to the various specimen and loading configurations, crack sizes, shapes, orientation have been determined by various workers. Some examples of the more widely used stress-flaw size relations are presented in Figure 2.

One of the underlying principles of fracture mechanics is that unstable fracture occurs when the stress intensity factor at the crack tip reaches a critical value K_C. For Mode I deformation (see later), and for small crack-tip plastic deformation (plane-strain conditions), the critical stress intensity factor for fracture instability is designated K_{IC}. K_{IC} represents the inherent ability of a material to withstand a given stress field intensity at the tip of a crack and to resist progressive tensile crack extension under plane-strain conditions. Thus K_{IC} represents the fracture toughness of the material and has units of $(MN/m^{3/2})$. However, this material-toughness property depends on the particular material, loading rate and

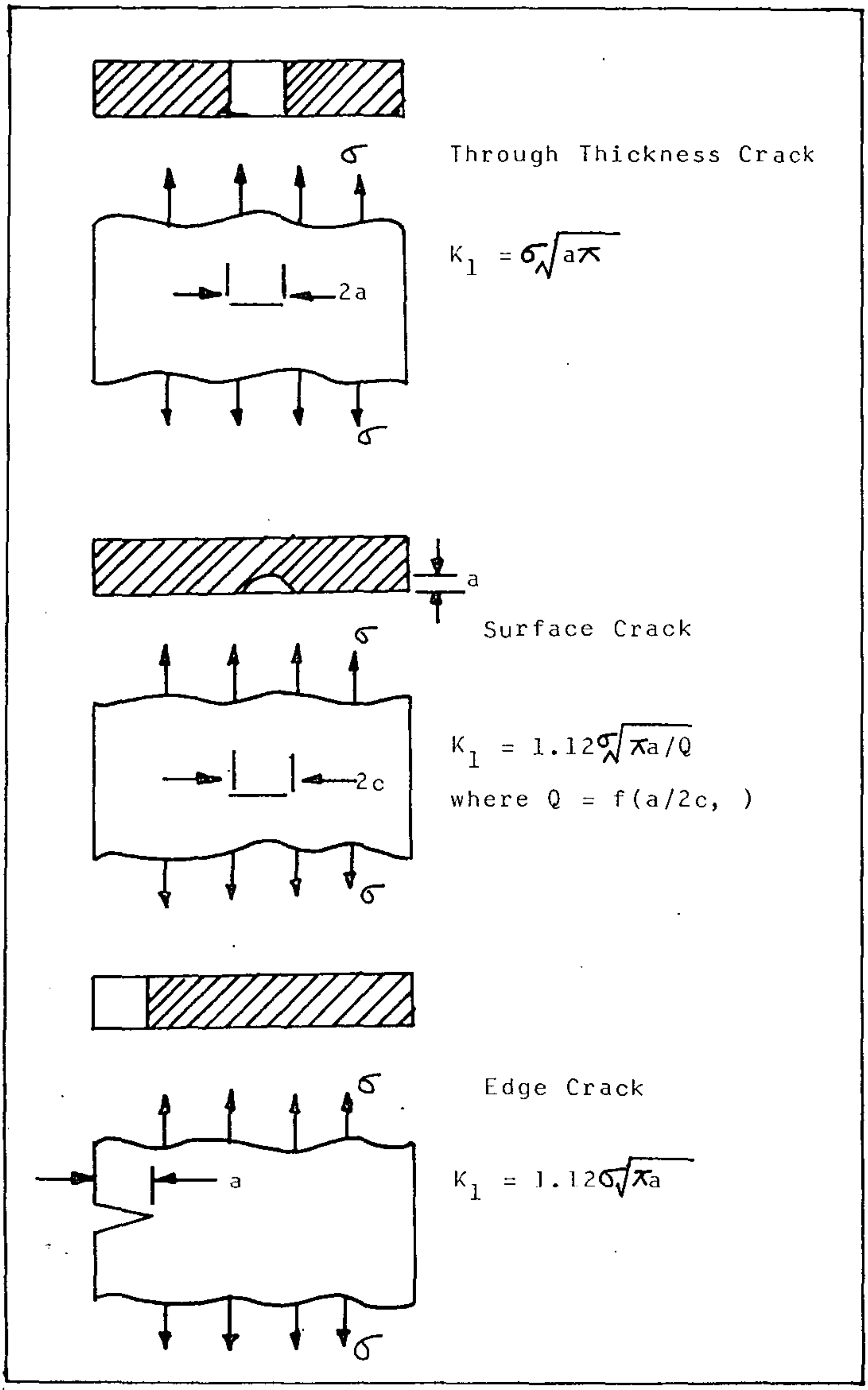

Fig. 2 Values for Various Crack Geometries

constraint as follows:

K_C = critical stress intensity factor for static loading under plane-strain conditions of variable constraint. Thus, this value depends on specimen thickness and geometry, as well as on crack size.

K_{IC} = critical stress intensity factor for static loading under plane-stress conditions of maximum constraint. Thus, this value is a minimum value for thick plates.

Where K_C or $K_{IC} = Y\sigma\sqrt{a}$

Where Y = constant, function of specimen and crack geometry

σ = nominal stress (MN/m^2)

a = flaw size (in m)

Each of these values is also a function of temperature, particularly for those structural materials exhibiting a transition from brittle to ductile behaviour. By using a method that was developed by Westergaard, Irwin found that the stress and displacement of field in the vicinity of the crack tips subjected to the three modes of deformation are given by:- [8]

Mode I: Opening

$$\sigma x = \frac{K_I}{(2\pi r)^{\frac{1}{2}}} \cos\frac{\theta}{2}\left[1 - \sin\frac{\theta}{2}\sin\frac{3\theta}{2}\right]$$

$$\sigma y = \frac{K_I}{(2\pi r)^{\frac{1}{2}}} \cos\frac{\theta}{2}\left[1 + \sin\frac{\theta}{2}\sin\frac{3\theta}{2}\right] \qquad (1)$$

$$\tau xy = \frac{K_I}{(2\pi r)^{\frac{1}{2}}} \sin\frac{\theta}{2}\cos\frac{\theta}{2}\cos\frac{3\theta}{2}$$

$$\sigma_z = \nu(\sigma_x + \sigma_y), \quad \tau_{xz} = \tau_{yz} = 0$$

$$U = \frac{K_I}{G}\left[\frac{r}{2\pi}\right]^{\frac{1}{2}} \cos\frac{\theta}{2}\left[1 - 2\nu + \sin^2\frac{\theta}{2}\right]$$

$$V = \frac{K_I}{G}\left[\frac{r}{2\pi}\right]^{\frac{1}{2}} \sin\frac{\theta}{2}\left[2 - 2\nu - \cos^2\frac{\theta}{2}\right]$$

$$W = 0$$

Mode II: Edge Sliding Mode

$$\sigma_x = -\frac{K_{II}}{(2\pi r)^{\frac{1}{2}}} \sin\frac{\theta}{2}\left[2 + \cos\frac{\theta}{2} \cos\frac{3\theta}{2}\right]$$

$$\sigma_y = \frac{K_{II}}{(2\ r)^{\frac{1}{2}}} \sin\frac{\theta}{2} \cos\frac{\theta}{2} \cos\frac{3\theta}{2} \qquad (2)$$

$$\tau_{xy} = \frac{K_{II}}{(2\ r)^{\frac{1}{2}}} \cos\frac{\theta}{2}\left[1 - \sin\frac{\theta}{2} \sin\frac{3\theta}{2}\right]$$

$$\sigma_z = \nu(\sigma_x + \sigma_y), \quad \tau_{xz} = \tau_{yz} = 0$$

$$U = \frac{K_{II}}{G}\left[\frac{r}{2\pi}\right]^{\frac{1}{2}} \sin\frac{\theta}{2}\left[2 - 2\nu + \cos^2\frac{\theta}{2}\right]$$

$$V = \frac{K_{II}}{G}\left[\frac{r}{2\pi}\right]^{\frac{1}{2}} \cos\frac{\theta}{2}\left[-1 + 2\nu + \sin^2\frac{\theta}{2}\right]$$

$$W = 0$$

Mode III: Shear Mode

$$\tau_{xz} = -\frac{K_{III}}{(2\pi r)^{\frac{1}{2}}} \sin\frac{\theta}{2}$$

$$\tau_{yz} = \frac{K_{III}}{(2\pi r)^{\frac{1}{2}}} \cos\frac{\theta}{2} \qquad (3)$$

$$\sigma_x = \sigma_y = \sigma_z = \tau_{xy} = 0$$

$$W = \frac{K_{III}}{G}\left[\frac{2r}{\pi}\right]^{\frac{1}{2}} \sin\frac{\theta}{2}$$

$$U = V = 0$$

Where the stress components and the co-ordinates r and θ are shown in Figure 3, U, V and W are the displacements in the X, Y and Z directions, respectively, ν is Poisson's ratio; and G is the shear modulus of elasticity.

Equations (1) and (2) represent the case of plane strain (W = 0) and neglect higher-order terms in r. Because higher order terms in r are neglected these equations are exact in the limit as r approaches zero and are a good approximation in the region where r is small compared with other X-Y planar dimensions.

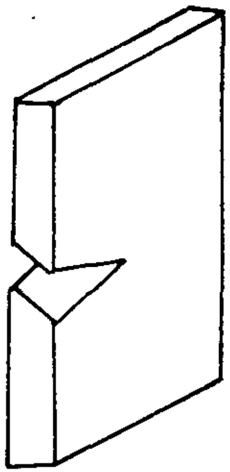

Fig. 5 Crack on 45 degree plane

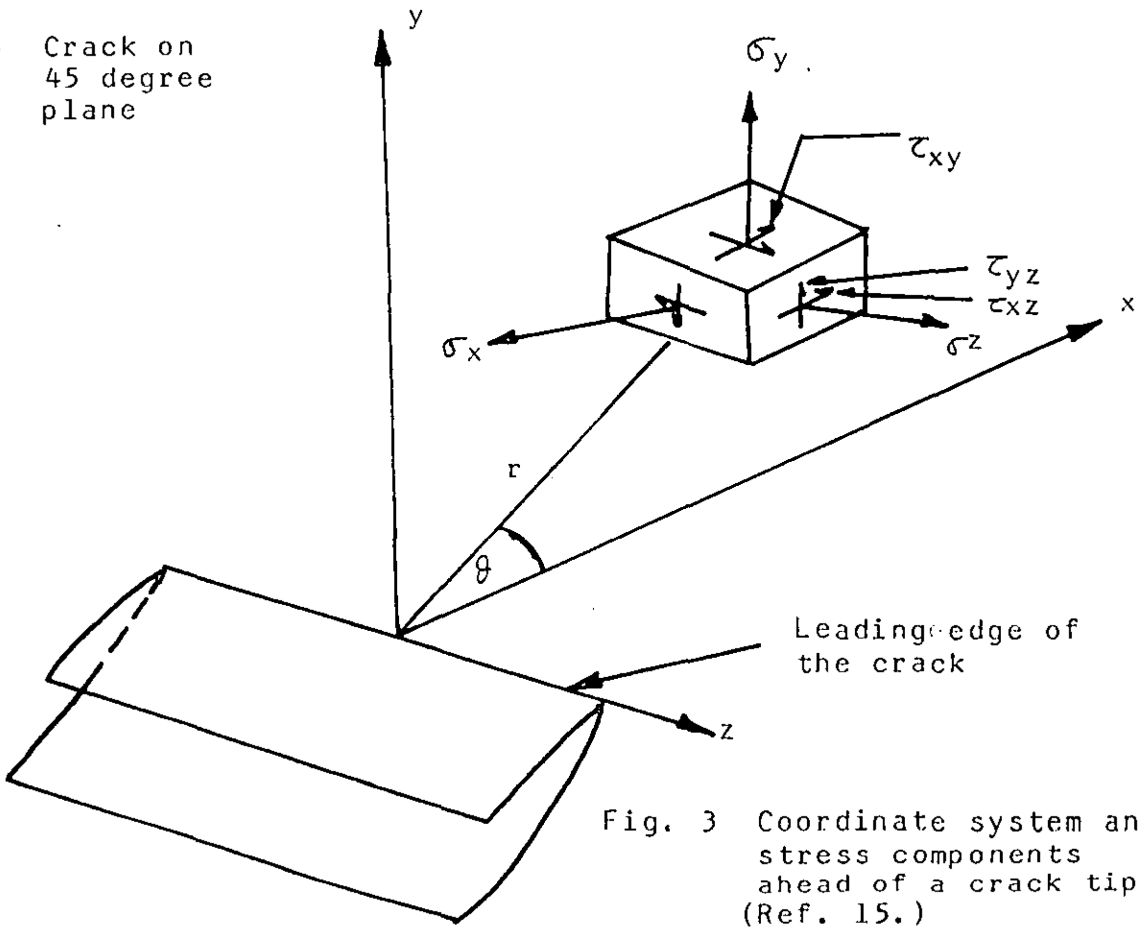

Fig. 3 Coordinate system and stress components ahead of a crack tip. (Ref. 15.)

2.1.2 Application of Stress Intensity Factor to Fatigue

The attainment of a Kc value at the crack tip clearly sets an upper bound to the value of the maximum stress intensity factor during fatigue cycling. Application of a cyclic applied stress to a body containing a crack-like defect corresponds to cycling the crack tip over a range of stress intensity values. In view of the success in relating brittle fracture to the attainment of a critical stress intensity factor at the crack tip, it seems reasonable to attempt to relate the progressive fatigue fracture process to the cyclic range of stress intensity experienced by the crack tip. The work of numerous researchers has now established this relationship.

In order to describe the progressive nature of fatigue cracking it is necessary to know the rate of crack propagation da/dN, where da represents the increment of crack length for an increment in number of fatigue cycles dN. Several crack propagation laws have been presented in the past years, which claim to be verified by the experimental data analysed in their respective papers. They are specifically, the work of Head [8] Frost and Dugdale, [10] McEvily and Illg, [11] Liu [12,13] and Paris.

The Paris general equation is

$$\frac{da}{dN} = C(\Delta k)^m \qquad (1)$$

where $\frac{da}{dN}$ = crack extension per cycle of load

Δk = stress intensity-factor range

C = material constant

m = a numerical exponent

Crack-propagation laws given in the literature take many forms. In general they treat cracks in infinite sheets subjected to a uniform stress perpendicular to the crack (or can be applied to that configuration) and they relate the crack length 2a, to the number of cycles of load applied N, with stress range σ and material constant C_i. The single form in which all crack propagation laws may be written is

$$\frac{da}{dN} = f(\sigma, a, C_i) \qquad (2)$$

σ = applied stress (range)

C_i = constants (which vary slightly with mean stress)

Chronologically the first crack-propagation law which drew wide attention was that of Head [9] in 1953. He employed a mechanical model which considered rigid, plastic work hardening elements ahead of a crack tip and elastic elements over the remainder of the infinite sheet. The model required extensive calculations and deductions to obtain a law which may be written as

$$\frac{da}{dN} = \frac{C_1 \sigma^3 a^{3/2}}{(C_2 - \sigma) W_o^{\frac{1}{2}}} \qquad \text{Head's Law} \qquad (3)$$

a = half crack length

W_o = plastic-zone size

Where C_1 depends upon the strain-hardening modulus, the modulus of elasticity, the yield stress and fracture stress of the material and C_2 in the yield strength of the material. Head defined W_o as the size of the plastic zone near the crack tip and presumed it was constant during crack propagation. However Frost [10] noticed that the plastic-zone size increased in direct proportion to the crack length in his tests. Irwin [10] has recently pointed out from analytical considerations that

$$W_o \approx \sigma^2 a \qquad (4)$$

for the configuration treated here which is in agreement with Frost's conclusions. Therefore, though Head adopted equation (3) with W_o considered constant as his crack-propagation law, we are forced here to introduced equation (4) into equation(3) to obtain a modified or corrected form of Head's crack-propagation law

i.e. $$\frac{da}{dN} = \frac{C_3 \sigma^2 a}{(C_2 - \sigma)}$$ (Head's corrected law) (5)

Frost and Dugdale (10) in 1958 presented a new approach to crack-propagation laws. They observed, as was introduced in equation (5), that Head's Law should be corrected for the variation of plastic-zone size with crack length. They deduced that the corrected result, equation (5) depends linearly on the crack length a. However, they also argued by dimensional analysis that the incremental increase in crack length da, for an incremental number of cycles dN, should be directly proportional to the crack length a. Hence they concluded that (independent of Head's model)

$$\frac{da}{dN} = Ba \quad (6)$$

where B is a function of the applied stresses. They observed that in order to fit their experimental data:

$$B = \frac{\sigma^3}{C_4} \quad (7)$$

Combining equations (6) and (7) they obtained the law:

$$\frac{da}{dN} = \frac{\sigma^3 a}{C_4}$$ (FROST'S AND DUGDALE'S LAW) (8)

About the same time McEvily and Illg (11) modified a method of analysis of static strength of plates with cracks used at NASA to obtain a theory of crack propagation. Their arguments were as follows: presuming that a crack tip in a material has a characteristic (fictitious) radius ρ_1, which allows computation of the stress σ_o, in the element at the crack tip using elastic stress concentration factor concepts, the stress σ_o is

$$\sigma_o = K_N \sigma_{net} \quad (9)$$

where KN is the stress-concentration factor and σ_{net} is the area stress at the cracked section. For the configuration used here, i.e. an infinite plate with uniform stress

$$KN = 1 + 2(a/\rho_1)^{\frac{1}{2}} \quad (10)$$

which is based on the elastic solution for an elliptical hole of semi-major axis a and end radius ρ_1.

$$\sigma_{net} = \sigma \quad (11)$$

and substituting equations (10) and (11) in to (a) gives

$$\sigma_o = \sigma(1 + 2(a/\rho_1)^{\frac{1}{2}}) \quad (12)$$

Based on considerations that under cyclic loading work-hardening at the crack tip will raise the local stress to a fracture stress, they concluded that the crack-extension rate will be a function of σ_o or

$$\frac{da}{dN} = F(\sigma_o) = F(K_N \sigma_{net}) \quad (13)$$

(McEvily and Illg's Law)

Therefore for the special configuration of interest here, i.e. introducing equations (9), (10), (11) and (12) into (13) we have

$$\frac{da}{dN} = F(\sigma(1 + 2(a/\rho_1)^{\frac{1}{2}})) \quad (14)$$

which is the desired form in the discussion upon considering ρ_1 to be a material constant, in likeness to the C_i.

McEvily and Illg go on in an empirical manner to obtain the form of the function F(), and suggest

$$\log_{10} \left(\frac{da}{dN}\right) = 0.0509\, K_N \sigma_{net} - 5.472 - \frac{34}{K_N \sigma_{net} - 34} \quad (15)$$

McEvily and Illg's Law empirically extended.

Independent of McEvily and Illg, Paris proposed a crack propagation theory at about the same time. It is based on the following arguments. Irwin's [14] stress intensity-factor reflects the effect of external load and configuration on the intensity of the whole stress field around a crack tip. Moreover, for various configurations the crack-tip stress field always has the same form, i.e. (distribution). Therefore it was reasoned that the intensity of the crack tip stress field as represented by K should control the rate of crack extension. That is to say:

$$\frac{da}{dN} = G(k) \qquad (16)$$

$$\text{where } k = \sigma a^{\frac{1}{2}} \qquad (17)$$

Whereupon equation (16) may be specialized to read:

$$\frac{da}{dN} = G(\sigma a^{\frac{1}{2}}) \qquad (18)$$

Somewhat later Liu [12] restated Frost and Dugdale's [10] dimensional analysis in a much more elegant form and argued that the crack-growth rule should depend linearly on the crack length, i.e.

$$\frac{da}{dN} = Ba \qquad \text{(Liu's Law)} \qquad (19)$$

which is the same result as equation (6). Liu then presumed that B was in general a function of stress range (and mean stress); i.e.

$$B = B(\sigma) \qquad (20)$$

In subsequent work Liu [13] notes that mean stress is of secondary influence and using a model of crack extension employing an idealized elastic-plastic stress-strain range diagram and a concept of total hysteresis energy absorption to failure, reasons that:

$$B(\sigma) = C_5 \sigma^2 \tag{21}$$

which, combined with equation (19), gives

$$\frac{da}{dN} = C_5 \sigma^2 a \quad \text{(Liu's modified Law)} \tag{22}$$

Similarities Between Crack Propagation Laws

The Laws of Head, equation (5), Frost and Dugdale, equation (8), and Liu, equation (19) and (22), can all be approximated by the form

$$\frac{da}{dN} = \frac{\sigma^n a^m}{C_o} \tag{23}$$

for the special configuration which is treated. Now it is evident that Paris' result for this configuration, equation (18), implies:

$$m = \frac{n}{2} \tag{24}$$

which can also be derived from McEvily and Illg's result, equation (14), for ρ_1 small compared to a.

It is pertinent to now show that determining m and n from a limited quantity of data is a doubtful practice. That is to say that plotting data from single test specimens on a logarithmic or semilogarithmic graph on which laws such as Head's, Frost's, and Liu's predict straight line relationshops is not a reasonable test of the validity of a crack propagation law.

If we consider cycling from zero stress to a maximum applied stress we note that:

$$\frac{da}{dN} = A(\Delta K)^2 \text{ from } \frac{da}{dN} = A\sigma^2 a.$$ (12,13)

The ΔK represents the range of the Irwin stress intensity factor experienced at the crack tip since, as we have previously seen, $k = Y\sigma(a)^{\frac{1}{2}}$. Paris and Erdogan [15] have reviewed the development of crack propagation laws extensively, and the results of many experimental investigations show that the relationship for many materials falls close to:

$$\frac{da}{dN} = A(\Delta K)^4$$

Such a law is very difficult to arrive at through dimensional arguments. It appears that the nature of the progressive rupture itself, within the plastic zone at the crack tip may introduce the extra factor. This may be a blunting process on the tensile cycle followed by folding of the increased crack tip perimeter to give an effective increase in crack length, or linking with voids in a damaged plastic zone to give an increase in crack length.[16] Indeed these are experiments which show clearly that ΔK should not be raised to any simple integral value,[17] but the values found for the power of ΔK always lie near to 4.

2.1.3 Mechanism of Crack Growth

2.1.3.1 Stages of Crack Growth

In principle fracture mechanics can also provide a frame work for the study of micro crack (Stage I) growth, which takes place on planes of maximum shear stress, see Fig. 4. On a macroscopic scale, fatigue fracture surfaces are generally flat and smooth in appearance. They tend to grow in Mode I (Fig. 4) irrespective of their initial orientation, so attention is largely confined to this mode. Other modes can occur when a crack follows a plane of weakness,[18,19] or in composite materials.[20] Crack growth in thin sheets is usually on 45^{o} through the thickness plane (Fig. 5). These cracks are formed by the applied stress. A crack which has grown entirely in Mode I is not necessarily straight, and crack trajectories are not readily determined. As a general rule a crack tends to be attracted by the nearest free surface and may follow a curved path even under initially symmetrical loading conditions. Cracks in structures are frequently found to follow complex paths. Ensuring that a crack maintains its initial direction is an important factor in the design of fracture mechanism test specimens.

2.1.3.2 Fracture Surface Relief

Fracture surface relief was the first experimental object in the study of the fatigue crack-propagation mechanisms, In many cases, the macroscopic appearance of the fracture surface gives direct information about the crack origin and about the crack length at which Stage II fatigue - crack-propagation was replaced by fracture of the remaining cross-section. Electron microscopy, mainly scanning electron microscopy of fracture surface and transmission electron microscopy of replicas of the fracture surface, have yielded a vast amount of information about microscopic features.

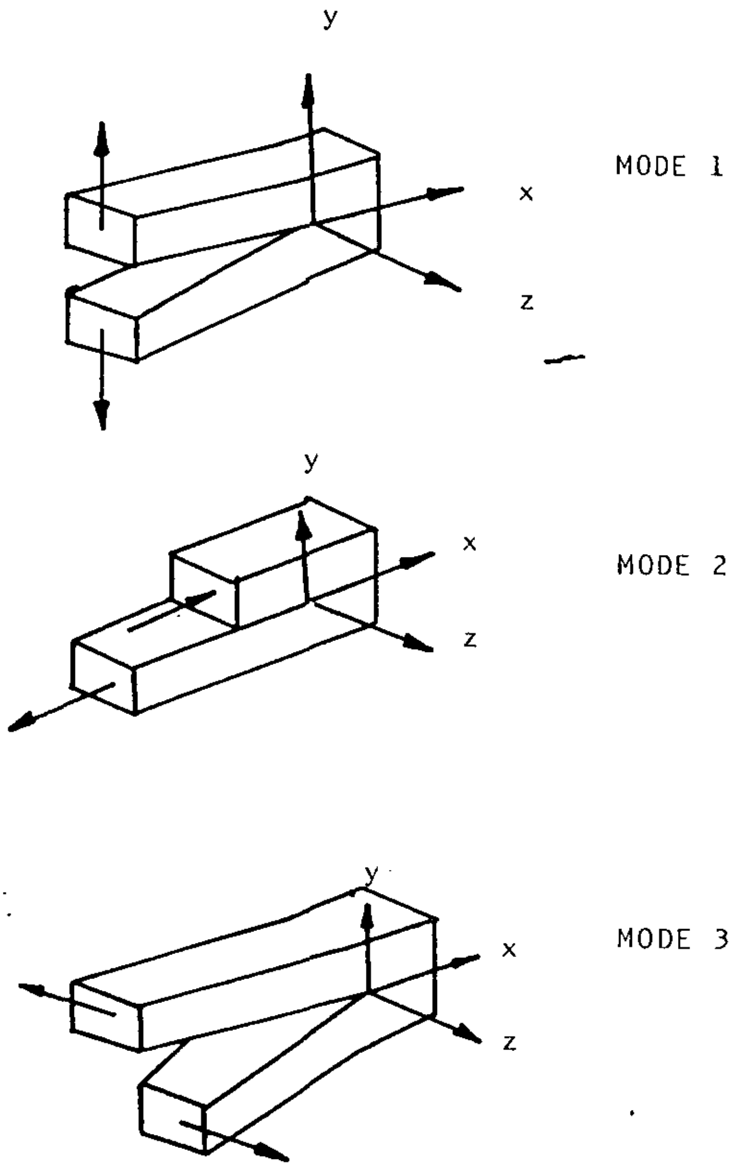

Fig. 4 The three basic modes of crack surface displacements. (Ref. 18)

The most frequent feature of the fatigue fracture surface is the presence of striations, which are a unique characteristic of fatigue. Fatigue striations can be clearly or poorly delineated and can take on several shapes from almost perfect straight lines to very curved lines.

As a rule fatigue striations can be observed in Stage II crack propagation, where the striations spacing is sufficiently large (of the order of a tenth of a micron or more). In Stage I propagation the crack rate and consequently the distance between striations, if they exist, are rather small (of the order of a hundredth of a micron and less) and fracture surface appears to be smooth. Some high-strength nickel-base alloys with very long Stage I crack propagation are an exception to the rule. In these alloys striations in Stage I propagation were observed.(21)

Even in materials exhibiting clearly delineated striation the fracture surface is not wholly covered. In some cases, mainly higher-strength materials, only a small part of the fracture surface was found to be covered with striations. On the basis of extensive experiments, Broek (22) showed that by employing suitable techniques, it was also possible to observe striations in places which appeared featureless when examined by usual methods. The extent of fatigue crack growth is determined by the fracture toughness of the material.

The micro relief of the fracture surface (as well as the crack propagation rate) depends strongly on the surrounding environment. The most prominent influence was observed by Pelloux,(23,24) who cycled specimens of aluminium alloys alternately in air and vacuum. The fracture surface corresponding to air cycling was covered by well delineated striations, whilst the fracture surface corresponding to vacuum cycling appeared featureless. From experiments of this type it follows that the deformation process at the crack tip, which also determines the crack propagation rate, depends not only on the material parameters of the metallic matrix, but also on interactions with the surrounding environment.

2.1.3.3 Models of Crack Propagation

Descriptive models of fatigue-crack propagation are based mainly on the micro relief of the fracture surface and on direct observation of the crack-tip behaviour at high strain amplitude, low frequency cycling.

In Stage II propagation the crack rate, striation spacing and markedness of striation are much higher than in Stage I propagation. The existence of fatigue striations are the common feature of fatigue and of the one to one correspondence between striations and cycles means that fatigue crack propagation is a repetitive process. To understand the crack propagation mechanism, it is then sufficient to know the process in one leading cycle.

Laird [25] performed direct observation on some ductile metals with the crack-tip geometry corresponding to different stages of the stress cycle. The mechanism of crack propagation deduced from these observations is now called the plastic blunting process or Laird's model and is described in Figure 6.[25,26] The initial zero-load position corresponds to a well developed Stage II crack, with the fracture surface exhibiting striations (a). As the tensile load is applied, the metal yields plastically due to high stress concentration. This plastic deformation is highly concentrated in the slip zones along planes of maximum shear stress, i.e. along planes at 45^{o} to the stress axis (b). When the load is further increased, the slip zones at the tip broaden and the crack tip blunts to a semi circular configuration. The crack tip is thus effectively shifted (c). The application of compressive load reverses the slip direction in the zone, the distance between the matching surface decreases, but the new surface created in tension cannot be - at least not completely - removed by the "cold weld", i.e. the rejoining of atomic bonds. The new surface is partly folded by buckling into a double notch at the tip (d). The final configuration under maximum compressive load is again a sharp crack tip; the crack length has increased by $\Delta \ell$ which is equal to the striation spacing (e).

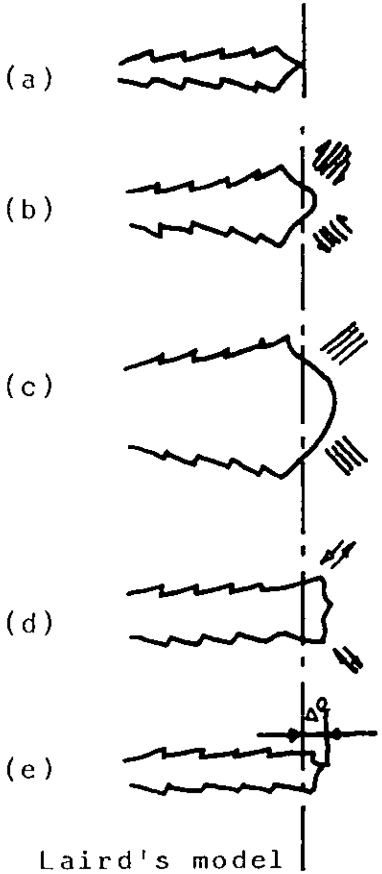

Fig. 6 Laird's model of fatigue crack propagation

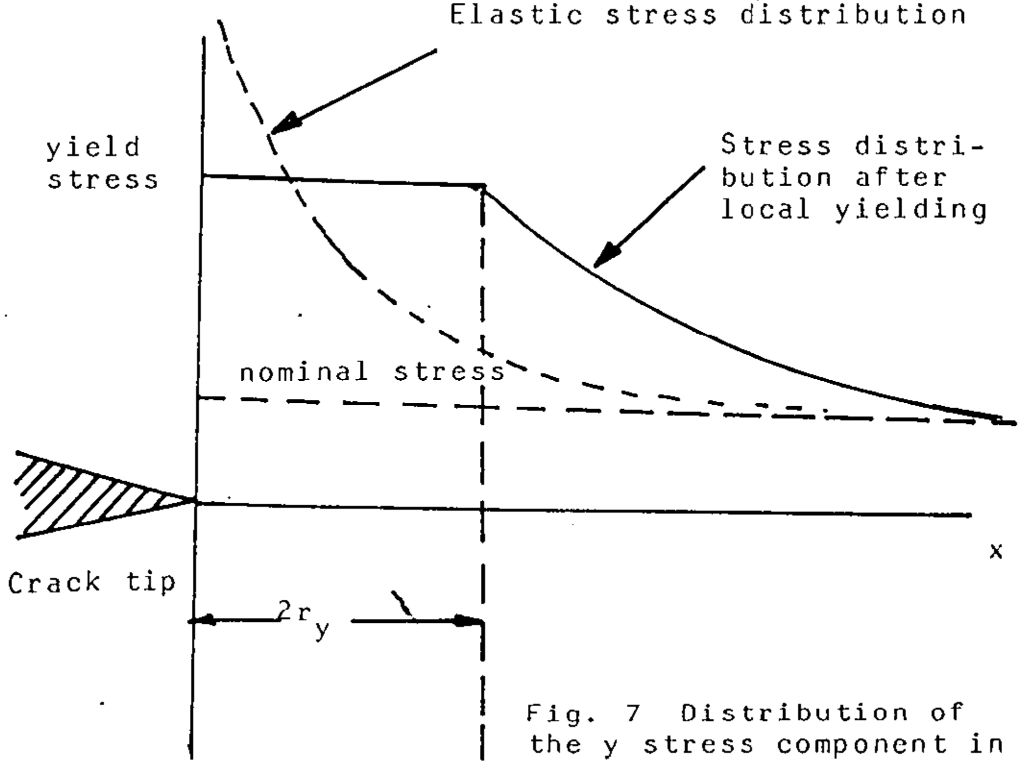

Fig. 7 Distribution of the y stress component in the crack-tip region

This mechanism of repeated plastic blunting and re-sharpening of the crack tip is probably the most general descriptive model of fatigue-crack propagation.

Laird's mechanism explains in a compact way the formation of fatigue striations on the fracture surface. The model does not make any assumptions about the dislocations mechanism at the crack tip, or about the relationship between the substructure and the surface relief.

The model of repeated plastic blunting and resharpening may at least partly account for the difference of fracture surface appearance in air and in vacuum. During compressive load (Figure 6c and d) the newly created surface can be re-welded to some extent.(27) This process is inhibited by oxide layers which form very quickly on fresh clean metallic surfaces, thus in vacuum are shallower and more closely spaced than in air.

In summary, the basic features of the crack propagation mechanism are well understood in ductile materials exhibiting fatigue striations. Here, the repetitive process of plastic deformation at the crack tip, whatever its specific form, is applicable. For more brittle materials or those with inclusions and inhomogenities which do not exhibit regularly fatigue striations as a feature of the fracture surface, the mechanism of repeated plastic blunting and resharpening does not directly explain all the experimental observations of the fracture surface or the macroscopic behaviour of cracks.

2.1.4 Plasticity During Fatigue Cycling

Crack-tip deformation

The stress-field equations, Equations (1), (2) and (3), show that the elastic stress in the vicinity of a crack tip where $r \ll a$ can be very large. In reality, such high stress magnitudes do not occur because the material in this region undergoes plastic deformation thus creating a plastic zone that surrounds the crack tip.

Figure 7 is a schematic presentation of the change in the distribution of the Y component of the stress caused by the localized plastic deformation in the vicinity of the crack tip.

The size of the plastic zone, r_y, can be estimated from the stress-field equations by treating the problem as one of the plane stress and setting the Y component of the stress σ_y equal to the yield strength, σ_{ys}, which results in (28)

$$r_y = \frac{1}{2\pi}\left(\frac{K}{\sigma_y}\right)^2 \qquad \text{(Plane Stress)} \qquad (4)$$

The plastic zone size under plane-strain conditions can be obtained by considering the increase in tensile stress for plastic yielding caused by plane-strain elastic constraint. This produces a plane strain plastic zone size of

$$r_y = \frac{1}{6\pi}\left(\frac{k}{\sigma_y}\right)^2 \qquad \text{(Plane Strain)} \qquad (5)$$

The material ahead ofthe crack front in a thick specimen is subjected to plane-strain conditions in the centre portion of the crack front where w = o. The material at the surfaces of the material will be subject to plane-stress conditions where $\sigma_2 = 0$. Consequently, Equations (4) and (5) indicate that the plastic zone in the centre of a thick specimen is smaller than at the surface of the specimen. A schematic representation of the variation of the plastic zone size along the front of a crack in a th[illegible]k specimen is shown in

Figure 8. More refined estimates ofthe sizes and shapes of crack tip plastic zones may be obtained by applying the von Mises and Tresca criteria to take into account the effect of tri-axial stresses on the yield stress of a material.

In order to investigate the plastic zones during fatigue cycling it is convenient to envisage initial loading to a stress σ , and instead of simple unloading we superimpose a stress $-\Delta\sigma$. This process can go on indefinitely but the $\Delta\sigma$ will always give rise to the production of a new plastic zone of reversed plastic shears. It follows that in the initial tension cycle of fatigue a plastic zone will be produced of radius r_y given by equation (4) at peak load.

2.1.5 Fatigue Crack Growth Data

Fatigue crack growth tests are relatively straight forward and over the past 20 years large numbers have been carried out. It is now usual practice to analyse data in terms of stress intensity factors. These provide a particularly convenient means of correlating fatigue crack growth data. In general the opening mode stress intensity factor is given by:-

$$K_I = \sigma a^{\frac{1}{2}} Y.$$

Where σ is the applied stress, a the crack length and Y a geometrical term describing the specimen, crack and the loading geometries.

The fatigue cycle is usually described by Δk, the range of stress intensities with the material at the crack tip experienced in one load cycle. Δk = Kmax - Kmin, where Kmax and Kmin are maximum and minimum values of the opening mode stress intensity factor K_I calculated from the maximum and minimum stresses applied during the fatigue cycle. If the minimum stress is compressive, Kmin is usually taken as zero, as it is assumed that a compressive stress does not contribute to crack growth. In practice, however, a crack may close at above or below zero load, and a number of modifications have been proposed to take the level of mean stress into account.

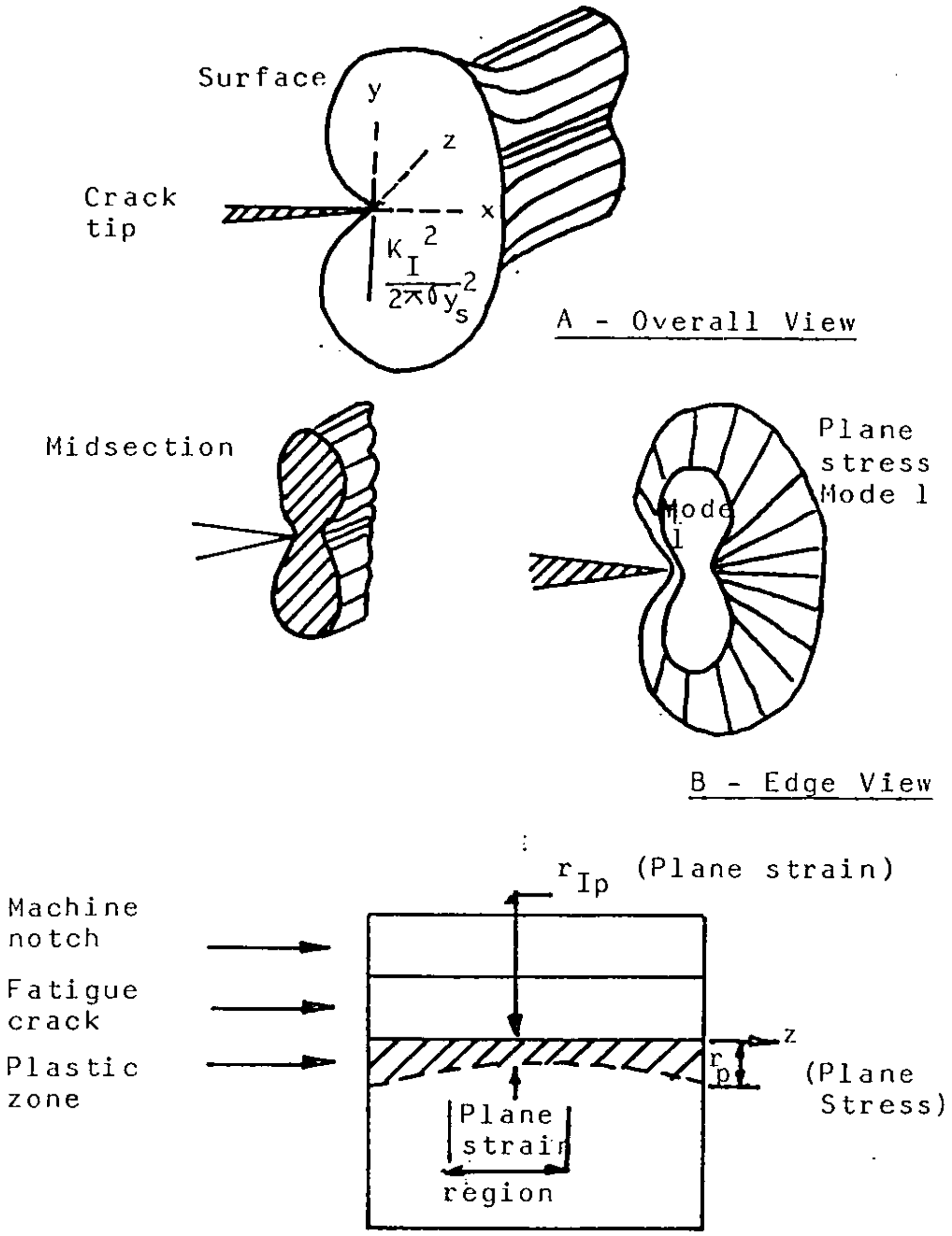

Fig. 8 Schematic representation of plastic zone ahead of crack tip. (Ref. 8)

It has been shown experimentally that Δk has the major influence on fatigue crack growth and in general, if Δk is constant the fatigue crack growth rate is constant. For many materials the rate of fatigue crack growth can be expressed by equation

$$\frac{da}{dN} = C(\Delta k)^m \quad \text{(Paris-Erdogan Law Equation)}$$

Where N is the number of cycles, C is a material constant, and m an exponent, usually about 3 - 4. Crack propagation data are usually presented in the form of a plot of the logarithm of Δk versus the logarithm of the growth rate da/dN which allows determination of power of Δk for a particular material (Figure 9)*.

The more recent research investigations have demonstrated that in a typical log-log plot of fatigue crack growth rate da/dN versus stress intensity factor range Δk, the Paris-Erdogan Law Equation is only valid for the intermediate range of growth rates typically 10^{-8} - 10^{-6} m $cycle^{-1}$ (region B in Fig. 9). The variation of growth rate da/dN with Δk is actually sigmoidal in form, defined in a range of Δk values bounded at its extremes by K_{IC} or K_C (the plane strain or plane stress fracture toughness), and threshold parameter Δko (Fig. 9). At the low end of the Δk scale, crack growth is slow but rises rapidly with increasing Δk. At the higher end of the Δk range when k max. of the fatigue cycle approaches the fracture toughness (K_{IC}, K_C), the crack accelerates and the above equation $da/dN = C(\Delta k)^m$ underestimates the high growth rates which are commonly observed (region C in Fig. 9). The precise shape of da/dN versus Δk plot is therefore strongly influenced by fracture toughness and threshold behaviour. For example, Stage C is strongly promoted in very low toughness materials and the intermediate Stage B can be significantly restricted or even lost. Also, some materials, particularly high strength steels in an aggressive environment do not show a well defined threshold.

* Figure 9 is from "Ritchie"; <u>Metal Science</u>; (1977).

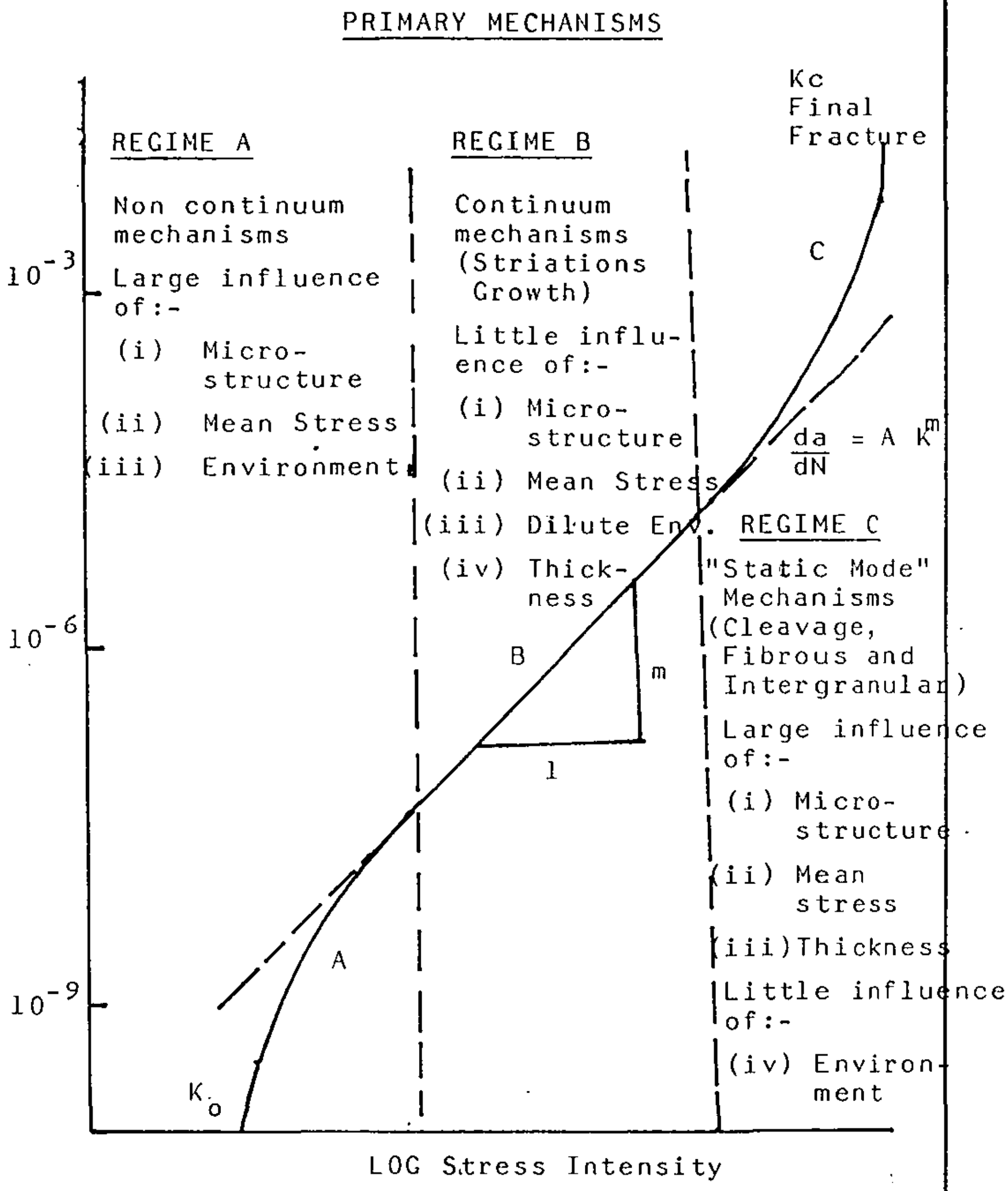

Fig. 9 Summary diagram showing the primary fracture mechanisms associated with sigmoidal variations of fatigue crack propagation rata da/dN with alternating stress intensity. K_o is the threshold intensity for crack growth and K_c the stress intensity at final failure.

The equation $da/dN = C(\Delta k)^m$ is sometimes modified to allow for the increase in crack growth rate, which usually occurs as Kmax approaches K_C the critical value of K_I at which brittle fracture takes place, and for the effect of mean stress, which influences fatigue crack growth rates in some materials. The availability of a master curve relating da/dN and Δk enables a designer to predict growth rates for any cracked body configuration, and he is not limited to situations similar to those pertaining to the cracked specimen geometry used to generate the original data.

2.1.6 Mechanism of High Temperature Fatigue

Introduction

Fatigue at elevated temperatures is a complex subject. In general we are dealing with a creep-fatigue interaction that depends sensitively on temperature, frequency, mean stress and environment.

The fatigue process can occur in three stages: first, nucleation and early growth of cracks within the plastic zone developed at the notch root; second, crack propagation of a stable crack through the plastic zone; third, propagation of the crack through the elastic zone, the crack generating its own plastic zone, until fracture of the structure results, either by sudden fracture, linkage, or by excess vibration or deformation. These stages are shown in Fig. 10.[31]

From Fig. 10 can be seen some of the many disciplines which must be brought to bear on the problem. Consider first plastic zone. Identification of the appropriate stresses and strains are required through analytical tools, such as finite element analyses. This requires the selection of appropriate material information and constitutive equations, heat transfer analysis etc., with the aid of appropriate failure criteria, the conditions for the occurrence of micro cracks or for nucleation and early growth can be specified. Elastoplastic analysis further aids in the specification of conditions for crack growth through the

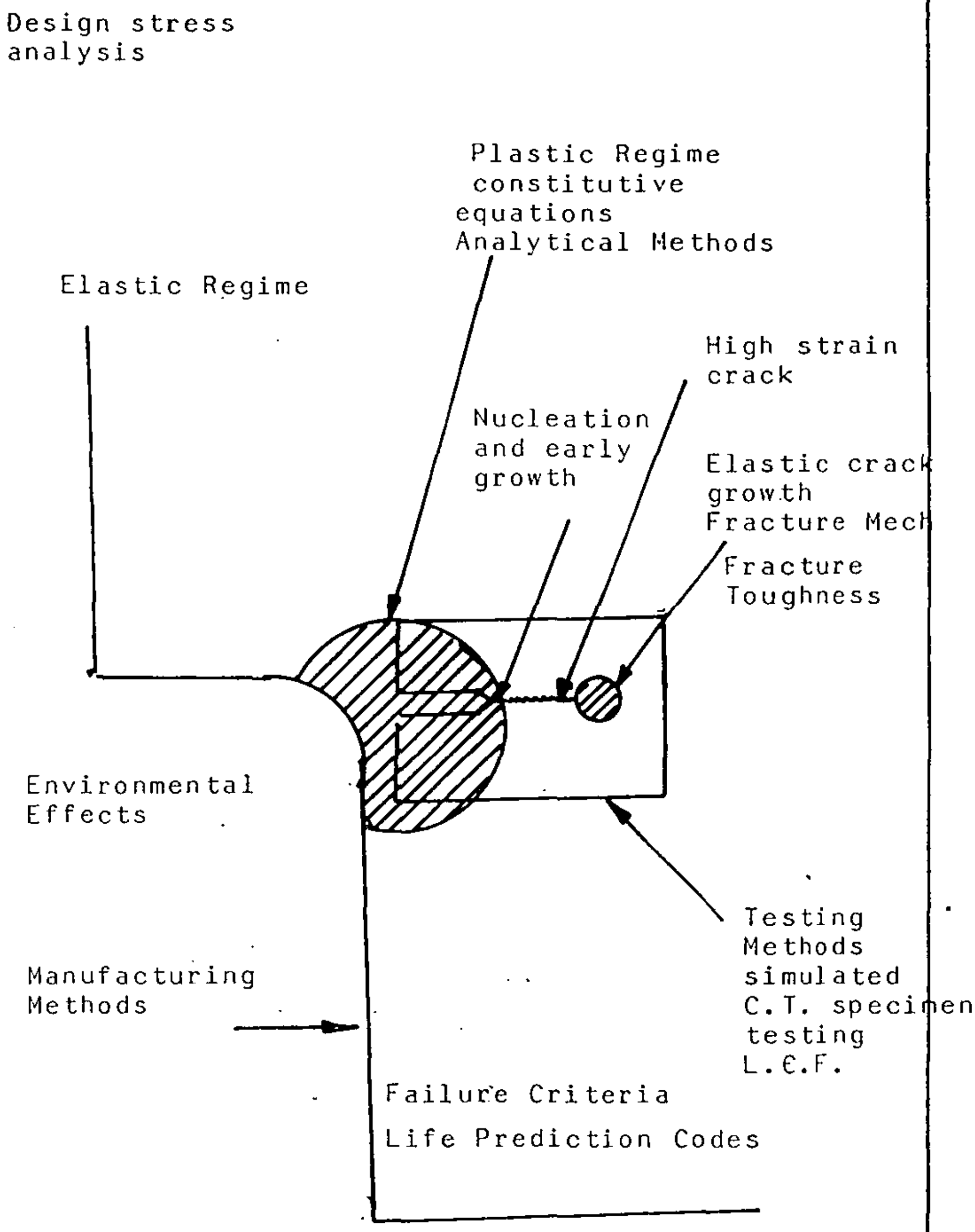

Fig. 10 Schematic view of high-temperature fatigue problem showing physical stages in failure process and relevant disciplines

plastic zone, again coupled with an appropriate fracture criterion. Finally, elastic stress analysis and fracture mechanics concepts allow the determination of crack growth in the elastic regime. Along the way we can identify several additional disciplines. Included are environmental effects on nucleation and growth, manufacturing techniques for surface preparation in the critical area, choice of material, testing methods for developing failure criteria, low cycle fatigue studies, development of high and low-strain crack growth rules, time dependency, fractography etc. Groups of these and other disciplines are lumped together into such activities as life prediction, design, code development, etc. There is also a whole structure of disciplines directed towards other aspects of the problem such as metal physics, corrosion and electrochemistry, physical and process metallurgy, statistics and others.

2.1.6.1 Grain boundary damage processes in low cycle fatigue at elevated temperature

Intergranular fracture is usually considered as one of the damage processes typical of high temperature low cycle fatigue. Mechanisms of damage leading to grain boundary fracture in high temperature fatigue, include the following[32]

(i) intergranular fracture due to environmental effects;

(ii) grain boundary sliding

(iii) other grain boundary damage. For instance aging reactions leading to grain boundary impurity segregation or precipitation can be deleterious for fatigue life. Another effect which has not perhaps received enough attention is also the influence of strain rate and temperature on slip character.

2.1.6.2 Oxidation effect

Oxidation may be most the important parameter in elevated temperature low cycle fatigue at least in certain cases. However, the mechanisms which account for the reduction in fatigue life in air as compared to the endurance in vacuum still need further investigation. In particular especially devised experiments which could allow the determination of the respective part of oxidation on either crack initiation or crack propagation would be very useful for better understanding of the interactions between strain cycling and oxidation. It has been shown that oxidation without stress is clearly inapplicable to the highly strained crack tip and the oxidation rate per cycle is a function of the plastic strain range.[33]

As far as grain boundaries are concerned, generally they offer less resistance to oxidation. This is due to chemical segregation and the presence of carbides, especially in the case of Ni-base alloys. Moreover it can also be thought that grain boundary sliding, where it is important, could also enhance grain boundary oxidation since the localisation of the strain along them may also contribute to oxide spalling.

2.1.6.3 Grain boundary sliding

Many studies have shown that integranular rupture at elevated temperature is associated with grain boundary sliding, especially in the case of structural alloys which contain second phase particles along grain boundaries.[34,35] Grain boundary sliding produces a typical form of grain boundary damage which is either the formation of wedge cracks at grain boundaries triple points on the formation of cavities along grain boundaries (Fig. 11). Most of these studies are based on monotonic creep experiments. They suggest that intergranular fracture observed in high temperature low cycle fatigue might also be associated with grain sliding.

2.1.6.4 Influence of temperature and strain rate on slip character

A concept which is particularly useful in rationalizing the various fatigue cracking modes and their dependence on variables such as strain rate and temperature is that of slip character.[36,37,38] Qualitatively, slip character is a

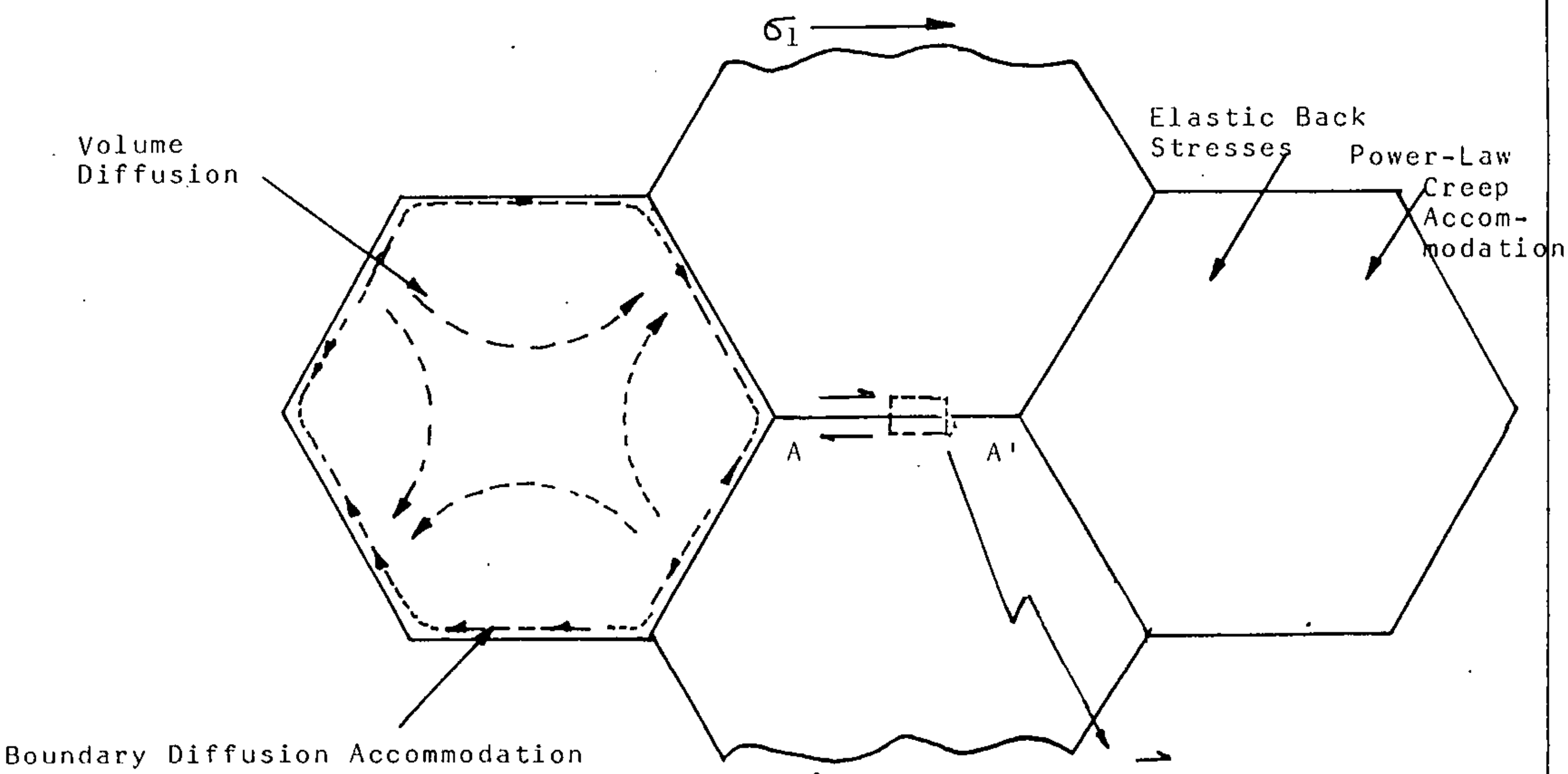

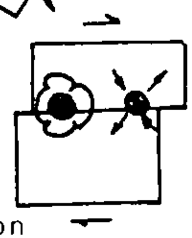

Fig. 11 Grain boundary sliding along the segment AA' can produce stress concentrations at the particles contained in the grain boundary. These stress concentrations, however, are transient since sliding along the segment AA' produces back stresses in the neighbouring grains. Steady state rate of sliding is controlled not by the accommodation around the particles, but by the rate of deformation of the grains (by diffusion or by power law creep).

measure of the degree to which dislocations tend to disperse during plastic deformation. Materials deforming by planar shear offsets are produced on polished surface. This type of deformation is favoured by a low stacking fault energy, ordering of the presence of coherent precipitates, low temperature, and small strains. The initial stage of fatigue cracking in planar slip materials is along slip planes and is referred to as Stage I cracking. For planar slip materials the degree of slip homogeneity is important in determining the rate of slip band crack initiation and propagation.

Wavy slip or homogeneously deforming metals exhibit uniformly distributed, non planar dislocation arrangements and a general surface rumpling. This type of deformation is favoured by a high stacking fault energy, incoherent precipitates or particles, and large strain, but most importantly, by temperatures greater than $\sim 0.4T_m$.[36,37,38,39,40,41] Most metals regardless of their slip character at low temperatures, exhibit wavy slip at temperatures $> 0.4T_m$ because thermal activation allows dislocations to cross slip and climb out of their original slip planes. Fatigue cracking under wavy slip conditions can occur in two modes: transgranular cracking perpendicular to the principal stress axis which is called Stage II fracture or intergranular cracking. An additional parameter of importance at temperatures $> 0.4T_m$ is frequency of cycling, that is, strain rate. The reason for this is that dislocation climb and cross slip are time dependent processes so the amount of slip dispersal occurring at a crack tip in given cycle will depend upon the frequency of cycling.

2.1.6.5 Temperature

Most materials exhibit reduced cycles to crack initiation and failure with increased temperature. The yield strength of material usually declines with increased temperature, and thus, in a given fatigue cycle, there is greater cyclic plasticity as the proportion of the plastic strain to total strain range increases. Even at a constant plastic strain range fatigue properties are reduced with increasing temperature because of the transition from transgranular to intergranular cracking.

Fatigue properties may improve with increased temperature under certain circumstances. Most ferrous materials experience strain aging at temperature above room temp.[41] During strain aging, the pinning of dislocations by interstitial atoms such as the precipitation of phases on dislocation can lead to both a dispersal of planar slip and an increased yield strength. The former can lead to improved fatigue properties, while the latter can produce higher stress ranges for a given total strain range and reduce fatigue life.

2.1.6.6 Frequency

At low temperatures, large changes in frequency have little or no effect on fatigue properties except for frequencies approaching the ultrasonic range. At elevated temperatures where time dependent processes become significant, reductions in frequency generally produce major reductions in the cycles for crack initiation and propagation. One of the common explanations for the frequency effect is that elastic strain is converted into plastic strain as a result of creep deformation or stress relaxation. As with increased temperature, the effect of thermally activated deformation processes and oxidation on the promotion of intergranular cracking significantly accounts for lowered fatigue properties as frequency reduced.

2.1.6.7 Combined effects of temperature and frequency

Fig. 12 shows schematically the effect of frequency at different temperatures on the fatigue life of a wavy and a planar slip material. At low temperatures, T_0, for both materials there is no frequency effect. For the wavy slip material, there is a reduction in life with increased temperature and reduced frequency. For the planar slip material at T_2, the life first increases then falls with frequency. Raising the temperature to T_3 is equivalent to moving the T_2

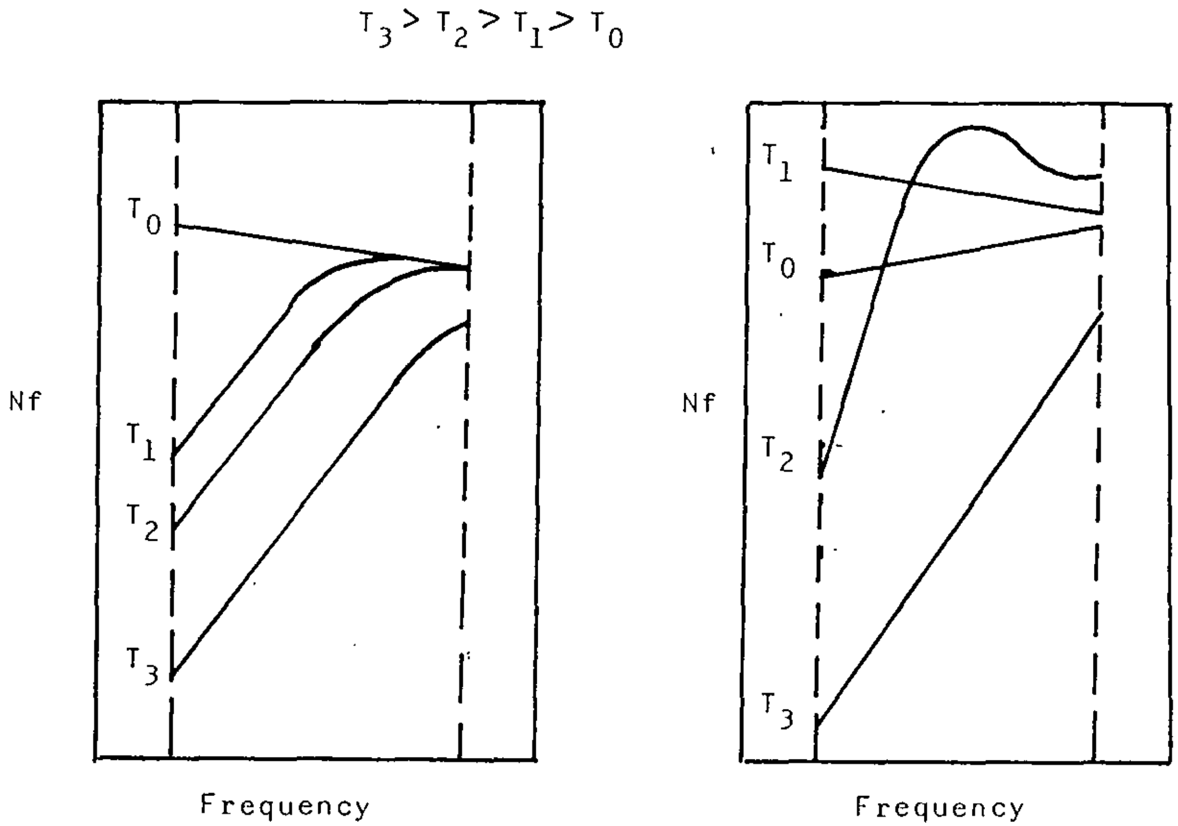

Fig. 12 The effect of temperature on fatigue life wavy and planar slip materials.

curve downwards and to the right, so that for frequency range indicated, there is only an increased fatigue life with increased frequency. Lowering temperature to T_1 is equivalent to moving the T_2 curve upward and to the left so that there is reduced fatigue life with increased frequency.

2.1.6.8 Dwell and mean stress effect

Increased tensile dwells and mean stress enhance thermally activated deformation, cavitation and intergranular cracking, and as a result, generally reduce fatigue life. The increased time per cycle upon introduction of a dwell period also promotes intergranular oxidation. One of the more interesting effects is that of a compressive dwell. There is evidence that compressive dwells retard or eliminate cavitation. On the other hand, once cavities are formed, the shape and therefore the rate of cavity growth may be dependent on whether a dwell is in tension or compression. A sharper flattened cavity can be produced with a compressive hold and a rounder one with tensile hold.[42]

2.1.6.9 Summary

Elevated temperature fatigue fracture can be intergranular (along grain boundaries) or transgranular (across grains). The rate of crack initiation and propagation is much faster when it occurs intergranularly than when it occurs transgranularly. It is therefore, important to be able to predict the mode of failure for given service conditions. If failure is transgranular, then it can occur in one of two modes: the Stage I mode is along slip planes and is in directions of high shear stress and the Stage II mode is non-crystallographic and normal to the principal stress direction.

The transition from transgranular to intergranular fracture and the rate of intergranular cracking can be related to the creep component and the amount of oxidation occurring in the fatigue cycle. Increasing the creep component and the degree of oxidation promotes intergranular cracking. The creep component is dependent on the temperature, frequency, hold time and normal stress. Cracking often starts in the form of cavities or microvoids and the surface of non-metallic precipitates in grain boundaries. It has been demonstrated that such cavity formation occurs more easily in the presence of a fatigue stress than for the case of simple creep. Oxidation attack also promotes intergranular cracking because grain boundaries and their environs are zones of chemical segregation and precipitations that have poor oxidation resistance. The preferential oxide penetration along a grain boundary is equivalent to a grain boundary notch of the same depth.

Perhaps the most success to date has been in relating the slip character and transgranular fracture mode of material to conditions of temperature and frequency. Planar slip is favoured by low temperatures, small strains, and high frequency in materials of low stacking fault energy.

The concepts of slip character, creep component, oxidation and fracture mode have been used in a qualitative manner to explain high temperature low cycle fatigue.

2.2 Fatigue Crack Propagation Behaviour of Ti-6Al-4V (IMI 318)

The extensive use of Ti-6Al-4V forgings in aircraft gas turbine structures has generated considerable interest in its low cycle fatigue behaviour. The availability of Ti-6Al-4V allowed an important step to be taken in the development of applications for titanium alloys in aircraft gas turbine engines, namely the use of titanium for compressor discs.

The Ti-6Al-4V alloy has modest quantities of both α-stabiliser (aluminium) and β-stabiliser (vanadium) thereby combining reasonable strength with good foregeability. The 0.2 per cent proof-strength-temperature relationship and low cycle fatigue properties of Ti-6Al-4V are compared with those other more recently developed titanium alloys in Fig. 13 and 14 [43] respectively. The relationship of strength to fracture toughness of titanium alloys [43] including Ti-6-4 is shown in Fig. 15.[43]

The α/β titanium alloys are most often used in the annealed condition and it should be noted that both microstructure and some mechanical properties may differ depending upon whether or not prior forming was carried out above or below the β-transus.

Table 2.1 compares the properties of the alloy Ti-6Al-4V forged in these conditions. It should be noted that although tensile properties are fairly similar, the samples forged in the $\alpha+\beta$ phase field (equi-axed grains) are more ductile, whereas fracture toughness and fatigue strength are both notably higher in β-forged and annealed material (acicular widmanstatten structure).

Work on Ti-6Al-4V rolled plate has indicated that the superior fatigue performance with the β-annealed conditions is associated with relatively slower rates of crack propagation, Fig. 17.[44] This effect, in turn, is attributed to the slower progress of cracks through the Widmanstatten structure, especially at stress intensities below a critical value (T in Fig. 17) when desirable crack branching occurs within packets of the α-laths.

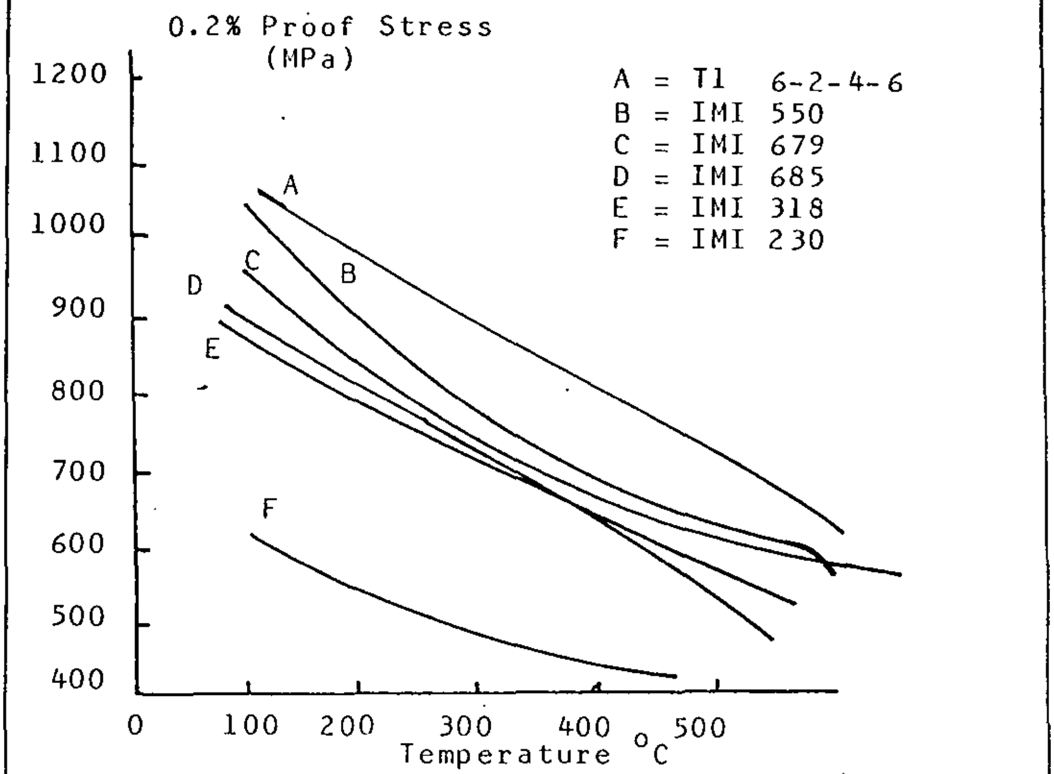

Fig. 13 Effect of temperature on the 0.2% proof stress of various titanium alloys. (Ref. 43)

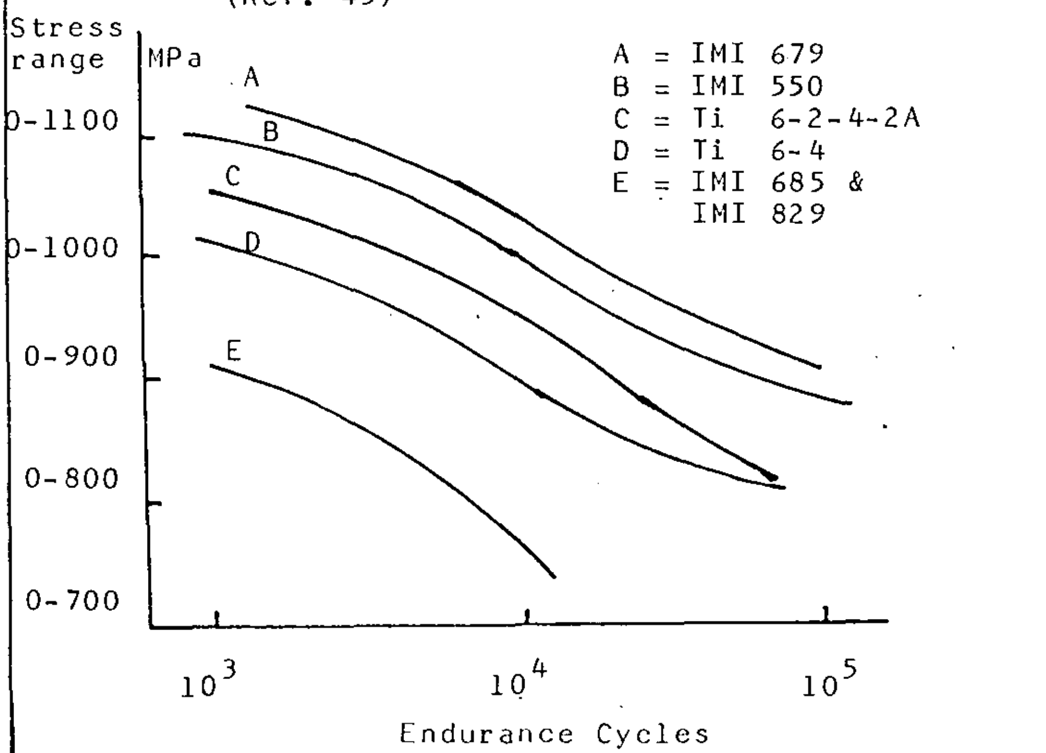

Fig. 14 Typical low cycle fatigue properties for various titanium alloys at 20°C. (Ref. 43)

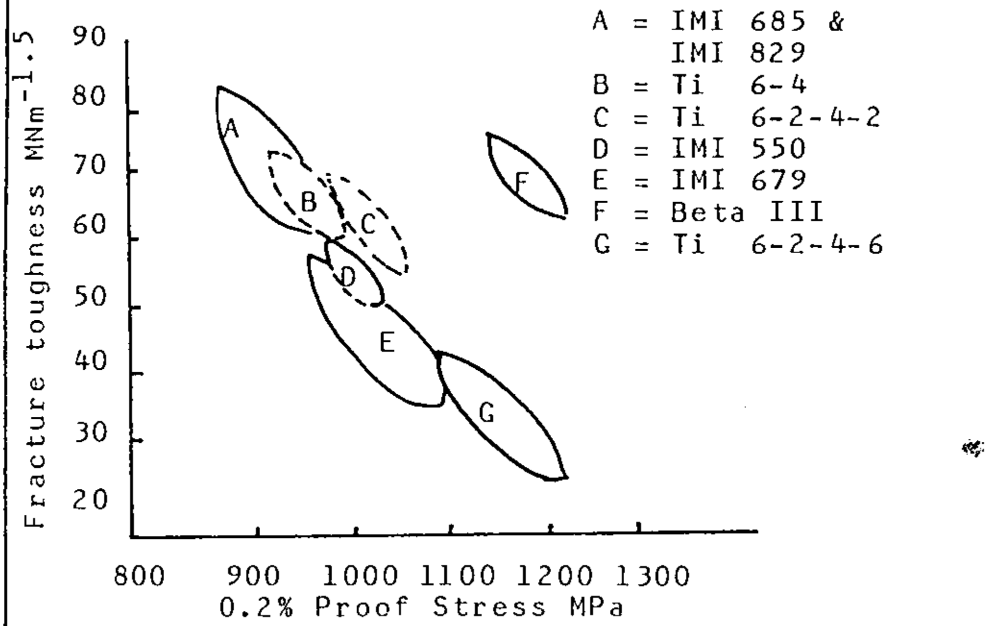

Fig. 15 Comparison of fracture toughness versus strength for various alloy types at 20°C. (Ref. 43)

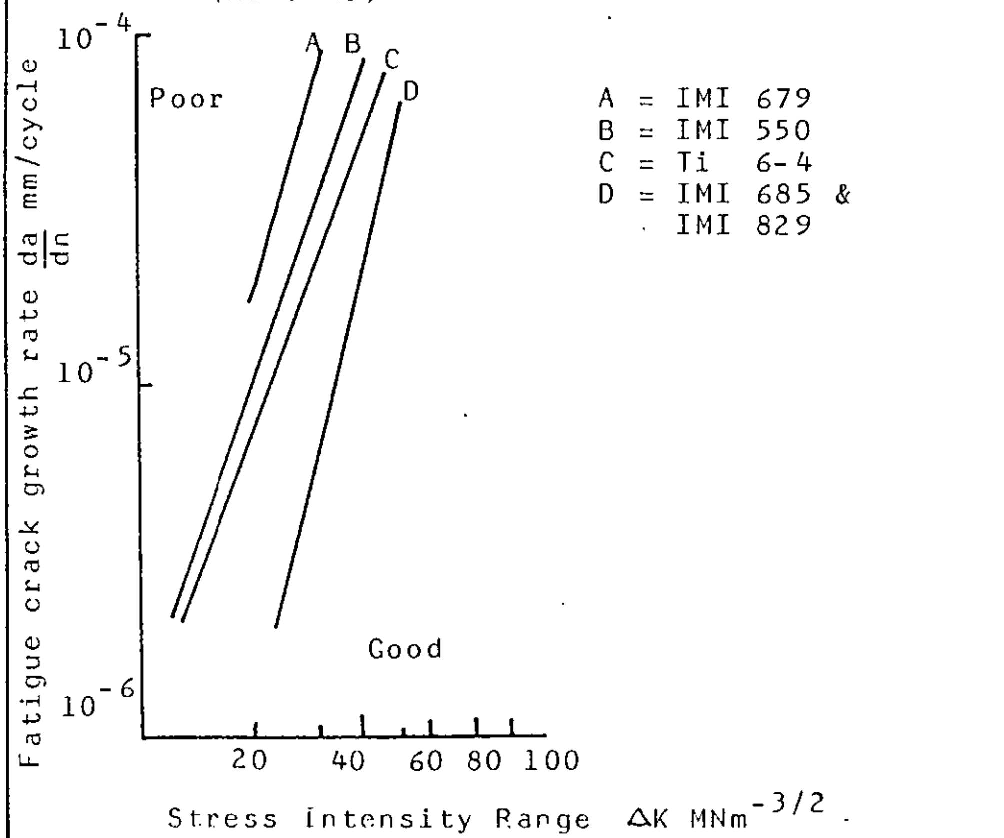

Fig. 16 Comparison of the crack propagation rates for various titanium alloys at 20°C. (Ref. 43)

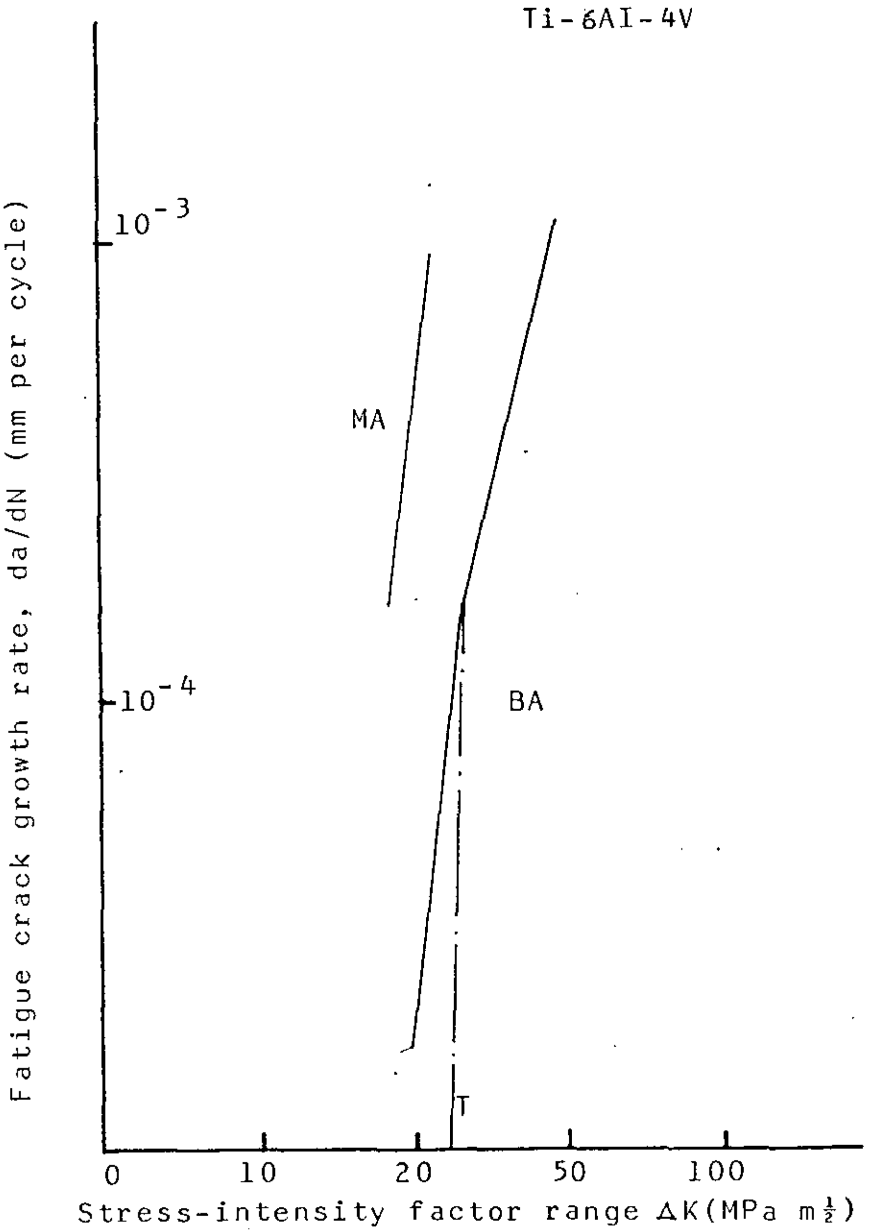

Fig. 17 Fatigue crack growth rates for Ti-6Ai-4V rolled plates in the β-annealed (BA) and mill-annealed (MA) conditions. BA = 0.5h 1038°C, air-cool to room temperature. Tests conducted at 5Hz using compact tension specimens. Ratio of minimum to maximum load = 0.1.

Table 2.1 Properties of annealed Ti-6Al-4V forgings (45)

Properties	Forging treatment $\alpha + \beta$ Phase field	β Phase field
Tensile Ultimate (MPa)	978	991
Tensile Yield (MPa)	940	912
Tensile Elongation (%)	16	12
Reduction in area (%)	45	22
Fracture toughness ($MPam^{\frac{1}{2}}$)	52	79
10^7 Fatigue limit (MPa)	$\pm$494	$\pm$744

Annealed 2 hours at 705°C, air cooled after forging
α/β transus 1005°C
Axial loadings = smooth specimen k_r = 1.0.

Fig. 16 illustrates the crack propagation rates of various titanium alloys at room temperature. IMI 685 exhibits lower crack propagation rates than IMI 318. This is due to the basket weave type microstructure of IMI 685.

There is general agreement in the literature and enough experimental evidence that refining the microstructure of the Ti-6Al-4V alloy results in an improvement of fatigue strength of smooth specimen.[46] Fatigue crack propagation rates were measured in the range between 10^{-9} and 10^{-7} m/cycle in vacuum, laboratory air, and 3.5 percent NaCl solution.[46] The results are shown in Figures 18-20. The vacuum tests revealed that the coarse equiaxed microstructure exhibited a slower crack propagation rate than the fine equiaxed structure (Figure 18). The bi-modal structure showed the slowest crack propagation rate, this is probably due to the lamellar portions of the structure. In the presence of an aggressive environment (laboratory air, Fig. 19 and 3.5 percent NaCl solution, Fig. 20), the crack propagation rates were faster and the difference between the three microstructures became smaller.

Fig. 18

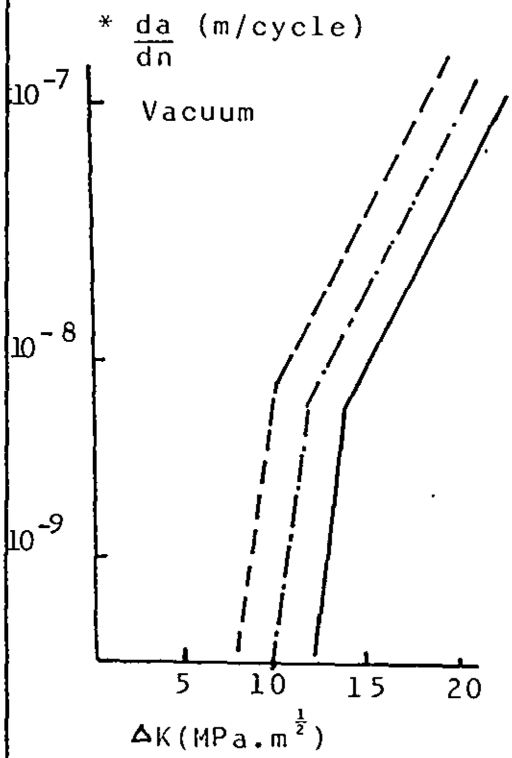

Fig. 19

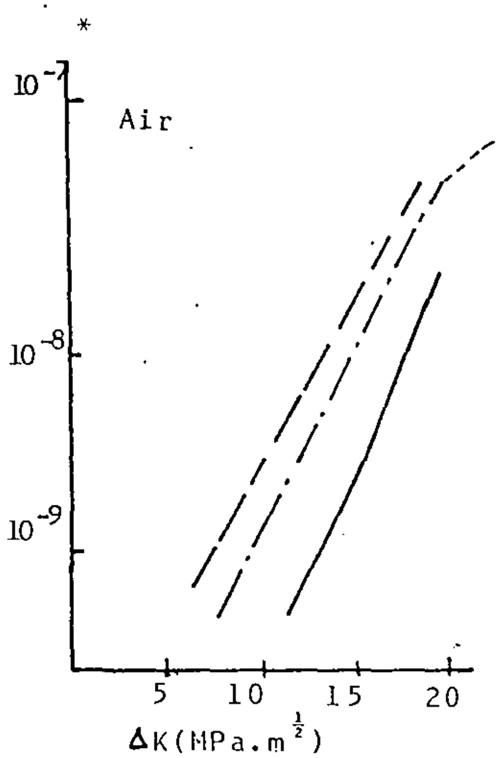

Fig. 20

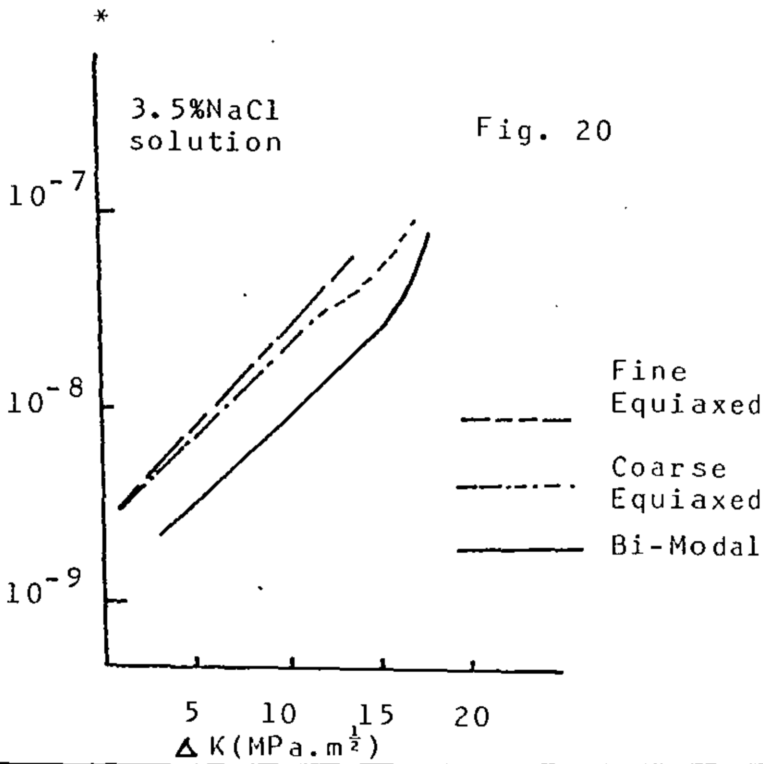

Recent studies of sustained load cracking in titanium alloys have shown that highly accelerated crack growth can occur at sub-ambient temperatures in alloys containing 100-300 ppm hydrogen.[47]

The influence of hold-time or dwell on fatigue properties of structural materials has been the subject of considerable interest over recent years. This interest has been generated in part by the fact that engineering structures are frequently subjected to this kind of loading sequence, and in part because surprisingly large effects are sometimes observed with relatively short hold times. These effects generally take the form of decreased fatigue life in conventional stress or strain versus life testing,[48] or in the form of increased fatigue crack growth rate in crack propagation tests.[49] In most materials, the increase in crack growth rate or decrease in life is accounted for on the basis of either an environmental interaction or alternatively can be ascribed to the influence of creep on deformation or cavitation during a tensile hold.[50]

The situation with titanium alloys is somewhat different in that hold time effects has been reported at temperatures below those at which significant environmental or creep effects take place. The work on crack propagation behaviour confirmed that a dwell period [51] at peak stress can significantly increase the rate of crack growth da/dN at a given range of stress intensity Δk. Previous work on IMI 318 clearly demonstrates that the crack propagation dwell sensitivity disappears at temperatures in the range 350 and 425k.

Fatigue crack growth studies on Ti-6Al-4V at growth rates of 10^{-7} - 10^{-4} mm/cycle in air have shown [52] that microstructural variations can produce variations in crack growth rate by a factor between 3 and 10 when testing at R (L min/L max ratio) of 0.35.

The effects of microstructure are considered to be the least important of the variables involved in fatigue crack growth.[53] Experimental work on the influence of microstructural parameters on fatigue lives have usually concluded that any improvement in fatigue ratio occurs through an improvement in initiation behaviour rather than increased resistance to fatigue crack growth.[54,55]

There have been a limited number of investigations into growth rates in Ti-6Al-4V material, most of them at medium to high growth rates with Δk levels of between 7 and 20 $MNm^{3/2}$ [56,57,58] Bucci et al [59] have performed a low growth rate investigation in Ti-6Al-4V and conclude that a threshold for crack growth exists at Δk values of 4-6 $MNm^{3/2}$, and that there is no significant effect of microstructure. At low growth rates they and Mayn [56] reported the observation of cleavage like features on the fracture face.

CHAPTER 3

3.0 REVIEW OF EXPERIMENTAL TECHNIQUES

3.1 Techniques of Crack Measurement

Introduction

It is generally recognised that failure by fast fracture of an engineering component is often preceded by slow crack growth. Consequently much effort has been devoted in recent years to studies of the initiation and propagation of such slowly growing cracks. Optical measurement of crack length in a laboratory test piece using a travelling microscope or similar instrument is both simple and inexpensive. There are many instances where this direct approach is unsuitable, however, perhaps for physical reasons as when the cracked material is enclosed in a furnace chamber or where tests take place over extended periods of time. Furthermore, optical measurements are in general restricted to the free surface and may be unrepresentative of the behaviour in the interior. For complicated experimental situations exemplified above, several indirect methods of measuring crack length have been developed.

One of the most popular techniques used both to determine the onset of cracking and to measure crack length growth rates has been the electrical potential method, with d.c. current or a.c. current. The electrical potential techniques have been in use for over 15 years for measuring crack lengths in metallic fatigue and fracture specimens. Briefly this entails passing a constant current through a cracked test piece under load, and measuring the potential difference across the crack. As the crack extends, the uncracked cross sectional area of the test piece decreases, its electrical resistance increases, and the potential difference between two points on either side of the crack rises. By monitoring this potential increase (V_a) and comparing it with a reference potential (V_b) measured elsewhere on the test piece preferably in a region which is not affected by crack growth, the crack length to test piece width ratio (a/w) may be determined.

Direct current systems were the first to be used.(60-63) The initial systems involved measurements of electrical potential changes in the millivolt range.(60-61) Because of the low resistance of metallic specimens, high direct currents (on the order of tens of amperes) were needed. Measurements were typically made on a point-by-point basis because of the particular measurement (null) technique, and the need to have the current switched on only during measurements to minimise specimen heating. To avoid the use of these high direct currents, systems capable of measuring potentials in the microvolt range were later utilized.(62-63) Point-by-point measurements were made at first using a null technique (62-63) with the availability of low-noise, high-gain d.c. amplifiers, continuous recording systems are now commonly utilized.(64-65)

The d.c. systems are somewhat limited, however, because of their sensitivity to thermally induced electromotive force (emf) (associated with thermocouple effects) and the limited potential for further reduction in their sensitivity to "noise". To circumvent some of these limitations of the d.c. systems, alternating-current systems have been assembled to take advantage of the noise rejection capabilities of lock-in-amplifiers and the high gain associated with these amplifiers.(66-67) These systems, being a.c. systems, would be insensitive to thermally induced d.c. potentials, and are capable of sensitivity in the nanovolt range. Signal discrimination is facilitated in a.c. systems by the ability to tune the measuring instrument to the excitation frequency.

Both the d.c. and a.c. potential systemshave gained acceptance as reliable, accurate and cost-effective methods for measuring crack lengths in fatigue and in other fracture specimens. They can be readily integrated into a suitable data acquisition system for continuous monitoring of crack growth experiments. They can also form an integral part of automated materials testing systems for data acquisition and provide for control of simple and complex crack growth experiments.

3.1.1 The Direct Current System

The block diagram of a typical d.c. potential system is illustrated in Fig. 21. The system is composed of a "constant" current source and a means of measuring the potential differences which are produced across the crack plane. The constant current source should of course be highly stable for most accurate work and a capability of supplying up to 50 amps is required if the specimens of low resistivity and large size are to be used. (In the experimental work current of 10 amps was used for 12.7mm thick Ti-6Al-4v specimen).

Since the specimen resistance is very low (much less than 1ohm), the constant current source is often replaced by a constant voltage source, with suitable current limiting resistors to establish the desired current level. In addition to or in place of the recording instruments the output of the amplifier may be connected to a data acquisition system or to a digital computer.

The potential differences which are produced in a test are dependent upon the magnitude of the current, the specimen resistivity, the specimen shape and size, the length of the crack, and the current lead and potential probe positions.

The connection of the current leads to the specimen is achieved through brass bolts screwed into the specimen.

Sometimes specimens such as the CTS shown in Fig. 21 are insulated by using sheaths over the loading pins. Insulation at these points has caused problems with specimen temperature stability during fatigue testing, however, due to either friction heating effects or simply because of thermal insulation of the current-carrying specimen from the grip mass.[68] Whether insulated or otherwise, tight fitting loading pins must be avoided because of obvious friction problems. Tight, uninsulated pins also create an additional problem of a variable conducting path across the holes and consequent modification of the potential field in the specimen.

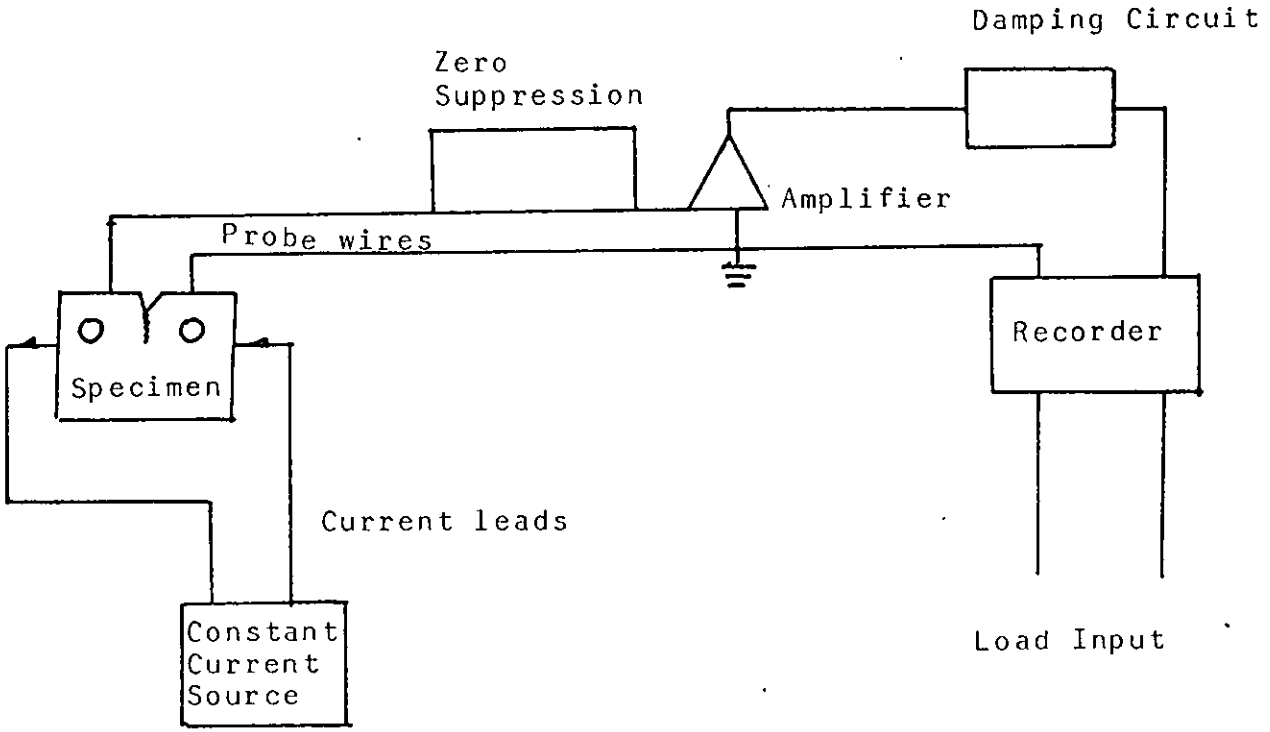

Fig. 21 A d.c. potential drop block circuit diagram

The above paragraphs have described the basic requirements of a d.c. potential drop system, but the sensitivity and accuracy may be improved by attention to the following points. These are of particular importance in an application where measurements of microvolt and submicrovolt potentials are required and where long term stability is at a premium.

(i) Thermal effects can be major sources of error and it is recommended that a controlled temperature room be used for the potential drop equipment if available. Alternatively, benefit can be obtained if the stabilised current source and the zero suppression facility are contained in a constant temperature enclosure.

(ii) Avoid dissimilar metal connections.

(iii) Avoid large-scale specimen plasticity. An error in potential measurements may occur when a substantial amount of plastic deformation occurs in the material ahead of the crack tip. Changes in potential can occur, caused by a change in shape of the crack tip and changes in potential resistivity of the plastically deformed material ahead of the crack tip. These changes in potential are not associated with an increase in crack length, making crack length measurement inaccurate.

(iv) Remove oxides from both the specimen and the lead wires, as they can introduce very large resistance into the excitation and measurement circuits. The presence of oxides at junctions can serve as a source of significant thermal emf errors in a d.c. potential system.

3.1.2 A.C. System

A typical a.c. potential system is illustrated in the block diagram in Fig. 22. The system is built around a lock-in amplifier and includes, in addition, a power amplifier (operated as a constant current operational amplifier), an isolation transformer, and appropriate recording and data acquisition systems. The power amplifier is driven by a reference signal from the lock-in amplifier to supply the specimen with a constant current a.c. excitation signal. The constant current level is determined by the wiring configuration of the power amplifier and the sampling circuit resistors. Typically this is approximately 0.75A.

The input signal consists of the desired potential signal at the reference frequency combined with broad-band noise picked up from stray magnetic and electrical fields and other sources. Since the potential signal at the specimen is small ($\sim$100 microvolts), the signal-to-noise ratio of the input signal may also be quite small and the resolution of the potential signal within the noise may be unacceptable. The frequency discrimination characteristic of the lock-in is used [(67)] to selectively amplify the desired potential signal for measurement. The noise rejection capabilities of available lock-in amplifiers allows them to handle signals with signal-to-noise ratios as low as 0.1.

3.1.3 Calibration

To use the potential systems for measuring crack lengths, the relationship between specimen crack length and potential for a particular specimen plan form must be established. This relationship can be determined experimentally, analytically,[(69)] or by numerical methods.[(70,71)] Analytical techniques are suitable for simple specimen geometries (such as center-cracked tension specimens), but are difficult to use because of problems encountered in modelling the complex geometry of most specimens. Numerical methods, unless they are quite sophisticated, tend to yield relatively crude results. Experimental determination with a specimen on the

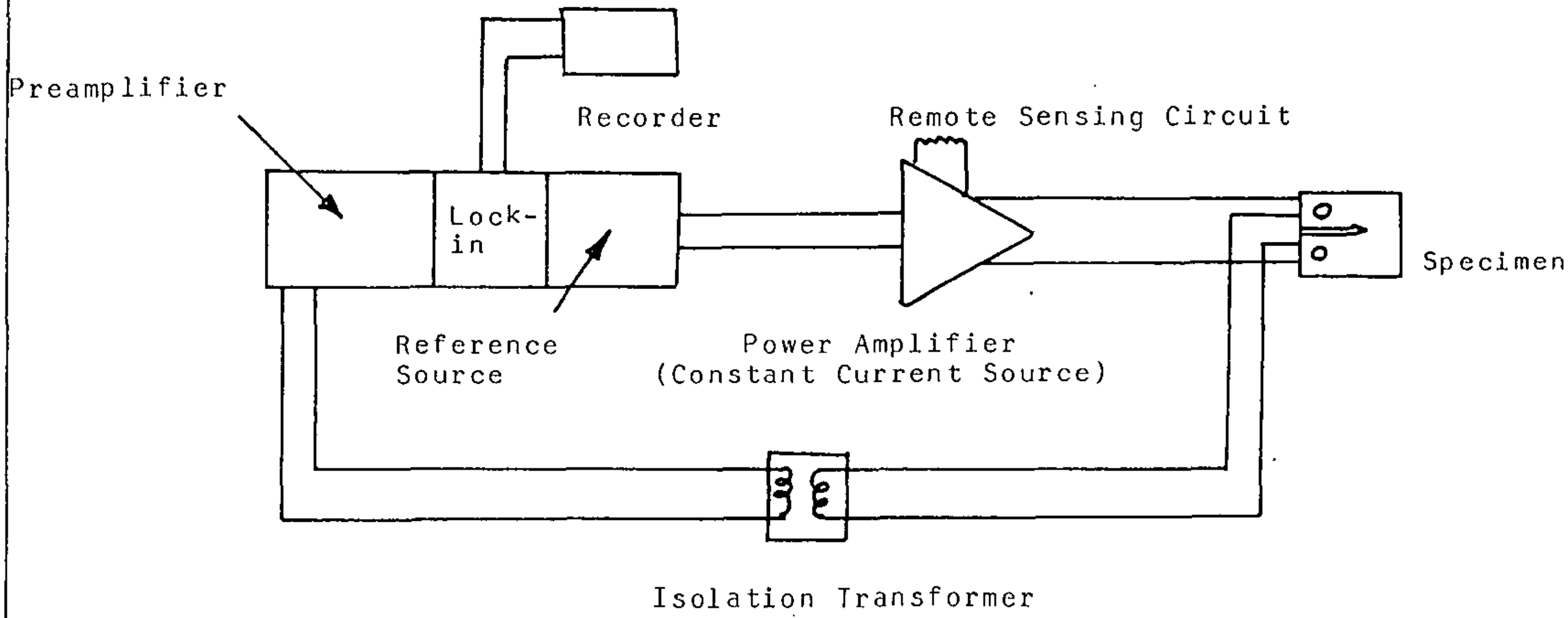

Fig. 22 Schematic diagram of the a.c. potential system

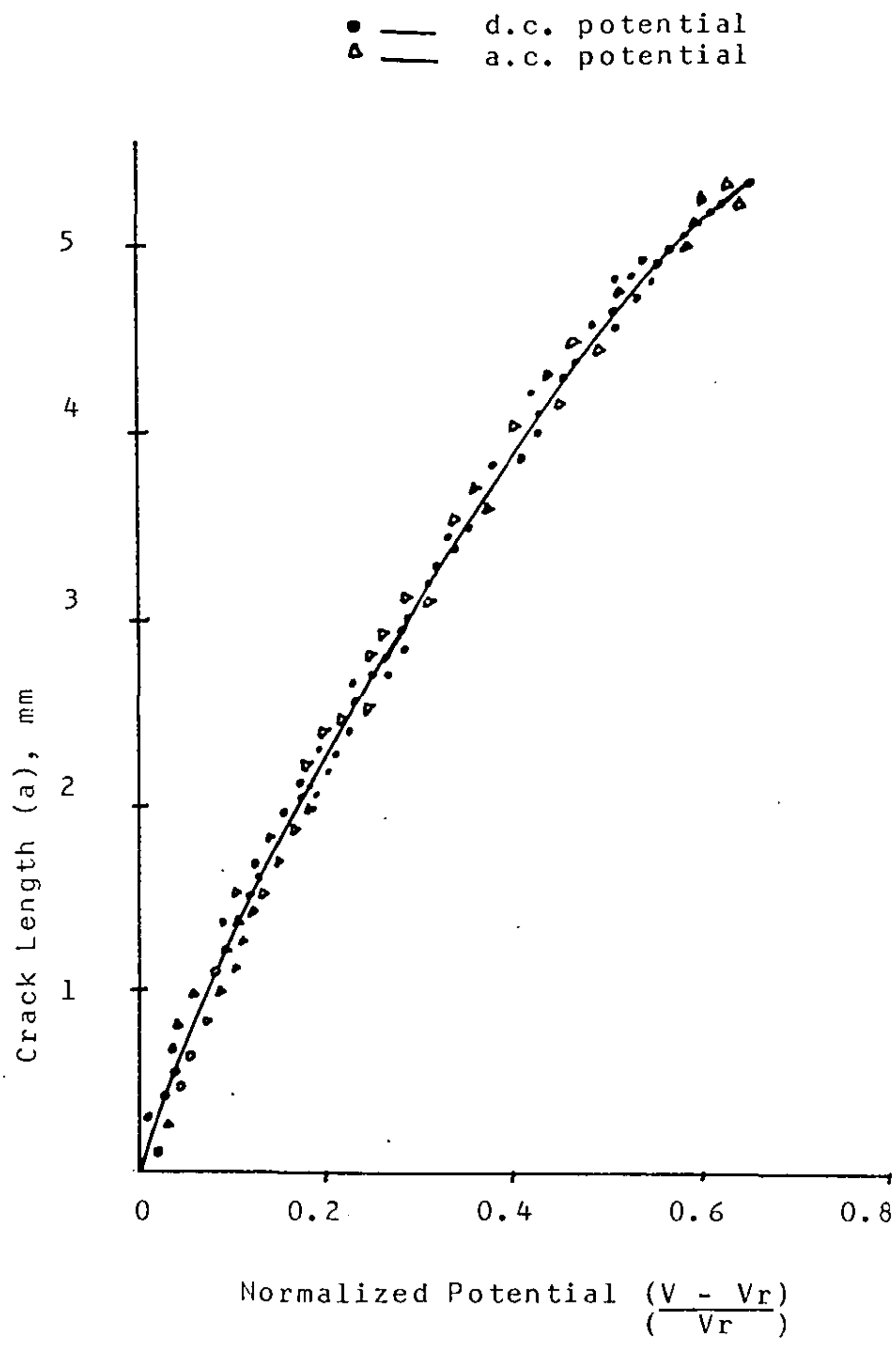

Fig. 23 Calibration curve for a.c. and d.c. potential systems (Ref. 67)

other hand, in the most straight forward actual operating conditions can be exactly duplicated. This method also provides data for making statistical estimates of the uncertainty in crack length measurements.

When determining specimen crack lengths from potential measurements it is desirable to eliminate specimen-dependent effect from these measurements. Normalization of potential readings with respect to a reference potential for each specimen is used to eliminate from these measurements any variations in potential caused by changes in specimen resistivity with temperature or by thickness difference from one specimen to another. Normalized potential, however, is only dependent on changes in specimen resistance produced by crack extension when all other variables remain constant. The normalised potential depends on the distributed electric field within the specimen and this specimen planform and probe position in general requires a separate calibration to determine how crack length is related to the normalized potential. Conversely, however, geometrically similar (but dimensionally different) specimens should exhibit the same normalized potential dependence on normalized crack length (that is, the ratio between crack length and the reference crack length). The normalized potential, from which crack length can be determined after calibration, is usually taken to be the ratio of the difference between the absolute and reference potentials (V-Vr) to the reference potential (Vr), or

$$V = \frac{V - Vr}{Vr}$$

The reference potential, Vr, is the specimen potential corresponding to a reference crack length.

Calibration data obtained with both a d.c. and a.c. potential system are shown in Fig. 23, along with a fitted polynominal curve for the data. Both systems show approximately a 50 percent increase in normalized potential occurring over the useful crack length range of the specimen, so that good crack length sensitivity is obtained. Data obtained from both systems are in agreement over the entire range of crack lengths.

TABLE 3.1

Crack Growth Measurement Techniques

Method	Usage	Advantages	Disadvantages
Microscopy techniques.	Sheet and plate test pieces. Photography sometimes used.	Cheap, easy installation.	Difficulty of crack tip location without stroboscopic light. Only surface measurements possible during test. Difficult to automate.
Mechanical methods	Roating bend test pieces, sheet, plate and others depending on displacement gauge used.	Used of compliance change which can be measured externally away from specimen.	Restricted to test where compliance calibration (relationship between specimen stiffness and crack length) is known.
Acoustic methods	Applicable to most types of test-piece.	Very small probe required, can be mounted easily; useful in low and high temperature tests.	Errors due to background noise and calibration is difficult.
Electrical techniques	Continuity gauge usually used on sheet and plate samples, could be used for surface measurements on other test pieces.	Electrical signal gives easy automation.	Difficulty of connecting wire and foil gauges. Gauges must break when crack passes. Only surface measurements.

Table 3.1 (continued)

Method	Usage	Advantages	Disadvantages
Eddy currents	Used on surface crack monitoring of sheet test pieces; others should be possible.	Easily adapted to automatic process - small probe which is not in contact with test piece.	Not yet used on thicker samples, may only be useful for surface measurement. Expensive.
Electrical resistance or potential measurement.	Used on sheet and plate test pieces.	Easily adapted to automatic process. Only four leads attached to specimen. Therefore ideally suited for high or low temperature tests.	Problems of insulating the test piece. Initial calibration problem thought to be overcome.
Ultrasonics	Ideally suited to compact fracture toughness test piece.	Easily adapted to automatic process. Internal measurement of crack front.	Expensive compared to other techniques. Measurement restricted to thicker type of test piece.

The equation of the experimental calibration curve can be expressed as

$$Q = 15.9 + 52.0\,V + 26.0\,V^2 - 41.4\,V^3 \quad (Q \text{ in mm})$$

The coefficients were determined from the experimental data by the method of least squares, and statistics on the precision of the data were used to select the order of the polynominal forthe calibration equation. Apart from the direct observation of the specimen's surface and techniques described in Section 3.0, various other means of crack measurements have been developed and these are summarised in Table 3.1.

3.2 The Servo-Hydraulic Test Machine

In recent years there has been a marked increase in the use of servo-hydraulically operated fatigue machines, Fig. 24.(72) In such systems the load generated by hydraulic cylinder is measured by a strain-gauged dynamometer or load cell in series with the specimen. The signal from load cell is amplified and compared in a differential amplifier with the desired signal obtained from the data input. The output of the differential amplifier is transmitted to a servo-valve which controls the cylinder. This system thus forms a closed-loop control circuit. The loop may also be closed from a displacement transducer or a strain gauge on the specimen instead of the load cell, if desired. The energy required is provided by a hydraulic power pack which operates at constant pressure (usually in the range 20-30 MNm^{-2}).

A major advantage of such machines is their flexibility of operation. Much larger specimen deflections are possible than can be achieved in electromechanical machines, although the operating frequencies for large strokes are necessarily low unless very large hydraulic pumping capacity is available. Thus, components involving large deflections as well as conventional stiff test-pieces can be accommodated. A more important advantage, however, is the versatility of the system regarding the input signal which can be accepted.

Fig. 24 Scheme of an Electro-Hydraulic Fatigue Machine with Servo-Control

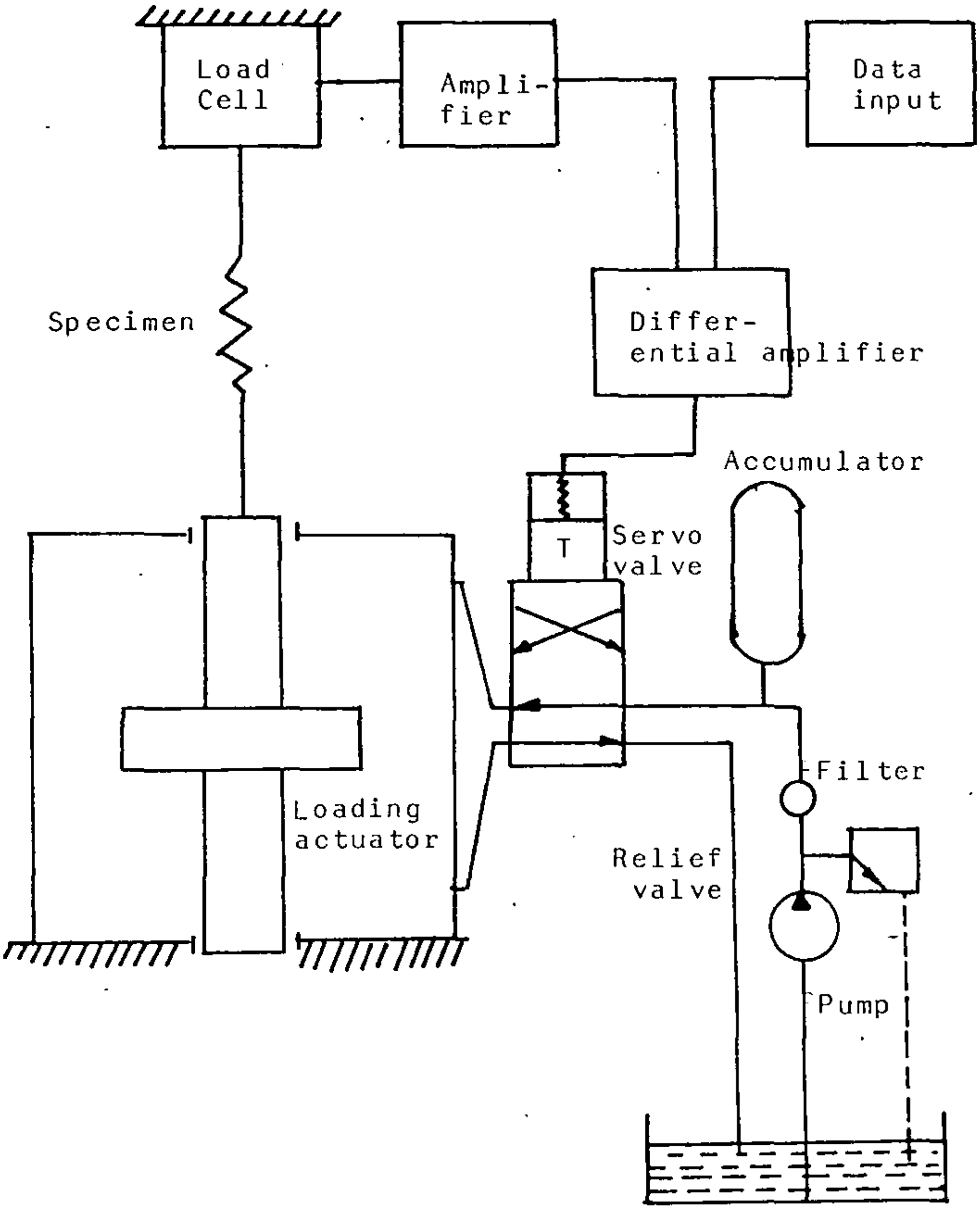

Virtually any analogue signal, for example, from a function generator, random noise generator, magnetic tape, or punched paper tape reader, can be used on input. Thus, not only constant amplitude waveforms or simple block programs. but also random waveforms, such as service-recorded stress histories, can be accommodated. Materials specimens or components, therefore can be subjected to much more realistic fatigue testing than is possible in conventional machines; this also applies to the use of servo-hydraulic actuators in loading-frame testing of components and structures. The major disadvantages of servo-hydraulic machines is that the power consumption is generally much higher than that of comparable conventional machines.

CHAPTER 4

Experimental Work

4.1 Introduction

Before crack growth studies can be performed on the test specimens, it is necessary to precrack the specimens to provide consistently sharp fatigue cracks of adequate size and straightness.

During precracking it is necessary to select a stress intensity amplitude such that the maximum stress intensity at the tip of the crack does not exceed the initial maximum stress intensity at the same point in the specimen during the actual crack growth test, in order that the residual plastic zone does not interfere with subsequent fatigue crack growth. As it is the intention to perform fatigue crack testing with a maximum stress intensity of 18 $MNm^{-3/2}$ it was decided that the maximum stress intensity at the tip of the crack should not be greater than about 15 $MNm^{-3/2}$ at the end of precracking.

One approach to precracking, then, is to select an appropriate load cycling range on the test machine to produce the stress intensity range of 1.5 - 15 $MNm^{-3/2}$ (using a R-ratio of 0.1) at the tip of a machined notch in a compact Tension type test specimen and cycle the load over this constant load amplitude until a precrack of the appropriate length is obtained. Whilst this approach is feasible, it is very inefficient as it will take a long time to initiate and grow a fatigue crack at the root of the notch at such a low stress intensity amplitude.

An alternative approach is to start the precracking with a much greater maximum stress intensity (25.5 $MNm^{-3/2}$ in this case) to encourage rapid crack initiation and initial growth, reduce the stress intensity range progressively as the crack extends, and finish precracking with crack growing at a maximum stress intensity value of 15 $MNm^{-3/2}$. This approach will reduce the precracking time drastically, but requires constant monitoring of crack length and periodic adjustment of reduction load limits. This can be done manually or by computer control of the testing machine. The design and implementation of the computer control approach is the subject of this project, details of which will be given in this chapter and Chapter 5.

4.2 The Size of the Crack Tip Plastic Zone

The material at the tip of a crack is assumed to remain elastic even though the stresses are very high. In practice, materials (especially metals) tend to exhibit a yield stress, above which they deform plastically. This means that there is always a region around the tip of a crack in a metal, where plastic deformation occurs, and hence a stress singularity cannot exist. The plastic region is known as the crack tip plastic zone.

The extent of the plastic zone ahead of the crack tip may be calculated by equating σy to the yield stress of the material (see diagram below). This gives the plastic zone size rp^*.

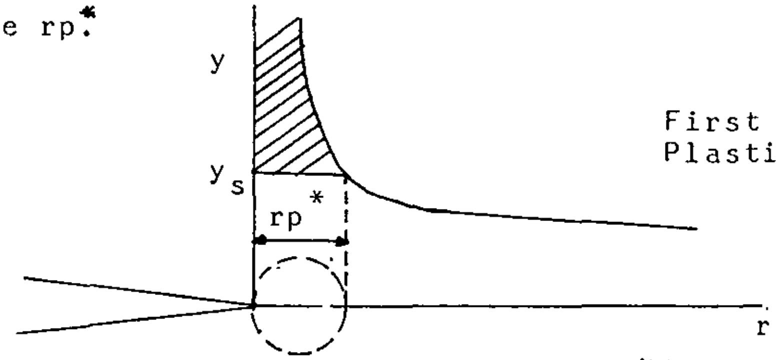

The σy stress ahead of the crack in the plane $\theta = 0$ is as shown until a distance rp^* from the crack tip $\sigma y > \sigma y_s$
To a first approximation rp^* = size of plastic zone.

$$\sigma y = \frac{K_I}{\sqrt{2\pi r}} \text{Cos } \theta/2 \ (1 + \text{Sin } \theta/2 \text{ Sin } 3\theta/2)$$

If $\theta = 0$, $\sigma y = \frac{K_I}{2\pi rp^*} .1 \ (1 + 0)$

Substitute $\sigma y = \sigma y_s$

we get

$$\sigma y_s = \frac{K_I}{\sqrt{2\pi rp^*}}$$

$$\text{or} \quad rp^{*} = \frac{(K_I)^2}{2\pi y_s^{\,2}} = \frac{\sigma^2 a}{2\sigma y_s^{\,2}} \tag{1}$$

4.3 Limiting Crack Lengths

The object of prefatigue cracking is to obtain a crack length of 1.6omm. It is the intention to perform subsequent fatigue crack propagation tests at peak stress intensities of 18 $MNm^{-3/2}$ and above. For this reason it is necessary to ensure that the limit of the crack tip plastic zone at the end of the precracking does not exceed the limit of the plastic zone caused by loading the specimen during the subsequent crack propagation tests.

This requires the calculation of the limiting crack lengths at which the stress intensity is reduced during pre-cracking.

A diagramation representation of the limiting crack lengths is shown below.

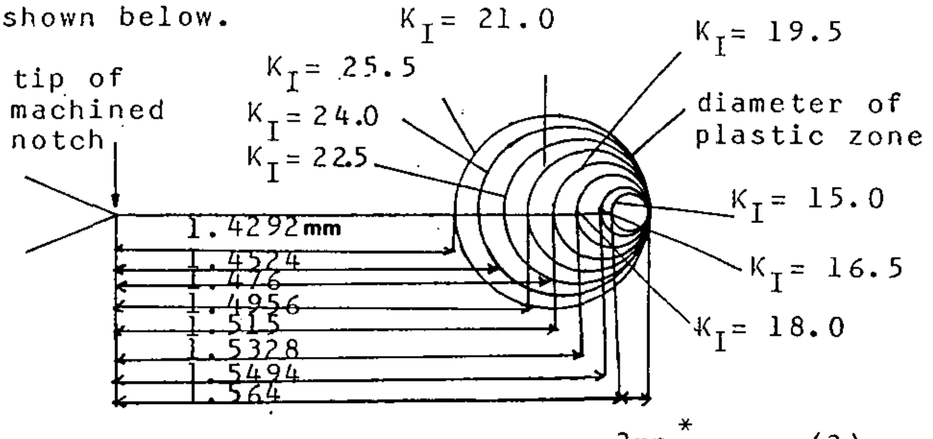

(2)

$$a_{min} = (1.60 - 2rp^{*}) - rp^{*} \quad (15)$$

$rp^{*}(15) = 0.0358$

The limiting crack lengths at which the stress intensities are progressively dropped are calculated from equation 2 where factor of 2 is used to work out the plastic crack tip sizes at all stress intensity levels to allow for any variations of the real crack tip plastic zone from the calculated sizes.

The maximum load applied during fatigue precracking cycling was calculated from the expression:

$$K_I = \frac{P}{BW^{\frac{1}{2}}}\left[29.6(a/w)^{\frac{1}{2}} - 185.5(a/w)^{3/2} + 655.7(a/w)^{5/2} - 1017(a/w)^{7/2} + 638.9(a/w)^{9/2}\right]$$

where K_I = maximum stress intensity in $MNm^{-3/2}$
P = Applied load in MN
a = Crack length in m
w = Width in m
B = Thickness in m

Table 4.1 shows different applied load for different stress intensities.

Table 4.1

K_I (MAX) $MNm^{-3/2}$	MAX LOAD APPLIED (KN)	2rp* (mm)	a/w Ratio	rp* (mm)	a_{min} (mm)
25.5	9.55	0.2068	0.3063	0.1034	1.4292
24.0	8.21	0.1836	0.3072	0.0918	1.4524
22.5	7.68	0.1610	0.3081	0.0805	0.1476
21.0	7.15	0.1404	0.3089	0.0702	1.4956
19.5	6.63	0.1210	0.3096	0.0605	1.515
18.0	6.11	0.1032	0.3103	0.0516	1.5328
16.5	5.60	0.0866	0.3110	0.0433	1.5494
15.0	5.08	0.0716	0.3116	0.0358	1.5644
-	-	-	0.31299	-	1.600

4.4 Material and Specimen Geometry

The material used for the precracking experiments was Ti-6Al-4V, manufactured by IMI Ltd., designated IMI 318, and was provided by Rolls Royce Ltd., Derby. The composition and mechanical properties as shown in Table 4.2. The material is two-phase α/β alloy, and was heat treated for one hour at 960°C, water quenched then annealed for two hours at 700°C. This heat treatment was carried out at Rolls Royce. In addition to providing stress-relief, this treatment results in the formation of an equi-axed structure composed of α - grains and grains of transformed β (Figure 25).

The compact tension (CT) specimen was used (Figure 26). The specimens were machined by Rolls Royce Ltd. The specimen is loaded through pins passing through the holes on both sides of the machined slot.

The pin-to-hole clearance are designed to minimise friction there by eliminating unacceptable and movement that would invalidate the specimen K-calibration.

The machined notch in the CT specimen must be at least 0.2W in length so that the K-calibration will not be influenced by small variations in the location and dimensions of the loading pin-holes.

Table 4.2

ALLOY	% Ti	% AL	% V	0.2% Proof Stress (MPa)	Tensile Strength (MPa)	% Elongation	Relative Density
IMI 318	BAL.	6.0	4.0	925	990	14	4.46

Figure 25(a). Micrograph of (Ti-6Al-4V). The structure consists of equi-axed grain of α (white) and transformed β (widmanstatten α) x 600. Etched in 10% HNO_3 + 2%HF + 88% H_2O.

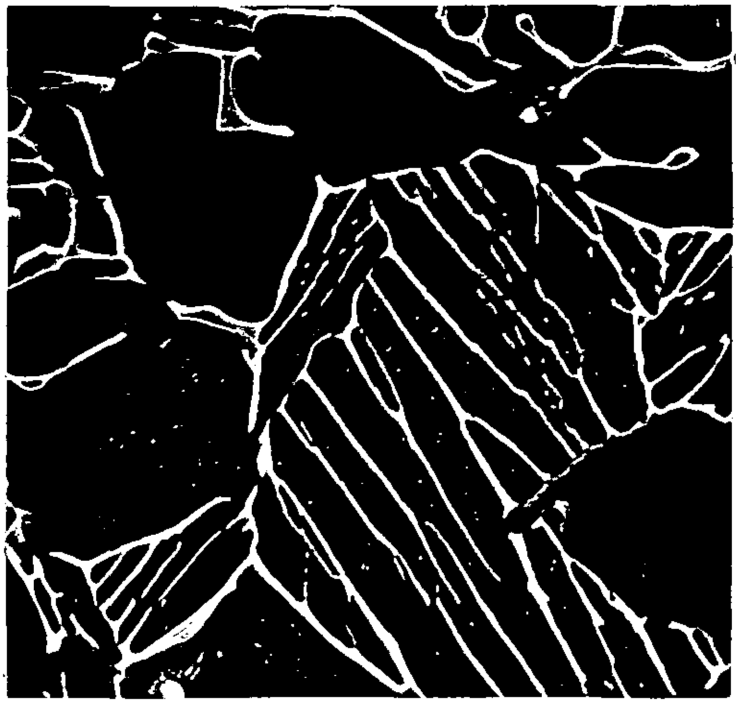

Figure 25(b). SEM micrograph of (Ti-6Al-4V) x 2400. Etched in 10% HNO_3 + 2%HF + 88% H_2O.

Figure 26

Compact tension test piece

(All dimensions in mm)

I = current I/O

A = P.d probes

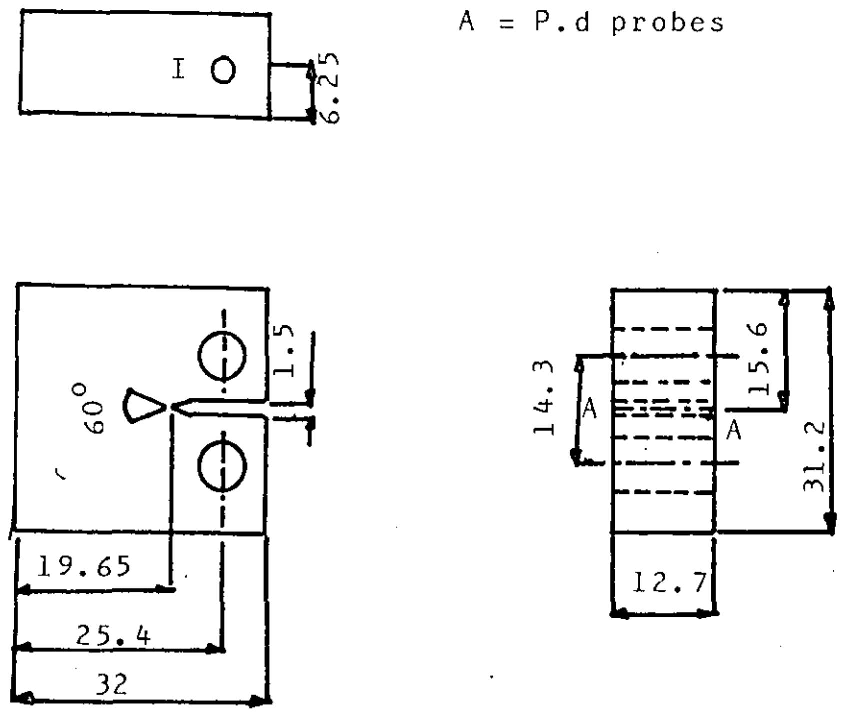

4.5 Crack Measurement

The crack lengths were determined using the d.c. potential drop method. The potential drop technique is a widely accepted method of monitoring crack initiation and growth in controlled laboratory tests. In its simplest form it involves passing a constant current through the test piece and measuring the electrical potential across the crack plane. As the crack propagates the resistance and hence the measured potential drop increases due to reductions in the uncracked cross section area of the test piece.

The potential drop technique has many advantages over optical measurements of crack length. It provides an average measurement, inclusion of crack front curvature, and because it does not require visual accessibility, test may be conducted in any sealed environment. Furthermore the output is the form of a d.c. signal which is continuous and which permits automated data collection and processing.

4.6 Current Supply

A constant current of 10 amps was supplied by a FARNELL (Model No. H30/100). The constant d.c. current was supplied to the top and bottom ends of the specimen. The leads from the power supply terminate in copper lugs which are fitted over the threaded studs on the ends of the specimen and screwed on by washers and nuts. To ensure that the current does not flow through the test machine the top loading bar of machine was insulated electrically from the rest of the test frame by the use of a "TUFNOL" disc pad and TUFNOL sleeves in the bolt holes.

4.7 Potential Drop Measurements

The potential drop across the uncracked ligament of the specimen was measured by spot-welding two fine chromel (20% Ni/80% Cr) wires to the end face of the specimen on both sides of the machined notch. As the electrical resistance of the specimen is very low the potential drop is correspondingly low (of the order of millivolts) and has therefore to be amplified before it can be easily recorded or fed into the computer. A gain valve of approximately 1000 was used, the actual gain setting was so selected that the initial d.c. signal was just over 8 volts. The actual gain ofthe signal was unimportant as the crack calibration curve was based on the relative voltage drop V/VO, where VO is the initial voltage drop.

The amplifier used is a high gain (up to x 10,000) high stability d.c. strain gauge amplifier supplied by E.S.H. Ltd. as part of the test machine.

During the pre-cracking tests. the computer program was so written that crack length measurements were taken only when the specimen was at peak tensile load to ensure that the measurements were taken when the crack faces were open and therefore not in intermittent electrical contact with each other.

4.8 Crack-Calibration Curve

The calibration curve for measuring crack length was provided by Rolls Royce Ltd. Table 4.3 shows some of the calibration results extracted from the calibration curve. The voltage drops and crack lengths were normalised to V/VO = 1.000 at a/w = 0.244.

Table 4.3 $x = (V/V_0 \times 10) - 10$

V/VO	= x-axis	a/w = y-axis
1.000	0.000	0.244
1.095	0.95	0.300
1.195	1.95	0.350
1.265	2.65	0.400
1.395	3.95	0.450
1.460	4.60	0.500
1.60	6.80	0.550
1.685	6.85	0.600
1.805	8.05	0.650
1.965	9.650	0.700
2.105	11.050	0.750
2.280	12.80	0.800
2.600	16.00	0.850

A polynominal curve fitting exercise was performed on the above data to smooth the data or to allow interpolation. A polynominal equation of the form

$$y = a + bx + cx^2 + dx^3 + ex^4$$

where a, b, c, d and e are the coefficients of the polynominal. The data were fitted to a polynominal of the fourth order with the aid of a computer and following coefficients were obtained.

$e = 0.244050314$

$d = 0.0598413969$

$c = -1.11301128 \times 10^{-3}$

$b = 7.6149487 \times 10^{-6}$

$a = -1.2678003 \times 10^{-6}$

Since y = a/w and x = V/VO the equation giving normalised crack length in terms of normalised voltage drop is:-

$$a/w = 0.24405 + 0.05894\ (V/VO) - 1.113 \times 10^{-3}\ (V/VO)^2 + 7.615 \times 10^{-6}\ (V/VO)^3 - 1.2678 \times 10^{-6}\ (V/VO)^4$$

a = crack length

w = width

v = voltage drop

VO = initial voltage drop

The equation (together with the calibration data) is plotted out in Figure 27.

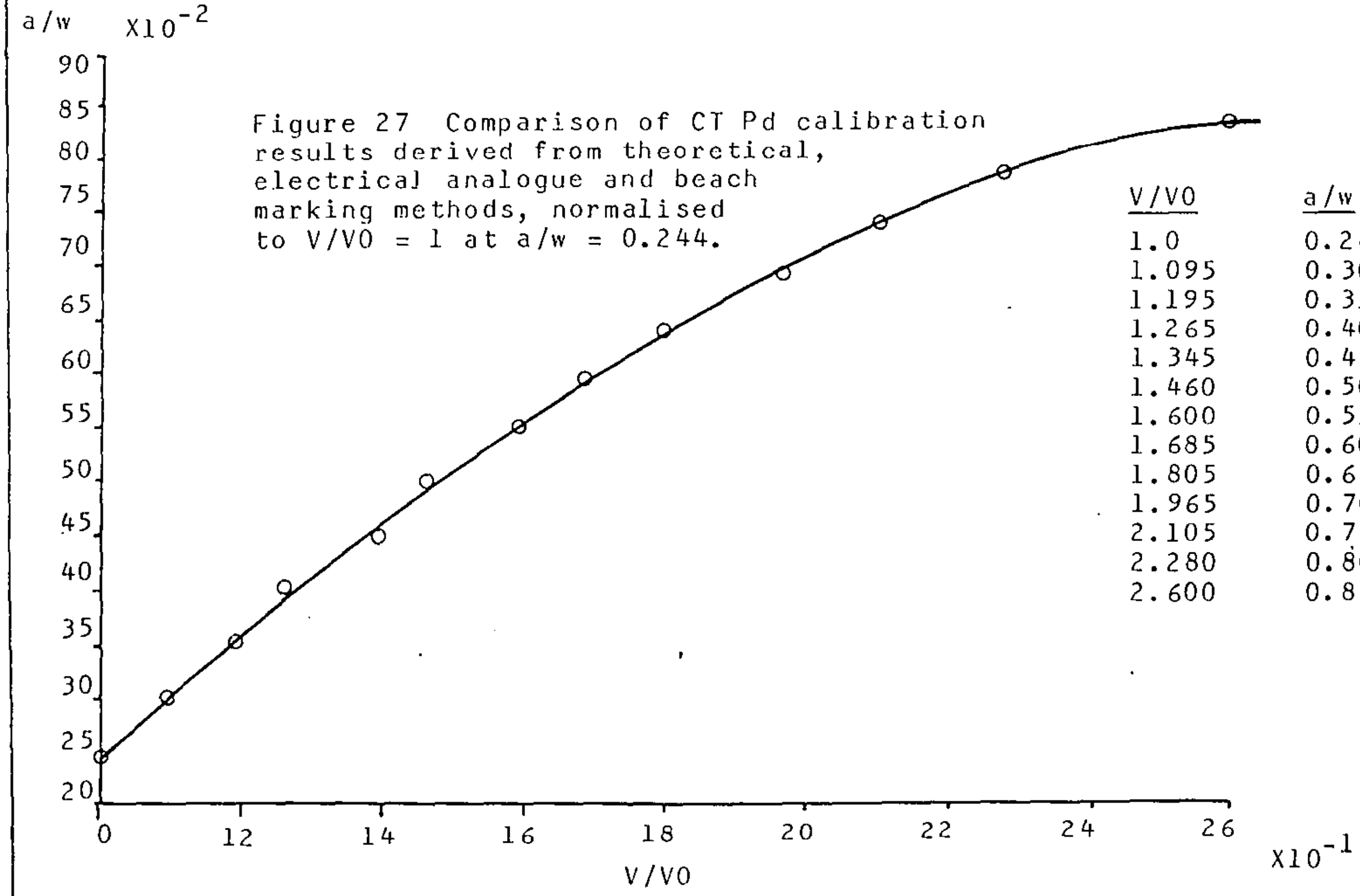

Figure 27 Comparison of CT Pd calibration results derived from theoretical, electrical analogue and beach marking methods, normalised to V/VO = 1 at a/w = 0.244.

V/VO	a/w
1.0	0.244
1.095	0.300
1.195	0.350
1.265	0.400
1.345	0.450
1.460	0.500
1.600	0.550
1.685	0.600
1.805	0.650
1.965	0.700
2.105	0.75
2.280	0.80
2.600	0.85

4.9 Test Procedure

In a closed-loop servo-controlled machine the specimen is loaded or strained according to the instantaneous magnitude of the analog command (or input) signal. The machine is equipped with analog ramp, sine wave, triangle wave and square wave signal sources. The frequency and amplitude of these waveforms are selected by manual setting of the potentiometers on the front of the instrument panels prior to the test. Once set the machine will maintain cycling at the constant frequency and amplitude. In fatigue precracking, however, it is necessary to vary the load amplitude (and therefore the stress intensity amplitude) in such a way that the stress intensity amplitude is rather high at the commencement of cycling (to encourage the early initiation of a crack) and progressively reduced as the crack propagates so that the maximum stress intensity when the crack has grown to the desired length is a little less than that attained during subsequent crack propagation testing. As it is not possible to make the machine alter the amplitude of signal produced by the signal sources mentioned above automatically as the crack grows, it is necessary to interface an APPLE II computer to it to perform the two functions necessary to do this:

(i) The computer must produce the analog signal of the appropriate frequency and amplitude (i.e. it must act as an analog signal source);

(ii) It must compare instantaneous crack length against preset crack lengths and decide whether or not to reduce load amplitude.

The lines of communication between the computer systems and typical closed-loop test are shown in Figure 28.

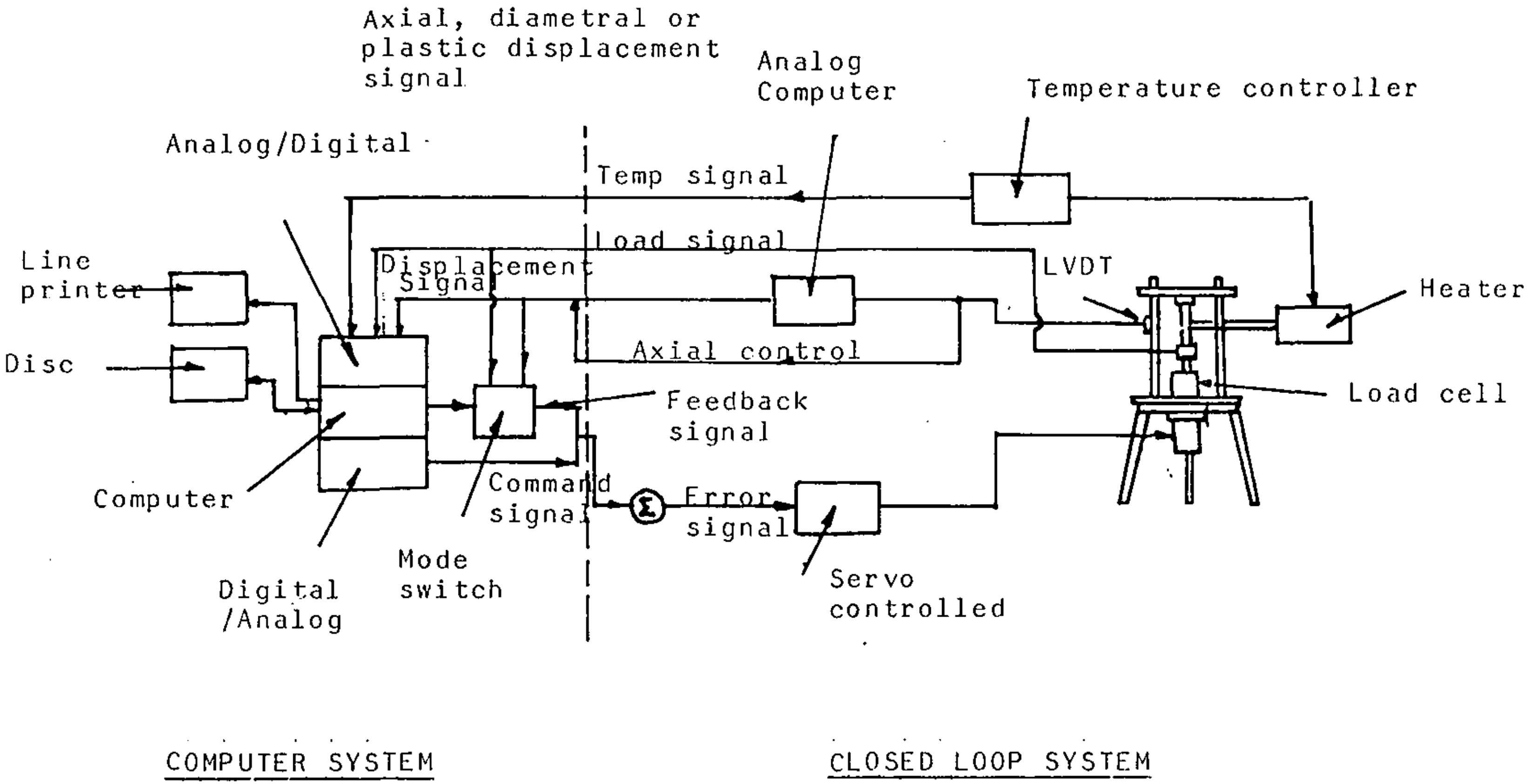

Figure 28. Block diagram of closed loop test system and computer system.

4.9.1 Precracking of the Specimens

A computer-controlled closed-loop servo-hydraulic fatigue precracking was carried out on compact tension specimens. These were performed at room temperature in air and at a frequency of 8Hz under sinusoidal push-pull cycling. Figures 29 to 31 show the experimental set up, i.e. testing system, control panel ofthe testing machine, grips and constant current supply.

The crack measurements were taken automatically after every 100 cycles at peak loads, when crack faces were open (i.e. not in electrical contact). The readings were taken and stored by computer on a file with a given name. These readings were in the form of a series of numbers and were converted to crack length measurements after the test with aid of computer program (see Results Section).

As the precracking progressed crack lengths were also taken with a travelling microscope. These readings will be compared to readings taken by the p-d method. The software developed consisted of four main types of routines:-

(i) determination of the test parameters necessary to conduct an experiment;

(ii) control of the command signal to the test system;

(iii) acquisition of necessary measurements (data);

(iv) analysis of data.

Figure 32 shows a block diagram of the various routines.

Figure 29(a). 300 KN - ESH Universal Servo-Hydraulic Testing Machine

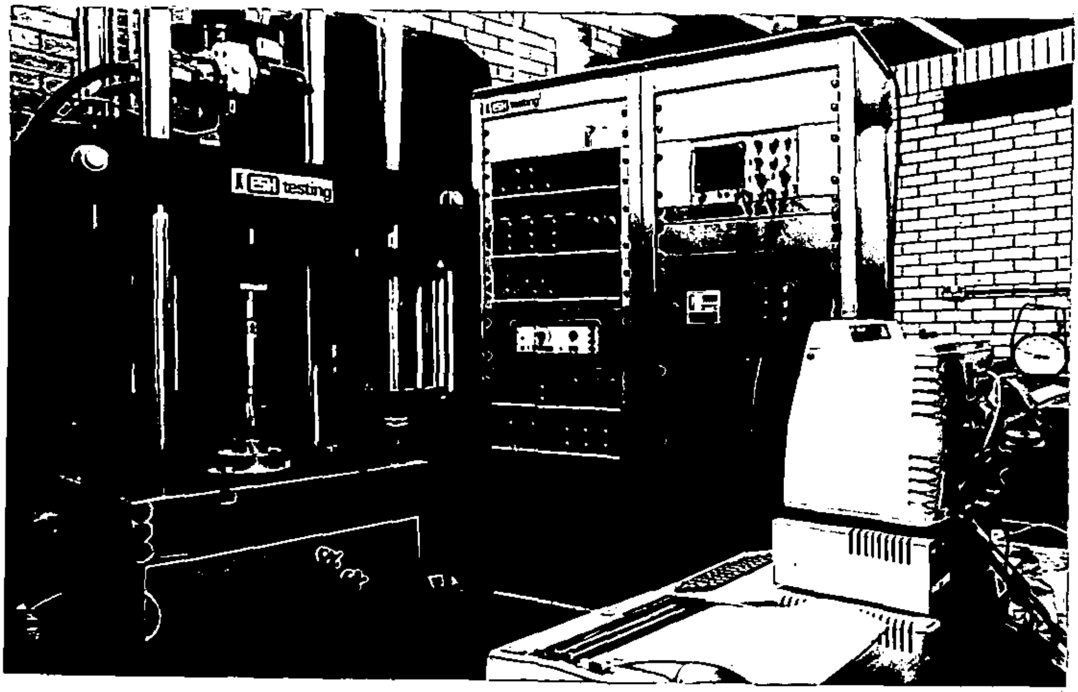

Figure 29(b). Control Panel of ESH Servo-Hydraulic Testing Machine

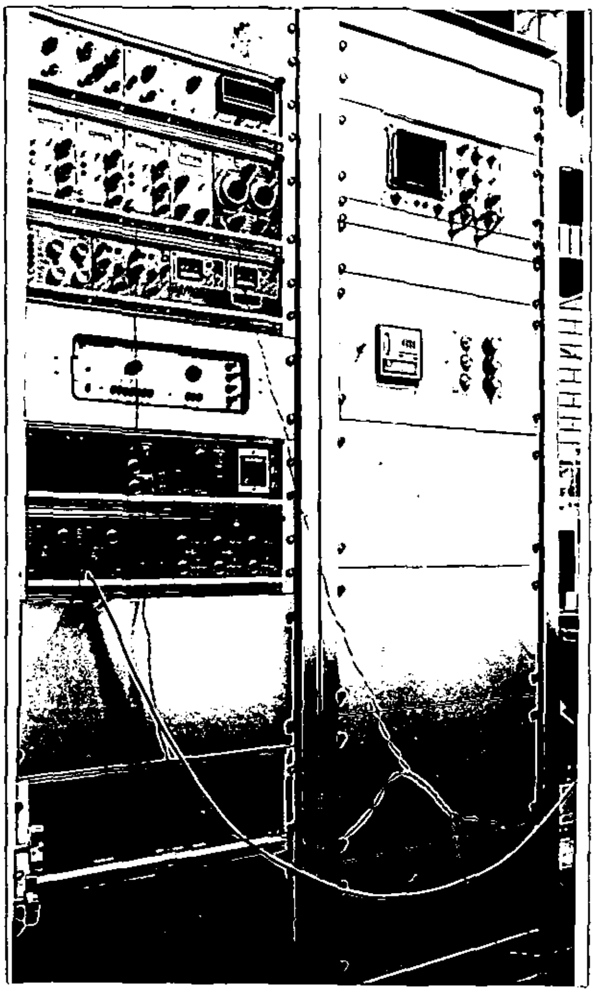

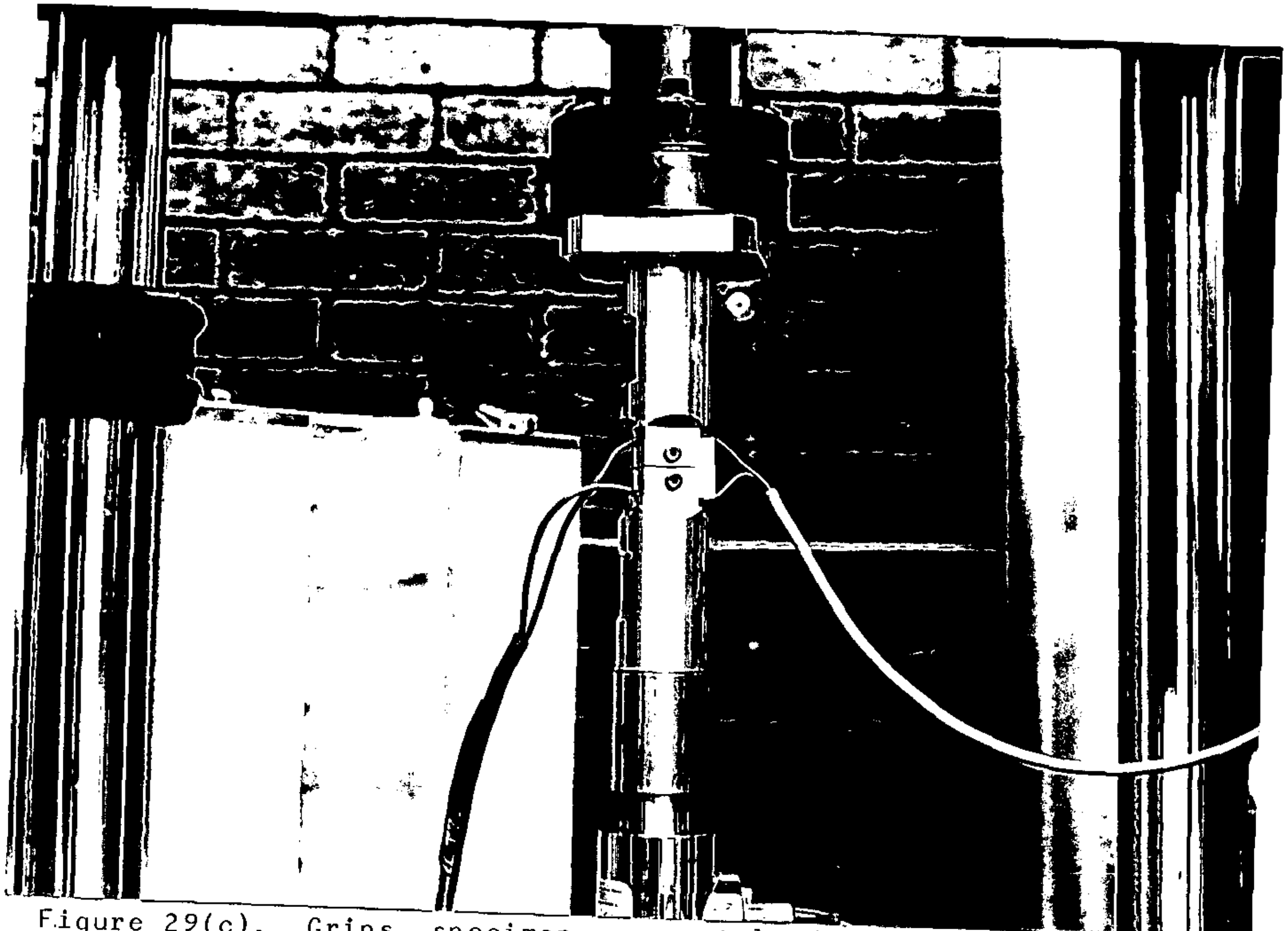

Figure 29(c). Grips, specimen, current leads, potential leads and load cell at the bottom.

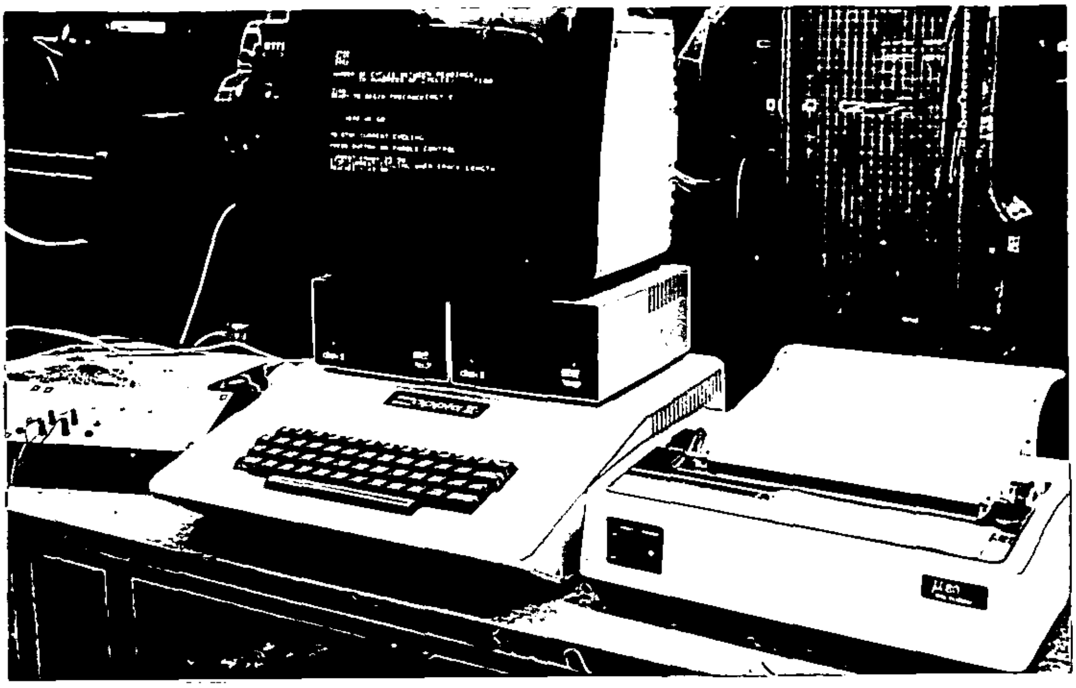

Figure 30. Apple II micro-computer

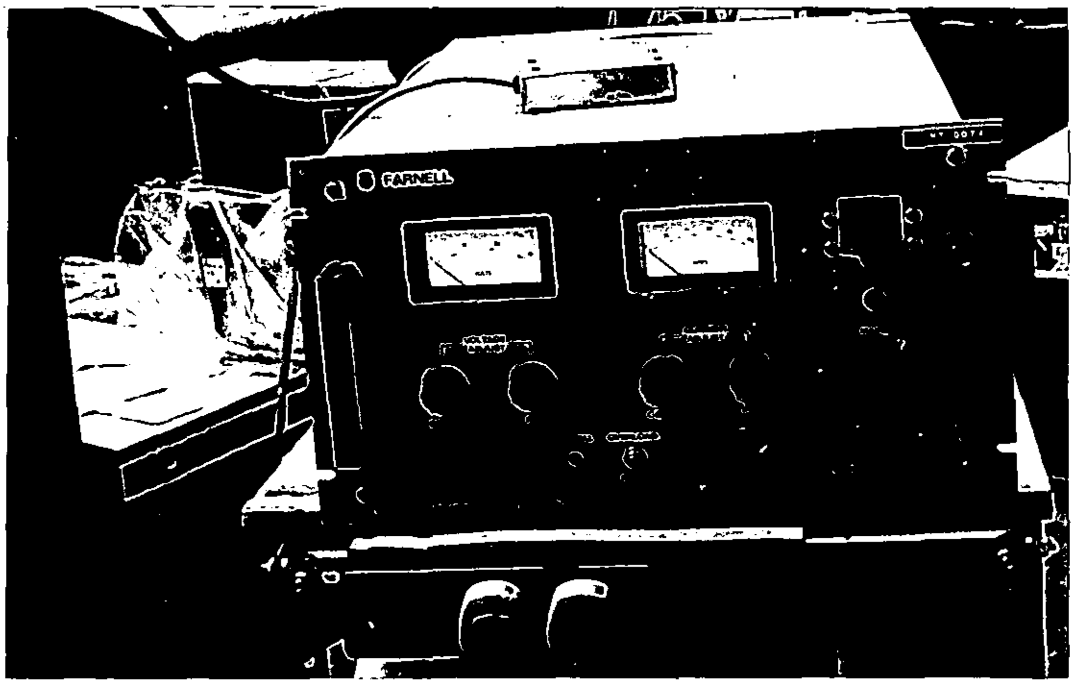

Figure 31. FARNELL Stabilised Power Supply (H30/100)

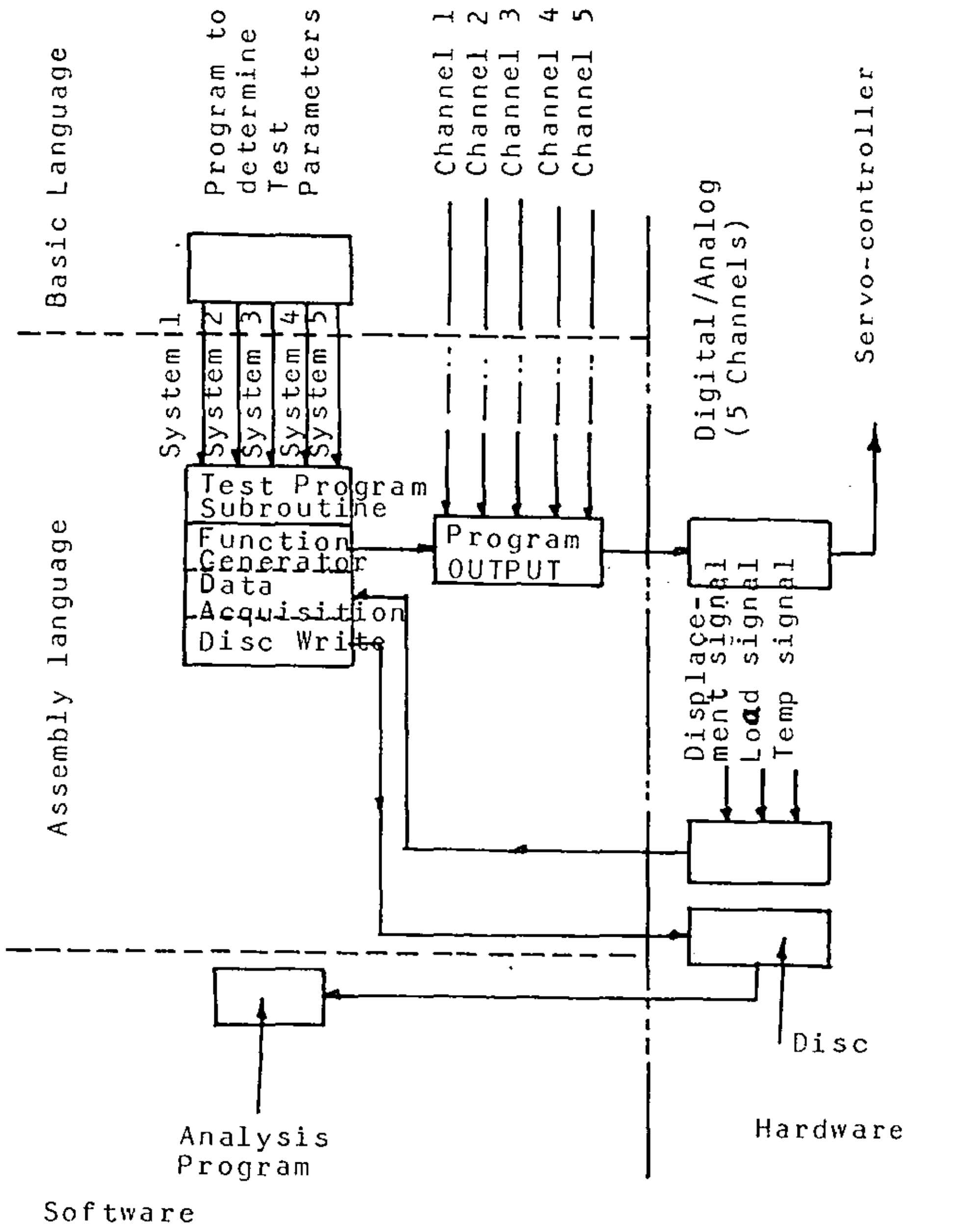

Figure 32 Block diagram of various routines and hardware links

CHAPTER 5

MICROCOMPUTER SOFTWARE

5.1 Software Languages

The 64K APPLE II microcomputer is supplied equipped with two high-level programming languages, Apple soft BASIC and Integer BASIC as well as the low-level 6502 Assembly Code language. The assembly-code language is fast and is in many ways suitable for machine control. However, much more effort is required to write the Program in assembly code than in a high-level language. Besides, it was considered unnecessary to have the very fast computing possible with Assembly Code for this application. For this reason only BASIC was used in the programs developed.

Both versions of BASIC were used to write the machine control programs described in Section 5.2. Integer BASIC runs much faster than Apple soft BASIC as it executes only integer numbers. Apple soft BASIC is, however, necessary to perform the calculations required during the setting up of the test since floating points mathematics are required at this stage. The solution adopted therefore was to write two programs, one for setting up the test parameters (written in Apple soft BASIC) and the other for running the test (in Integer BASIC). The relevant test parameters are passed from the first to the second program either through the computer memory or through disc memory.

To achieve fast execution of the second program, the BASIC program is written in such a way as to optimise the speed of execution. For that reason the program is not easily understood by another reader.

5.2 Computer-Programs to Control Specimen Precracking

The programs were written to control the precracking of the compact tension specimen to produce fatigue cracks of approximately 1.60 mm at room temperature. The program developed permits control of the stress intensity throughout the test. The value of stress intensity is decreased from 25.5 $MNm^{-3/2}$ to 15 $MNm^{-3/2}$ in steps of -1.5 as the crack length increases. Table 5.1 shows the load ranges needed for achieving the required stress intensity ranges during precracking.

TABLE 5.1

MAXIMUM STRESS INTENSITY ($MNm^{-3/2}$)	MAXIMUM LOAD (KN)	MINIMUM LOAD (KN)	MEAN LOAD (KN)
25.5	9.55	0.95	5.25
24.0	8.21	0.82	4.51
22.5	7.68	0.77	4.22
21.0	7.15	0.72	3.93
19.5	6.63	0.66	3.65
18.0	6.11	0.61	3.36
16.5	5.6	0.56	3.08
15.0	5.08	0.51	2.79

5.2.1 Flow Chart for Test Set-Up Program (in Applesoft BASIC)

The software development will be discussed in relation to the numbered boxes as shown in Figure 33 with cross reference to the corresponding segment of the program where appropriate. The listing of the program is given in Figure 36.

Box No. 1 INPUT DATA

This consists of the manual keying of the following data:

(i) The maximum stress intensity to be used;
(ii) thickness of the specimen;
(iii) width of the specimen;
(iv) R-Ratio (i.e. ratio of minimum to maximum stress intensities);
(v) load range setting on the machine (KN);
(vi) crack measurement voltage off-set;
(vii) name of the data file on which data will be stored.

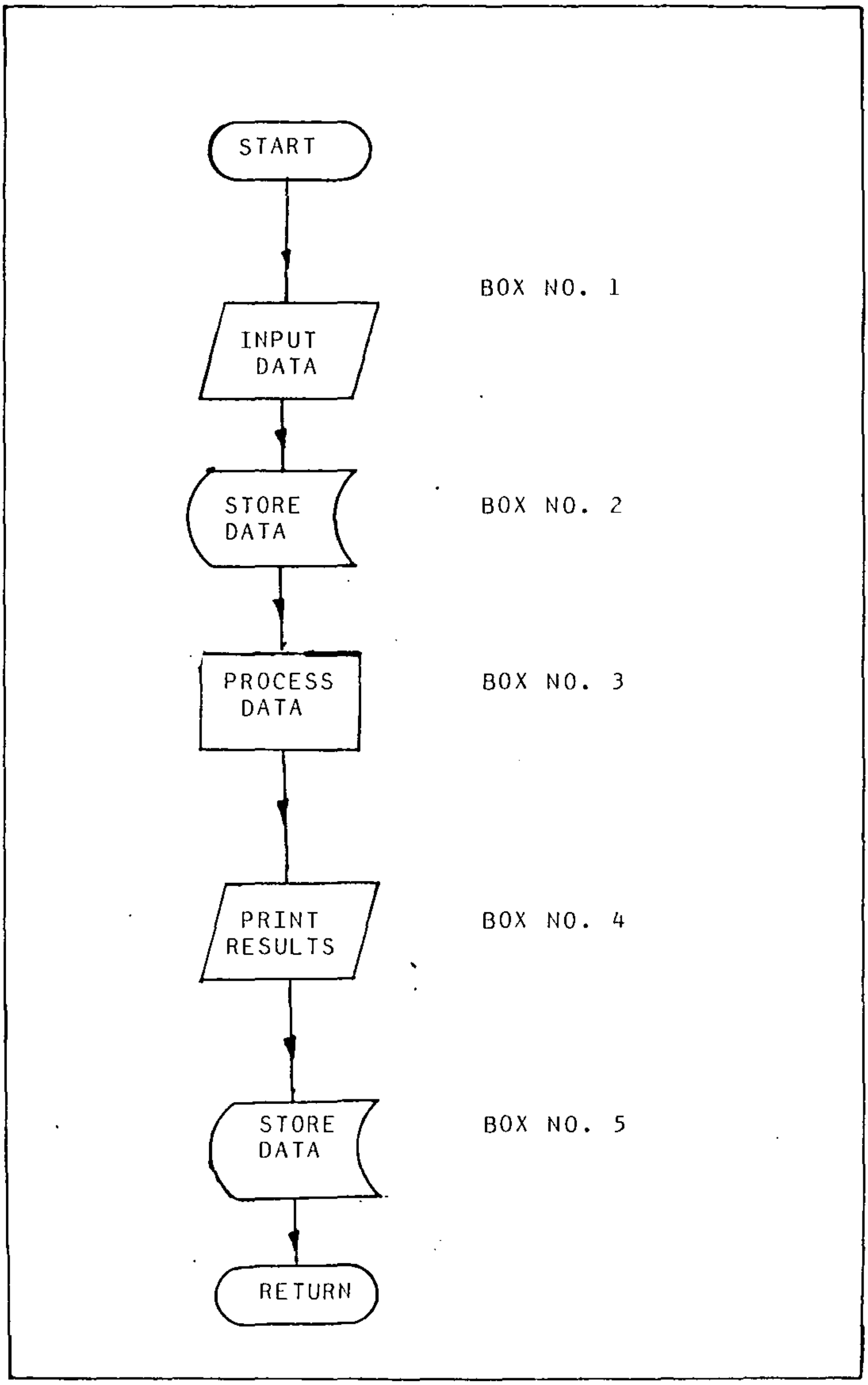

Figure 33. Flow Chart for Test Set-Up Program

Line numbers 70-190 in the program contain the data input instructions.

Box No. 2 STORE DATA

The POKE instruction in lines 260-290 store the relevant control parameters in memory locations within the computer for subsequent use by the second program.

Box No. 3 PROCESS DATA

From the stress intensity, maximum load; minimum load and mean load can be calculated. The load used for different given stress intensity can be calculated from the following equation:-

$$K_I = P/BW^{\frac{1}{2}}\left[29.6(a/w)^{\frac{1}{2}} - 185.5(a/w)^{3/2} + 655.7(a/w)^{5/2} - 1017(a/w)^{7/2} + 638.9(a/w)^{9/2}\right]$$

where:

K_I = Maximum stress intensity ($MNm^{-3/2}$)
P = Load (MN)
B = Thickness (m)
W = Width (m)
a = Machined notch length (m)

$$\therefore \text{ Maximum load} = \frac{(P \times 100 + 0.5)}{100} \quad (MN)$$

$$\text{Minimum load} = \frac{(P/R \times 100 + 0.5)}{100} \quad (MN)$$

where R = 10.0

$$\text{Mean Load} = \frac{(P \times 0.55 \times 100 + 0.5)}{100} \quad (MN)$$

Line numbers 300-360 in the program contain the instruction to process the data entered in the earlier parts of the program. Table 5.1 shows the calculated values of maximum load, minimum load and mean load.

After the load ranges had been calculated the numbers (within the range 0-255) necessary to produce the appropriate sine wave are generated and stored in memory locations within the computer by lines 520-560.

Box No. 4   PRINT RESULTS

The maximum load; minimum load and mean load required to be set on the testing machine is printed out on the TV screen with different values of stress intensities, i.e. from 25.5 $MNm^{-3/2}$ to 15 $MNm^{-3/2}$ in steps of -1.5.

Box No. 5   STORE DATA

Some data is stored on disc using the nominated file number. The file contains the maximum load, R-ratio, and off-set voltage. This information is stored on disc as permanent information and will be added to by the second program with data on crack growth during precracking.

5.2.2 Flow Chart for Precracking Program (in Integer BASIC)

The flow chart shown in Figure 34 is for the controlling program (i.e. run program), which carries out the testing. This program is written in Integer BASIC. It generates the load functions for the fatigue test. It is interactive with the operator before, during and after the test.

The crack length is converted to certain numbers and when that number is reached, the stress amplitude decreases automatically as shown in Table 5.2.

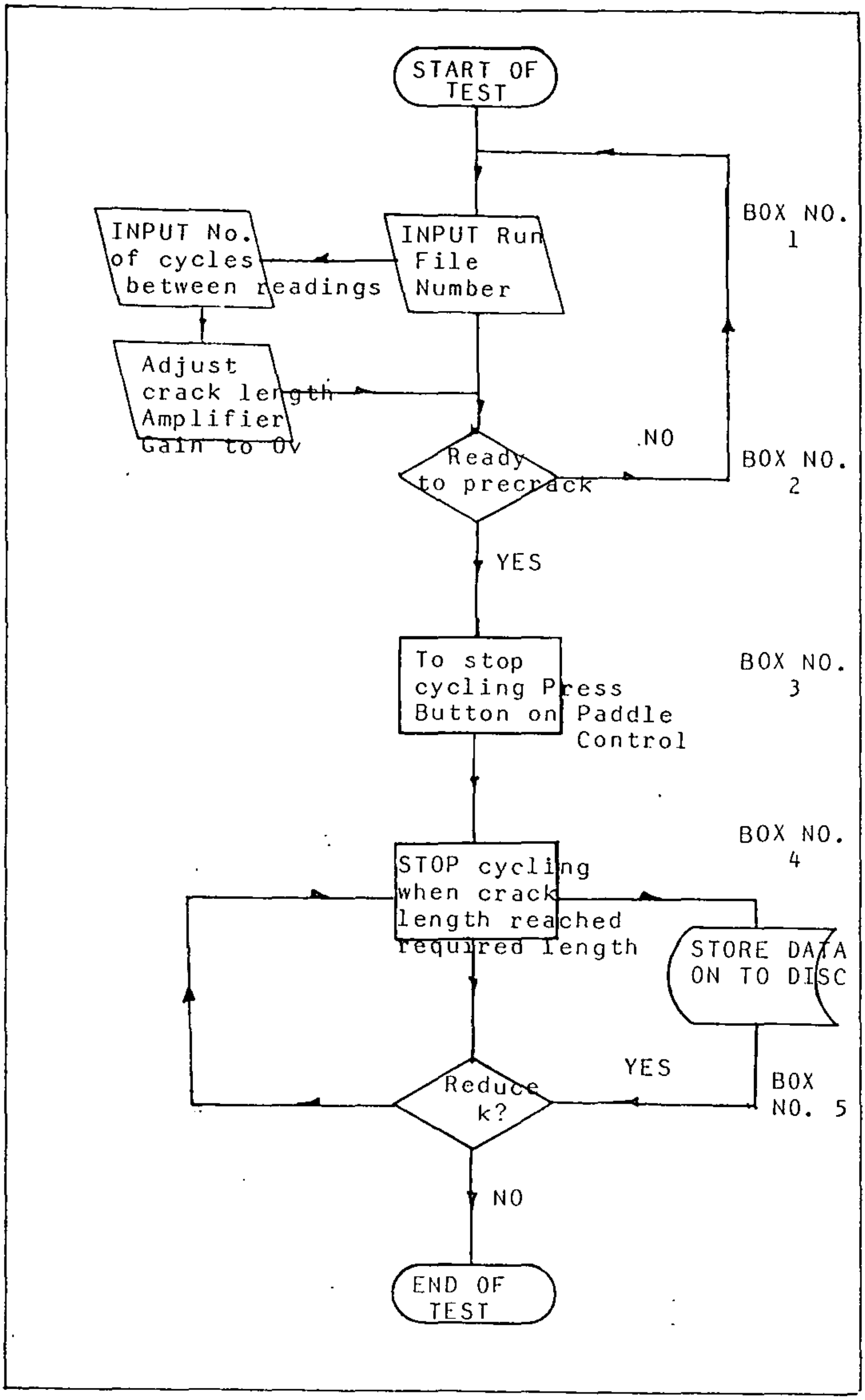

Figure 34. Flow Chart of Precracking Program

TABLE 5.2

MAXIMUM STRESS INTENSITY ($MNm^{-3/2}$)	DIGITAL NUMBERS	REQUIRED CRACK LENGTH (mm)
25.5	3168	1.43
24.0	3220	1.45
22.5	3272	1.47
21.0	3317	1.49
19.5	3359	1.51
18.0	3398	1.53
16.5	3437	1.57
15.0	3552	1.60

The crack length readings were taken automatically and optically after every 100 cycles and the automatical readings were stored on the disc using the nominated file number.

The software developed is discussed in relation to the numbered boxes as shown in Figure 34 with cross reference to the corresponding segment of the program where appropriate. The listing of the program is given in Figure 37.

Box No. 1 INPUT INSTRUCTIONS

This consists of the manual keying in of the following:-

(i) Name of run file number. This will be from the first program. The file will contain maximum load, R-ratio, and offset voltage;

(ii) number of cycles between crack length readings. In this case crack length readings were taken after every 100 cycles;

(iii) the crack length amplifier gain was adjusted to 0 volts.

Line numbers 500-555 in the program contain the input instructions.

Box. No. 3   STOP THE TEST

The test was stopped after 100 cycles, using the push button on the games paddle control, to check the fatigue crack length optically with a travelling microscope.

Box. No. 4 - No. 5   TESTING PROCEDURE

The cycling was stopped automatically when the crack length reached the required length (See Table 5.2). The data was stored on the disc under a given file. The stress intensity amplitude was decreased automatically and the cycling was re-started. This was repeated with different stress intensity amplitudes. The test was stopped when a final crack length of 1.60 mm was obtained at a stress intensity amplitude of 15 $MNm^{-3/2}$.

Line numbers 100 to 250 in the program contain the testing procedure.

5.3 A Program to Evaluate the Test Results

This program reduces the crack length versus cycle data to da/dN versus Δk by incremental polynominal method. Part of this program was translated from a FORTRAN program as used by Dowling and Walker.[73]

This method for computing da/dN involves fitting a second order polynominal (parabola) to sets of (2n + 1) successive data points, where n is usually 1, 2, 3 or 4. The form of the equation for the local fit is as follows:-

$$a_j = b_0 + b_1 \frac{(N_j - C_1)}{C_2} + b_2 \frac{(N_j - C_1)}{C_2} \qquad (1)$$

where $-1 \leqslant \frac{(N_j - C_1)}{C_2} \leqslant +1$

and b_0, b_1 and b_2 are the regression parameters that are determined by the least squares method (that is minimization of the square of the deviations between the observed and fitted values of crack length) over the range $a_j - n \leqslant a_j + n$.

The value a_j is the fitted value of crack length at $N_{\hat{j}}$. The parameters

$$C_1 = \tfrac{1}{2}(N_{j-n} + N_{j+n}) \quad \text{and}$$

$$C_2 = \tfrac{1}{2}(N_{j-n} - N_{j-n})$$

are used to scale the input data, thus avoiding numerical difficulties in determining the regression parameters. The rate of crack growth at N_j is obtained from the derivative of the above parabole, which is given by the following expression:-

$$\left(\frac{da}{dN}\right)_{a_{\hat{j}}} = \frac{b_1}{C_2} + 2b_2(N_j - C_1)/C_2^{\,2} \qquad (2)$$

The value of Δk associated with this da/dN value is computed using the fitted crack length $a_{\hat{j}}$ corresponding to N_j.

5.3.1 Definition of Input Variables for the Program

ID(I) = Specimen identification, for example specimen number, heat treatment, material, etc.

NPTS = Number of paired (a,N) data points.

Type = Type 1 for compact tension specimen.

Pmin = Minimum load (0.955 KN)

Pmax = Maximum load (9.55 KN)

F = Frequency used (8 Hz)

B = Thickness of specimen (12.7 mm)

W = Width of specimen (25.4 mm)

AW = Machined notch length (6.35 mm)

ENV = Test environment (air)

TEM = Test temperature (room temperature)

1/s = 0.2% yield stress of the specimen (1000 MPa)

A(I) = Crack length a, measured from machine notch

N(I) = Elapsed cycles N.

A (MEAS) and A (REG) are values of notch crack length obtained from measurement and from the regression equation (1) respectively. The goodness fit of equation is given by the multiple correlation coefficient, MCC. (Note that MCC = 1

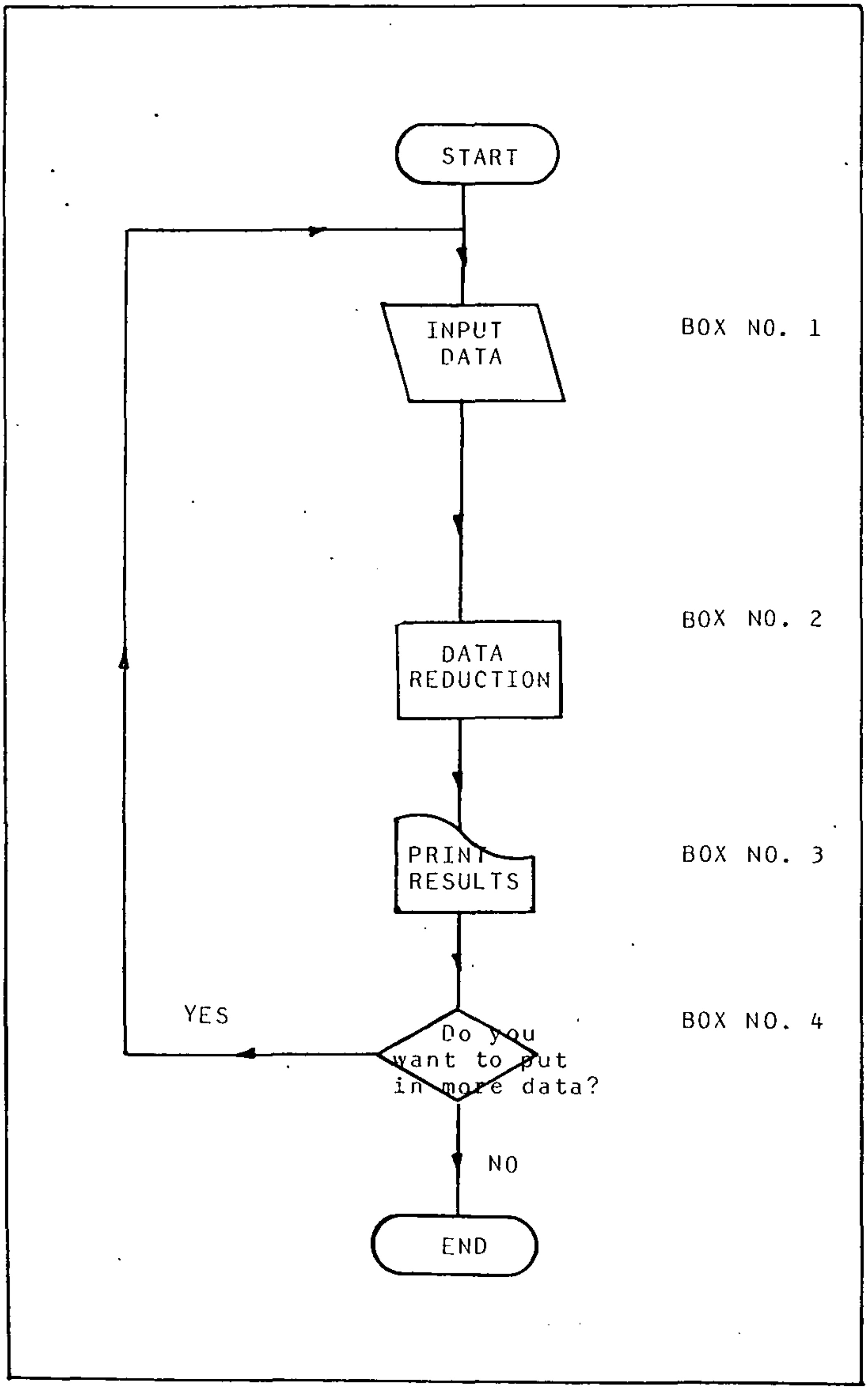

Fig. 35. Flow Chart for a Data Reduction Analysis

represents a perfect fit). Values of Del K (Δk) and DA/DN (da/dN) are given by the same unit $MNm^{-3/2}$ and m/cycles respectively.

The software will be discussed in relation to the numbered boxes as shown in Figure 35, with a cross reference to the corresponding segment of the program where appropriate. The listing of the program is given in Figure 38.

Box No. 1 INPUT DATA

This section consists of: specimen identification, for example specimen number; number of paired (a,N) data points these are stored on the file during the testing and are read automatically when input data; maximum and minimum load applied; specimen geometry, i.e. thickness and width; test frequency used; test temperature; type of specimen; test environment.

Box No. 2 DATA REDUCTION

Fatigue crack growth rates were obtained from the crack length versus cycles data (a V_s N), by the incremental polynominal procedure. In this procedure a second order polynominal is fitted through the first seven data points. The first derivatives of this polynominal is then evaluated at the central data point to obtain a cyclic crack growth rate da/dN. The same operation is then applied to the second through eighth, third through ninth, etc., data points to obtain crack growth rates at various number of cycles during the test.

Values of stress intensity range Δk, suited for correlating with the crack growth rates were obtained from the maximum applied load and measured crack length.

The stress intensity Del k (Δk) is calculated by the following expression:-

$$\Delta k = P/BW^{\frac{1}{2}}\left[29.6(a/w)^{\frac{1}{2}} - 185.5(a/w)^{3/2} + 655.7(a/w)^{5/2} - 1017(a/w)^{7/2} + 638.9(a/w)^{9/2}\right]$$

Where B = Thickness (m)
W = Width (m)
a = crack length (m)

An example of the output from the program is given in the results section. Information on the specimen, loading variables and environment are also listed with the tabulated values of the raw data and processed data. A (Measured) and A (Regression) are values of crack length obtained by measurement and from the regression equation respectively. The goodness of fit of this equation is given by the multiple correlation coefficient, MCC (note that MCC = 1 represents a perfect fit).

Line numbers 450-1040 in the program contain the data reduction instructions.

```
10  REM   ** FATIGUE PRECRACKER **
20  REM        ** 11 JUNE 1982 **
30  POKE  - 15615,0: HOME
40  VTAB 12: HTAB 5: INVERSE : PRINT "AUTOMATIC FATIGUE PREC
RACKER": NORMAL : PRINT : PRINT
50  FOR W = 1 TO 1500: NEXT W: HOME
60  PRINT : PRINT :NUM = 49:PI = 3.14159:ADDR = 7500:J = 0:N
N = 0:AK = 7457
70 N1 = 25.5
80  PRINT "INITIAL MAX STRESS INTENSITY                    (IN
MN-M UNITS)        = ";N1
90  PRINT
100 R = 10
110  PRINT "MAXIMUM/MINIMUM RATIO=";R
120  PRINT
130 B = 12.7
140  PRINT "THICKNESS OF SPECIMEN=";B
150  PRINT
160  PRINT "LOAD RANGE SETTING? (KN) ": INPUT "(CONFIRM SETT
ING NOW!) ";LR
170  PRINT : INPUT "BACK-OFF VOLTAGE?       ";VB
174  PRINT
175  INPUT "FATIGUE RUN FILE NUMBER? ";G$
180 V0 = VB / 1.01011
190  FOR I = 1 TO 9: READ VV(I):V(I) = V0 * VV(I):VL(I) =  I
NT ((V(I) - VB) * 4095): NEXT
200 B = B / 1000:W = 2 * B: PRINT : PRINT
201 D$ =  CHR$ (4)
210  FOR N = N1 TO 15 STEP  - 1.5
220 NN = NN + 1
225 VP = 10 * VV(NN) - 10
230 A = W * (.24405 + .05894 * VP - 1.113E - 3 * VP ÷ 2 + 7.
615E - 6 * VP ÷ 3 - 1.2678E - 6 * VP ÷ 4)
240 AM = (A - B / 2) * 1000
250  PRINT "MAXIMUM STRESS INTENSITY= ";N
260  POKE (AK + (NN * 4)), INT (N)
270  POKE (AK + (NN * 4) + 1), INT ((N -  INT (N)) * 10)
280  POKE (AK + (NN * 4) + 2), INT (AM)
290  POKE (AK + (NN * 4) + 3), INT ((AM -  INT (AM)) * 100)
300 AW = A / W
305  PRINT AW
310 C = 29.6 * AW ÷ 0.5 - 185.5 * AW ÷ 1.5 + 655.7 * AW ÷ 2.
5 - 1017 * AW ÷ 3.5 + 638.9 * AW ÷ 4.5
320 P = N * B * W ÷ .5 / C * 1000
330  IF P ) LR THEN  FLASH : PRINT : PRINT : PRINT "LOAD RAN
GE EXCEEDED": PRINT "RE-RUN TEST AND SELECT": PRINT "LOWER I
NITIAL STRESS INTENSITY ": PRINT "OR HIGHER LOAD RANGE": NOR
MAL : END
340 P2 =  INT (P * 100 + .5) / 100
350 P1 =  INT (P / R * 100 + .5) / 100
360 PM =  INT (P * .55 * 100 + .5) / 100
370  PRINT "MAXIMUM LOAD= ";P2;" KN"
380  PRINT "MINIMUM LOAD=  ";P1;" KN"
390 AP =  INT ((P - P / R) / 2 * 255 / LR)
400 OFFSET =  INT (P / R * 255 / LR)
410  PRINT "MEAN LOAD    = ";PM;" KN"
415  IF N = N1 THEN PL = (2 * AP + OFFSET) / 255 * LR
420  GOSUB 520
430  PRINT : PRINT
435  NEXT N
440  POKE 7500,NN
441  PRINT D$;"OPEN FATIGUE RUN FILE. #";G$
442  PRINT D$;"WRITE FATIGUE RUN FILE. #";G$
443  PRINT PL: PRINT R: PRINT VB: PRINT NN
444  FOR N = 1 TO NN + 1: PRINT VL(N): NEXT
```

Figure 36. Listing of Apple soft BASIC Computer Program for Test Set-Up.

```
500  PRINT : PRINT : PRINT : PRINT  TAB( 10)"LOADING RUN PRO
GRAM"
510  PRINT  CHR$ (4);"RUN AUTO FTPC"
520  FOR I = 0 TO NUM
530 J = J + 1
540 X =  INT (OFFSET + .5 + AP + AP *  SIN (2 * PI * I / NUM
 + PI / 2))
550  POKE (ADDR + J),X: PRINT X;" ";
560  NEXT I
570  RETURN
600  DATA  1.01013
610  DATA  1.1078
620  DATA  1.1094
630  DATA  1.1110
640  DATA  1.1124
650  DATA  1.1137
660  DATA  1.1149
670  DATA  1.1161
690  DATA  1.11965
```

Figure 36 continued

```
  100 E=E+O: IF PEEK (U))W THEN GOTO M: FOR I=A TO N: POKE S
, PEEK (I): NEXT I: IF E MOD X#Q THEN GOTO X: POKE Z,Y:J= PE
EK (Z1)*Z2+ PEEK (Z): IF J)C THEN GOTO D: IF E/X MOD K#Q THE
N GOTO X
  102 B=B+O:V(B)=J:E=0: PRINT J: GOTO X
  105 T=T+1: PRINT J,C:C=VL(T): IF T=3 THEN GOTO 210: GOTO 2
19
  110 INPUT "CONTINUE CYCLING AT CURRENT LEVEL? ",C$
  122 IF C$="N" THEN 130
  125 IF C$="Y" THEN 100
  127 GOTO 110
  130 IF L= PEEK (7500) THEN GOTO 225
  135 PRINT
  140 INPUT "REDUCE DELTA K AND CONTINUE CYCLING? ",C$
  170 IF C$="N" THEN 250
  180 IF C$="Y" THEN 219
  190 GOTO 140
  210 INPUT "LOAD DATA ON DISC? ",C$: IF C$="N" THEN GOTO 21
9
  211 PRINT "";"OPEN FATIGUE DATA FILE. #";F$
  212 PRINT "";"WRITE  FATIGUE DATA FILE. #";F$
  213 PRINT P$,R$,V$,K,B
  215 FOR H=1 TO B: PRINT V(H): NEXT H
  216 PRINT "";"CLOSE"
  218 PRINT "";"PR#1": FOR H=1 TO B: PRINT V(H);" ";:V(H)=0:
 NEXT H: PRINT : PRINT : PRINT "";"PR#0"
  219 A=A+50:N=N+50:G=G+1:E=0
  220 NEXT L
  225 PRINT "END OF TEST": FOR H=1 TO 100: POKE -15614,255:
NEXT H: POKE -15614,0
  226 POKE -15615,0
  230 END
  250 PRINT "TEST STOPPED...."
  255 GOTO 226
  500 CALL -936
  505 I=0:A=7501:N=7550:S=-15615:E=0:K=10:W=127:X=100:O=1:Q=
0:U=-16287:Z=-16256+16*5:Y=34:B=0:D=105:Z1=Z+1
  510 J=0:C=0:Z2=256:AK=7457:M=110
  515 DIM V(500),C$(5),VL(20)
  516 DIM P$(20),R$(20),V$(20),F$(6)
  518 PRINT : PRINT : INPUT "RUN FILE NUMBER ",F$
  520 PRINT "";"OPEN FATIGUE RUN FILE. #";F$
  522 PRINT "";"READ FATIGUE RUN FILE. #";F$
  523 INPUT P$,R$,V$,NN: PRINT P$,R$,V$,NN
  529 FOR H=1 TO NN+1: INPUT VL(H): PRINT VL(H): NEXT H
  530 PRINT "";"CLOSE"
  532 PRINT : INPUT "NUMBER OF CYCLES BETWEEN READINGS
      (IN HUNDREDS OF CYCLES)    ",K
  535 T=2
  536 C=VL(T)
  537 PRINT C
  539 FOR H=1 TO PEEK (7501): POKE S,H: NEXT H: FOR H=1 TO 1
0: NEXT H
  540 POKE Z,Y: POKE Z,Y:V(0)= PEEK (Z1)*Z2+ PEEK (Z)
  550 PRINT "ADJUST CRACK LENGTH AMPLIFIER GAIN TO   REQUIRE
D VOLTAGE NOW!"
  555 PRINT "PRESS SPACEBAR TO PROCEED": PRINT
  560 POKE Z,Y: PRINT PEEK (Z1)*Z2+ PEEK (Z): IF PEEK (-1638
4)(=127 THEN GOTO 560
  590 INPUT "READY TO BEGIN PRECRACKING? ",C$
  592 PRINT : PRINT : PRINT "     HERE WE GO......."
  594 PRINT : PRINT : PRINT "TO STOP CURRENT CYCLING, ": PRI
NT : PRINT "PRESS BUTTON ON PADDLE CONTROL"
  596 PRINT
```

Figure 37. Listing of Integer BASIC Computer Program for Precracking of Compact Tension Specimens

```
  696 PRINT "CURRENT KMAX= "; PEEK (AK+(L*4));"."; PEEK (AK+
1+L*4);PRINT
  697 PRINT "STOP CURRENT CYCLING WHEN CRACK LENGTH": PRINT
"REACHES "; PEEK (AK+L*4+6);"."; PEEK (AK+L*4+7);" MM": PRIN
T
  698 RETURN
  700 REM  **AUTOMATIC FATIGUE RUN PROGRAM**
  720 REM           ** 7 JULY 1982**
  730 REM   OUTPUT AO02, CH.1, CH.2
  740 REM  INPUT AI13, CH.2
```

Figure 37 continued

```
5  GOTO 5000
10  HOME
20  DIM N(200),BB(6),DADN(200),DK(200),ID(7),AA(20),NN(20),A
R(200),R2(200)
30 ID$ = F$
35 NR = NPTS
40  PRINT : PRINT : FOR I = 1 TO 1000: NEXT : HOME
50  PRINT  TAB( 5)"PLEASE PUT IN THE FOLLOWING DATA "
60  PRINT
70  INPUT "MAXMIUM LOAD (KN )= ";P1: PRINT
80  INPUT "MINMIUM LOAD (KN )= ";P2: PRINT
85 B = 12.7
100  PRINT "THICKNESS     (MM )= ";B
110  PRINT :W = 25.4
120  PRINT "WIDTH         (MM )= ";W: PRINT
130 AW = 6.35
140  PRINT "NOTCH LEN.    (MM )= ";AW: PRINT
150  INPUT "TEST FREQ.    (HZ )= ";F: PRINT
160  PRINT "TEST ENVIRONMENT  = AIR ";: PRINT
170  PRINT
180  INPUT "TEST TEMP(DEG.C. )= ";TEM: PRINT
190  INPUT "0.2% Y.STRESS(MN )= ";YS: PRINT
200  PRINT "SPECIMEN TYPE.     = COMPACT TYPE ": PRINT
210  PRINT
220 R =  INT ((P2 / P1) * 10000) / 10000
225  PRINT : PRINT : PRINT
230  PRINT  TAB( 6)"PRESS ANY KEY TO CONTINUE ";: GET A$
240  HOME
260  FOR I = 1 TO NPTS
275 A(I) = A(I) / 1000
280 N(I) = N(I - 1) + 100
282 N(1) = 0
285  PRINT N(I),A(I)
290  NEXT I: HOME
310  VTAB 10: PRINT  TAB( 5)"SEVEN POINT INCREMENTAL POLYNOM
IAL ": PRINT : PRINT  TAB( 8)"METHOD FOR DETERMINING DA/DN"
339  PRINT  CHR$ (4);"PR#1": PRINT  CHR$ (31): POKE 36,8: PR
INT "FATIGUE DATA ANALYSIS": POKE 36,8: PRINT "------------
--------": PRINT
340  PRINT : PRINT : PRINT "      SPECIMEN IDENTIFICATION =
";ID$: PRINT : PRINT "      NUMBER OF DATA POINTS    = ";NPTS
345 P1 = P1 / 1000:P2 = P2 / 1000:B = B / 1000:W = W / 1000:
AW = AW / 1000
350  PRINT : PRINT "      MAXIMUM LOAD        (MN ) = ";P1
360  PRINT : PRINT "      MINMIUM LOAD        (MN ) = ";P2
370  PRINT : PRINT "      THICKNESS           ( M ) = ";B
380  PRINT : PRINT "      WIDTH OF SPECIMEN   ( M ) = ";W
390  PRINT : PRINT "      NOTCH LENGTH        ( M ) = ";AW
400  PRINT : PRINT "      TEST ENVIRONMENT          = AIR "
410  PRINT : PRINT "      TEST TEMPERATURE    (C )  = ";TEM
420  PRINT : PRINT "      TEST FREQUENCY      (HZ ) = ";F
430  PRINT : PRINT "      R-RATIO (P1/P2)           = ";R
433  PRINT  CHR$ (4);"PR#0": PRINT : PRINT : PRINT
435  PRINT  TAB( 6)"PRESS ANY KEY TO CONTINUE ";: GET A$: PR
INT
437  HOME
438  PRINT : PRINT "AM"; TAB( 8)"AR"; TAB( 16)"MCC"; TAB( 22
)" DK"; TAB( 28)"DA/DN"
440  FOR I = 1 TO NPTS
455  NEXT I
460 K = 0:PI = 3.1416:P3 = P1 - P2
465  FOR I = 1 TO 3: PRINT : PRINT N(I); TAB( 8)A(I): NEXT I
470 NPTS = NPTS - 6
480  FOR I = 1 TO NPTS
```

Figure 38. Listing of Apple soft BASIC Program for Reducing Crack length versus Cycle Data to da/dN versus Δk by the Seven Point Incremental Polynominal Technique.

```
500  FOR J = K TO K1
510 L = L + 1:AA(L) = A(J)
520 NN(L) = N(J)
530  NEXT J
540 C1 = 0.5 * (NN(1) + NN(7))
550 C2 = 0.5 * (NN(7) - NN(1))
560 S1 = 0:S2 = 0:S3 = 0:S4 = 0:S5 = 0:S6 = 0:S7 = 0
570  FOR J = 1 TO 7
580 X = (NN(J) - C1) / C2
590 YY = AA(J)
600 S1 = S1 + X
610 S2 = S2 + X ^ 2
620 S3 = S3 + X ^ 3
630 S4 = S4 + X ^ 4
640 S5 = S5 + YY
650 S6 = S6 + X * YY
660 S7 = S7 + YY * X ^ 2
670  NEXT J
680 DN = 7.0 * (S2 * S4 - S3 ^ 2) - S1 * (S1 * S4 - S2 * S3)
 + S2 * (S1 * S3 - S2 ^ 2)
690 T2 = S5 * (S2 * S4 - S3 ^ 2) - S6 * (S1 * S4 - S2 * S3)
+ S7 * (S1 * S3 - S2 ^ 2)
700 BB(1) = T2 / DN
710 T3 = 7 * (S6 * S4 - S7 * S3) - S1 * (S5 * S4 - S7 * S2)
+ S2 * (S5 * S3 - S6 * S2)
720 BB(2) = T3 / DN
730 T4 = 7 * (S2 * S7 - S3 * S6) - S1 * (S1 * S7 - S3 * S5)
+ S2 * (S1 * S6 - S2 * S5)
740 BB(3) = T4 / DN
750 YB = S5 / 7
760 RS = 0:TS = 0
770  FOR J = 1 TO 7
780 X = (NN(J) - C1) / C2
790 YH = BB(1) + BB(2) * X + BB(3) * X ^ 2
800 RS = RS + (AA(J) - YH) ^ 2
810 TS = TS + (AA(J) - YB) ^ 2
820  NEXT J
830 R2(I) = 1.0 - RS / TS
840 DADN(I) = BB(2) / C2 + 2 * BB(3) * (NN(4) - C1) / C2 ^ 2
850 X = (NN(4) - C1) / C2
860 AR(I) = BB(1) + BB(2) * X + BB(3) * X ^ 2
865 AR(I) =  INT (AR(I) * 1000000) / 1000000
890 QQ = I + 3
900 T = AR(I) / W
910 DK(I) = P3 / (B * W ^ 0.5) * (29.6 * T ^ 0.5 - 185.5 * T
 ^ 1.5 + 655.7 * T ^ 2.5 - 1017 * T ^ 3.5 + 638.9 * T ^ 4.5)
1005  PRINT
1010  PRINT A(QQ); TAB( 8)AR(I);; TAB( 16) INT (R2(I) * 1000
00) / 100000; TAB( 22) INT (DK(I) * 100) / 100; TAB( 28)DADN
(I)
1020  GOTO 1040
1025  PRINT
1040  NEXT I
1050 J = NPTS + 4:K = NPTS + 6: FOR I = J TO K
1060  FOR I = J TO K: PRINT
1070  PRINT N(I); TAB( 8)A(I): NEXT
1080  PRINT : PRINT : INPUT "DO YOU WANT HARD COPY OF RESULT
S(Y/N)?";B$
1090  IF B$ = "N" THEN  GOTO 1230
1100  PR# 1: PRINT  CHR$ (29)
1110  PRINT : PRINT : PRINT
1120  POKE 36,20: PRINT "N(I)";: POKE 36,43: PRINT "A(I)";:
POKE 36,67: PRINT "A(R)";: POKE 36,80: PRINT "MCC";: POKE 36
,98: PRINT "DK(I)";: POKE 36,117: PRINT "DA/DN(I)"
1125  PRINT
```

Figure 38 continued

```
)
1145  NEXT I
1150  IF NR =  ( 7 THEN 1190
1160  FOR I = 4 TO (J - 1): PRINT
1170  POKE 36,20: PRINT N(I);: POKE 36,38: PRINT A(I);: POKE
 36,63: PRINT AR(I - 3);: POKE 36,80: PRINT  INT (R2(I - 3)
* 100000) / 100000;: POKE 36,98: PRINT  INT (DK(I - 3) * 100
0) / 1000;: POKE 36,116: PRINT DADN(I - 3)
1180  NEXT
1190  FOR I = J TO K
1200  PRINT : POKE 36,20: PRINT N(I);: POKE 36,38: PRINT A(I
)
1210  NEXT
1220  PR# 0
1225  PRINT : PRINT : PRINT
1230  INPUT "DO YOU WANT TO PUT MORE DATA IN(Y/N)";A$
1240  IF A$ = "N" THEN  GOTO 2000
1250  IF A$ = "Y" THEN  GOTO 10
2000  END
5000  HOME
5010  DIM C(200),V(200),A(200)
5020 V0 = 8
5030 D$ =  CHR$ (4)
5040  INPUT "FILE NUMBER? ";F$
5045  PRINT
5050  INPUT "HOW MANY DATA POINTS? ";NPTS
5060  PRINT D$;"READ FATIGUE DATA FILE. #";F$
5070  FOR I = 1 TO NPTS
5080  INPUT C(I)
5090 V(I) = (8 + C(I) / 4095) / V0
5100 VP = 10 * V(I) - 10
5110 A(I) = 25.4 * (.24405 + .05894 * VP - 1.113E - 3 * VP ^
 2 + 7.615E - 6 * VP ^ 3 - 1.267E - 6 * VP ^ 4)
5115  PRINT
5120  PRINT V(I),A(I)
5130  NEXT I
5140  PRINT D$;"CLOSE FATIGUE DATA FILE. #";F$
5150  GOTO 10
```

Figure 38 continued

CHAPTER 6.0

RESULTS

6.1 Calibration of Load Cell (25 KN)

A 25 KN load cell was used during pre-cracking. The load cell was calibrated before use, and Table 6.1 shows the results for different load ranges. Figure 39 shows the calibration graph of LOAD against volts (mv). For this work a load of 10 KN range was used. It can be seen from the graph that the calibration of the load cell is reasonably accurate for this work.

Table 6.1

LOAD (KN)	LOAD (Kg)	VOLTS (mv) 2.5KN Range	VOLTS (mv) 5.0KN Range	VOLTS (mv) 10KN Range
0	0	0.00	0.00	0.00
0.0981	10	0.39	0.19	0.09
0.1962	20	0.79	0.39	0.19
0.2943	30	1.19	0.58	0.29
0.3924	40	1.58	0.78	0.39
0.4905	50	1.985	0.97	0.49
0.5886	60	2.390	1.17	0.59
0.6867	70	2.790	1.365	0.69
0.7848	80	3.20	1.565	0.78
0.8829	90	3.59	1.76	0.875

6.2 Crack Measurements

The crack length was measured after every 100 cycles. The readings were taken automatically by the computer and they were also measured optically using a travelling microscope.

The readings which were taken automatically by the computer, were a set of numbers which were then converted into crack lengths by the following expression:

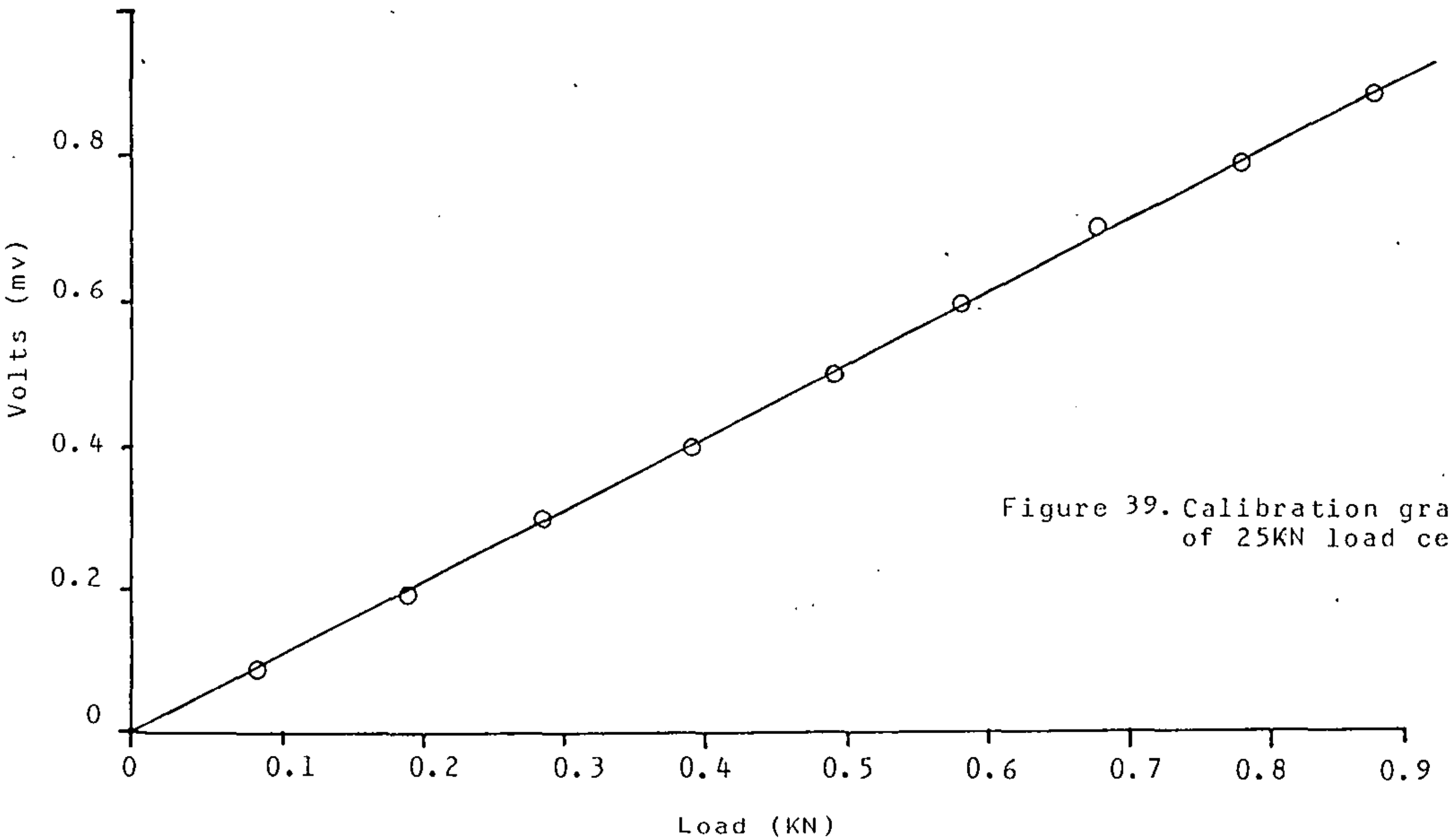

Figure 39. Calibration graph of 25KN load cell.

$$V = \frac{V_0 + C(I)/4095}{V_0}$$

where V_0 = Back off voltage (8 volts)

$C(I)$ = digital readings from computer

The value of V is then substituted in the following expression to determine the crack length:

$$A/W = 0.24405 + 0.05894 \times V - 1.13 \times 10^{-3} \times V^2 + 7.613 \times 10^{-6} \times V^3 - 1.267 \times 10^{-6} \times V^4$$

A = crack length

W = width of specimen (25.4 mm)

The above expression is a polynominal equation which is attained by a numerical curve fit of calibration graph of a/w against V/V_0 as shown in Figure 27. The crack length is measured from the tip of the machined notch of the specimen. Therefore the crack length (A) is given by:-

A = 6.35 + measured length of the growing crack. 6.35 is the distance from the tip of machined notch to line joining centres of holes, as shown below:

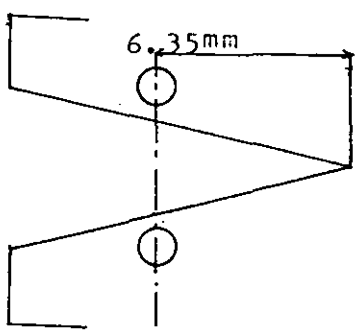

Tables from 6.3 to 6.5 show the calculated crack lengths and the crack lengths measured during pre-cracking tests for three specimens.

TABLE 6.3 Specimen CP.B2

MAX K_I $MNm^{-3/2}$	No. of cycles	Digital readings from computer	Converted crack length (m)	Optically measured crack length (m)
25.5	0	0	6.2032×10^{-3}	6.3500×10^{-3}
"	100	280	6.30201	CRACK NOT
"	200	300	6.3266	VISIBLE
"	300	290	6.3357	"
"	400	290	6.3312	"
"	500	308	6.3312	"
"	600	329	6.3393	"
"	700	350	6.3489	"
"	800	342	6.3584	"
"	900	297	6.3548	"
"	1000	302	6.3344	"
"	1100	313	6.3367	"
"	1200	370	6.3416	"
"	1300	364	6.3675	"
"	1400	323	6.3648	"
"	1500	356	6.3462	"
"	1600	336	6.3612	"
"	1700	256	6.3521	"
"	1800	379	6.36122	"
"	1900	370	6.37168	"
"	2000	348	6.3675	"
"	2100	366	6.3576	"
"	2200	383	6.3657	"
"	2300	363	6.3735	"
"	2400	340	6.3634	"
"	2500	343	6.3566	"
"	2600	384	6.3553	"

Table 6.3 continued

25.5	2700	384	6.3739×10^{-3}	6.35×10^{-3}
"	2800	390	6.3912	CRACK NOT
"	2900	383	6.3755	VISIBLE
"	3000	404	6.3735	"
"	3100	414	6.3831	"
"	3200	394	6.3876	"
"	3300	392	6.37851	"
"	3400	370	6.3776	"
"	3500	388	6.36759	"
"	3600	400	6.3757	"
"	3700	420	6.4494	"
"	3800	550	6.3985	"
"	3900	448	6.4030	"
"	4000	438	6.4030	"
"	4100	448	6.3867	"
"	4200	412	6.3967	"
"	4300	434	6.4167	"
"	4400	478	6.3948	"
"	4500	430	6.4067	"
"	4600	456	6.4139	"
"	4700	472	6.4203	"
"	4800	486	6.4148	"
"	4900	476	6.4026	"
"	5000	447	6.4267	"
"	5100	500	6.4194	"
"	5200	484	6.4398	"
"	5300	529	6.42306	"
"	5400	492	6.4494	"
"	5500	550	6.4471	"

Table 6.3 continued

25.5	5600	512	6.4321×10^{-3}	6.35×10^{-3}
"	5700	514	6.4421×10^{-3}	
"	5800	550	6.4698	CRACK NOT
"	5900	595	6.4776	VISIBLE
"	6000	612	6.4666	"
"	6100	588	6.4762	"
"	6200	609	6.4966	"
"	6300	654	6.5079	"
"	6400	679	6.5174	"
"	6500	700	6.51928	"
"	6600	704	6.51157	"
"	6700	687	6.5446	"
"	6800	760	6.5546	"
"	6900	782	6.5614	"
"	7000	794	6.5664	"
"	7100	808	6.5817	"
"	7200	842	6.5822	"
"	7300	843	6.5921	"
"	7400	865	6.627	"
"	7500	942	6.6107	"
"	7600	906	6.6279	"
"	7700	944	6.6667	"
"	7800	1030	6.6604	"
"	7900	1016	6.6875	"
"	8000		6.6970	"
"	8100		6.7137	"
"	8200		6.728	"
"	8300		6.74256	"
"	8400		6.7632	"
"	8500		6.7759	"
"	8600		6.7863	"

Table 6.3 continued

25.5	8700	-	6.8078×10^{-3}	6.35×10^{-3}
"	8800	-	6.83439	-
"	8900	-	6.83799	-
"	9000	-	6.613	-
"	9100	1134	6.9161	-
"	9200	1166	6.9143	-
"	9300	1198	6.9278	-
"	9400	1244	6.9386	-
"	9500	1295	6.9874	-
"	9600	1343	6.9932	-
"	9700	1295	7.0022	-
"	9800	1345	7.0232	-
"	9900	1402	7.0424	-
"	10000	1403	7.0424	-
"	10100	1462	7.0894	-
"	10200	1506	7.0978	-
"	10300	1584	7.1326	-
"	10400	1580	7.1264	-
"	10500	1610	7.1647	-
"	10700	1634	7.1999	-
"	10800	1734	7.2204	-
"	10900	1756	7.2396	6.36×10^{-3}
"	11000	1776	7.2760	6.40 "
"	11100	1823	7.3058	6.50 "
"	11200	1866	7.3258	6.56 "
"	11300	1866	7.3449	6.66 "
"	11400	1971	7.39722	7.02 "
"	11500	1990	7.4087	7.03 "
"	11600	2068	7.429	7.03 "
"	11700	2054	7.4587	7.04 "
"	11800	2140	7.4870	7.04 "

Table 6.3 continued

25.5	11900	2942	7.52063×10^{-3}	7.42×10^{-3}
"	12000	3001	7.54667	7.42 "
"	12100	3022	7.5559	7.51 "
"	12200	3100	7.59034	7.51 "
"	12300	8182	7.62647	7.56 "
24.0				
"	12400	3272	7.6660	7.666
22.5				
"	12500	3217	7.6418	7.7100
"	12600	3346	7.6986	7.7600
19.5				
"	12700	3351	7.70082	7.86
"	12800	3385	7.7157	"
18.5				
"	12900	3386	7.7162	"
16.5				
"	13000	3420	7.7311	"
"	13100	3434	7.734	"
15.0				
"	13200	3495	7.7640	7.88
"	13300	3489	7.7614	7.88
"	13400	3495	7.7640	"
"	13500	3499	7.7657	"
"	13600	3514	7.772	"
"	13700	3537	7.7824	"
"	13800	3564	7.7943	7.89

∴ Final crack length:-

Electrically measured $= 7.7943 - 6.2032 \times 10^{-3}$

$= \underline{1.5911 \times 10^{-3}\text{m}}$

Optically measured $= 7.89 - 6.35 \times 10^{-3}$

$= \underline{1.54 \times 10^{3}\text{m}}$

TABLE 6.4 Specimen CP.R2

MAXIMUM K_I $MNM^{-3/2}$	No. of Cycles	Digital readings from computer	Converted crack length (m)	Optically measured crack length (m)
25.5	0	-	6.2032×10^{-3}	6.35×10^{-3}
"	100	636	8.4884	
"	200	760	6.5446	CRACK NOT
"	300	844	6.5826	VISIBLE
"	400	859	6.5863	"
"	500	870	6.5944	"
"	600	894	6.6053	"
"	700	910	6.6125	"
"	800	924	6.6188	"
"	900	928	6.6207	"
"	1000	971	6.62068	"
"	1100	958	6.6401	"
"	1200	994	6.6342	"
"	1300	1006	6.6505	"
"	1400	990	6.6559	"
"	1500	1009	6.6487	"
"	1600	1036	6.6573	"
"	1700	1058	6.6695	"
"	1800	1042	6.6794	"
"	1900	1058	6.6722	"
"	2000	1091	6.6794	"
"	2100	1086	6.6943	"
"	2200	1112	6.69205	"
"	2300	1094	6.7037	"
"	2400	1105	6.6956	"
"	2500	1120	6.7006	"
"	2600	1171	6.70739	"
"	2700	1128	6.73039	"

Table 6.4 continued

"	2800	1128	7.7110×10^{-3}	6.35×10^{-3}
"	2900	1146	6.71912	
"	3000	1151	6.7213	CRACK NOT
"	3100	1180	6.7344	VISIBLE
"	3200	1187	6.7376	"
"	3300	1165	6.72816	"
"	3400	1206	6.7461	"
"	3500	1210	6.7479	
"	3600	1219	6.7520	
"	3700	1241	6.7619	
"	3800	1240	6.7614	
"	3900	1228	6.7560	
"	4000	1219	6.7632	
"	4100	1267	6.75207	
"	4200	1297	6.76419	
"	4300	1276	6.7736	
"	4400	1318	6.7872	
"	4500	1338	6.777	
"	4600	1332	6.7966	
"	4700	1351	6.8029	
"	4800	1336	6.81145	
"	4900	1362	6.8047	
"	5000	1404	6.8164	
"	5100	1418	6.8352	
"	5200	1426	6.8415	
"	5300	1454	6.8451	
"	5400	1422	6.8577	
"	5500	1472	6.8433	
"	5600	1496	6.8658	
"	5700	1520	6.8766	
"	5800	1538	6.8874	
"	5900	1524	6.8954	

Table 6.4 continued

25.5	6000	1582	$6.9116x10^{-3}$	$6.35x10^{-3}$
"	6100	1642	6.9152	
"	6200	1654	6.9421	CRACK NOT
"	6300	1665	6.9475	VISIBLE
"	6400	1708	6.9524	
"	6500	1727	6.9717	
"	6600	1734	6.9802	
"	6700	1778	6.9847	
"	6800	1802	7.0030	
"	6900	1829	7.0138	
"	7000	1864	7.0259	
"	7100	1888	7.0415	
"	7200	1946	7.0522	
"	7300	1975	7.0782	
"	7400	1971	7.0911	
"	7500	1999	7.0894	
"	7600	2047	7.10189	
"	7700	2060	7.1283	
"	7800	2119	7.1291	
"	7900	2163	7.1554	
"	8000	2175	7.1751	
"	8100	2239	7.1803	
"	8200	2306	7.1959	
"	8300	2332	7.2089	
"	8400	2367	7.2387	
"	8500	2379	7.2502	
"	8600	2422	7.26585	
"	8700	2486	7.2711	
"	8800	2508	7.2902	
"	8900	2566	7.3187	
"	9000	2591	7.3284	
"	9100	2664	7.3542	

Table 6.4 continued

25.5	9200	2761	7.3653×10^{-3}	6.35×10^{-3}
"	9300	2776	7.39766	"
"	9400	2851	7.4038	"
"	9500	2879	7.4406	6.62×10^{-3}
"	9600	2959	7.4472	6.73×10^{-3}
"	9700	3007	7.4804	6.75×10^{-3}
"	9800	3091	7.4928	6.75
"	9900	3139	7.5197	6.75
"	10000	3188	7.5281	6.76×10^{-3}
24.0				
"	10100	3166	7.6194	6.76×10^{-3}
"	10200	3212	7.6387	6.81×10^{-3}
"	10300	3207	7.6374	6.81×10^{-3}
"	10400	3241	7.6524	6.82×10^{-3}
22.5				
"	10500	3292	7.6748	6.82×10^{-3}
21.0				
"	10600	3279	7.6691	6.87×10^{-3}
"	10700	3297	7.67707	"
"	10800	3297	7.67707	"
"	10900	3300	7.67839	"
"	11000	3300	7.67839	"
19.5				
"	11100	3312	7.6836	6.89×10^{-3}
"	11200	3338	7.69509	"
"	11300	3340	7.69597	"
"	11400	3377	7.7122	"
18.0				
"	11500	3408	7.72585	6.93×10^{-3}
16.5				
"	11600	3424	7.7320	6.93×10^{-3}
"	11700	3385	7.71578	6.93×10^{-3}

Table 6.4 continued

16.5	11800	3348	7.6994x10^{-3}	6.93x10^{-3}
"	11900	3356	7.7030	"
"	12000	3410	7.7267	"
"	12100	3385	7.7157	"
"	12200	3381	7.71399	"
"	12300	3414	7.7284	"
"	12400	3409	7.72629	6.94x10^{-3}
"	12500	3423	7.7324	"
"	12600	3401	7.7227	"
"	12700	3395	7.72014	"
"	12800	3383	7.7148	"
"	12900	3423	7.7324	"
"	13000	3390	7.7179	"
"	13100	3417	7.7298	"
"	13200	3426	7.7337	"
"	13300	3433	7.7368	"
"	13400	3461	7.74912	"
15.0				
"	13500	3462	7.74956	6.94x10^{-3}
"	13600	3445	7.74209	6.94x10^{-3}
"	13700	3461	7.74912	6.95x10^{-3}
"	13800	3449	7.7438	"
"	13900	3459	7.7482	6.98x10^{-3}
"	14000	3474	7.7548	"
"	14100	3462	7.7495	6.99x10^{-3}
"	14200	3478	7.7565	"
"	14300	3465	7.75088	"
"	14400	3494	7.7636	"
"	14500	3614	7.8162	"

∴ Final crack length:-

Electrically measured: $7.8162 - 6.2032 \times 10^{-3} = 1.613 \times 10^{-3}$ m.

Optically measured: $6.99 - 6.35 \times 10^{-3} = 0.64 \times 10^{-3}$ m.

TABLE 6.5 Specimen CP.DA2

MAXIMUM K_I $MNM^{-3/2}$	Number of Cycles	Digital readings from computer	Converted crack length (m)	Optically measured crack length (m)
25.5	0	0	6.2032×10^{-3}	6.35×10^{-3}
"	500	102	6.2454	
"	1700	260	6.3074	CRACK NOT
"	1800	283	6.31477	VISIBLE
"	1900	293	6.3279	
"	2000	268	6.33527	
"	2100	304	6.32115	
"	2200	321	6.3375	
"	2300	342	6.3452	
"	2400	357	6.3548	
"	2500	364	6.36167	
"	2600	398	6.3648	
"	2700	442	6.38033	
"	2800	448	6.40034	
"	2900	490	6.4030	
"	3000	514	6.42215	
"	3100	566	6.43306	
"	3200	605	6.45667	
"	3300	625	6.47438	
"	3400	639	6.4834	
"	3500	658	6.4898	
"	3600	726	6.4984	
"	3700	750	6.52925	
"	3800	814	6.54012	
"	3900	841	6.5691	
"	4000	890	6.5813	
"	4100	954	6.6035	
"	4200	998	6.6324	

Table 6.5 continued

25.5	4300	1008	6.6523×10^{-3}	6.35×10^{-3}
"	4400	1049	6.56683	
"	4500	1096	6.67535	
"	4600	1128	6.69665	
"	4700	1182	6.7087	
"	4800	1222	6.7353	
"	4900	1297	6.75337	6.51×10^{-3}
"	5000	1344	6.78715	
"	5100	1401	6.8083	6.65×10^{-3}
"	5200	1452	6.8339	"
"	5300	1513	6.85687	"
"	5400	1535	6.8843	"
"	5500	1615	6.89415	"
"	5600	1675	6.9300	6.75×10^{-3}
"	5700	1753	6.95694	"
"	5800	1780	6.9569	"
"	5900	1852	6.99189	"
"	6000	1902	7.0084	6.76×10^{-3}
"	6100	1947	7.03619	"
"	6200	2037	7.05856	"
"	6300	2111	7.07866	"
"	6400	2169	7.1188	"
"	6500	2230	7.15186	6.85×10^{-3}
"	6600	2300	7.1777	"
"	6700	2388	7.20489	"
"	6800	2431	7.23605	"
"	6900	2513	7.2751	"
"	7000	2555	7.2943	"
"	7100	2645	7.3307	"
"	7200	2697	7.3493	"
"	7300	2774	7.3892	"
"	7400	2451	7.4122	6.99×10^{-3}

Table 6.5 continued

25.5	7500	2923	7.4463×10^{-3}	7.15×10^{-3}
"	7600	3007	7.4804×10^{-3}	7.19
"	7700	3123	7.5122	7.25
"	7800	3140	7.5493	7.29
"	7900	3241	7.6004	7.35
"	8000	3241	7.6004	7.40
24.0				
"	8100	3271	7.6656	7.52×10^{-3}
22.5				
"	8200	3214	7.6713	
21.0				
"	8300	3342	7.6972	7.53×10^{-3}
19.5				
"	8400	3433	7.7232	7.54×10^{-3}
16.5				
"	8500	3478	7.7368	"
15.0				
"	8600	3524	7.7565	"
"	8700	3535	7.7767	7.65×10^{-3}
"	8800	3545	7.7815	"
"	8900	3538	7.7859	"
"	9000	3561	7.7929	7.55×10^{-3}

∴ Final crack length:-

Electrically measured: $7.7929 - 6.2032 \times 10^{-3}$

$= \underline{1.5897 \times 10^{-3}\ \text{m}}$

Optically measured: $7.55 - 6.35 \times 10^{-3}$

$= \underline{1.20 \times 10^{-3}\ \text{m}}$

Figures from 40 to 42 show the graphs of different specimens of crack length measured optically and automatically against number of cycles.

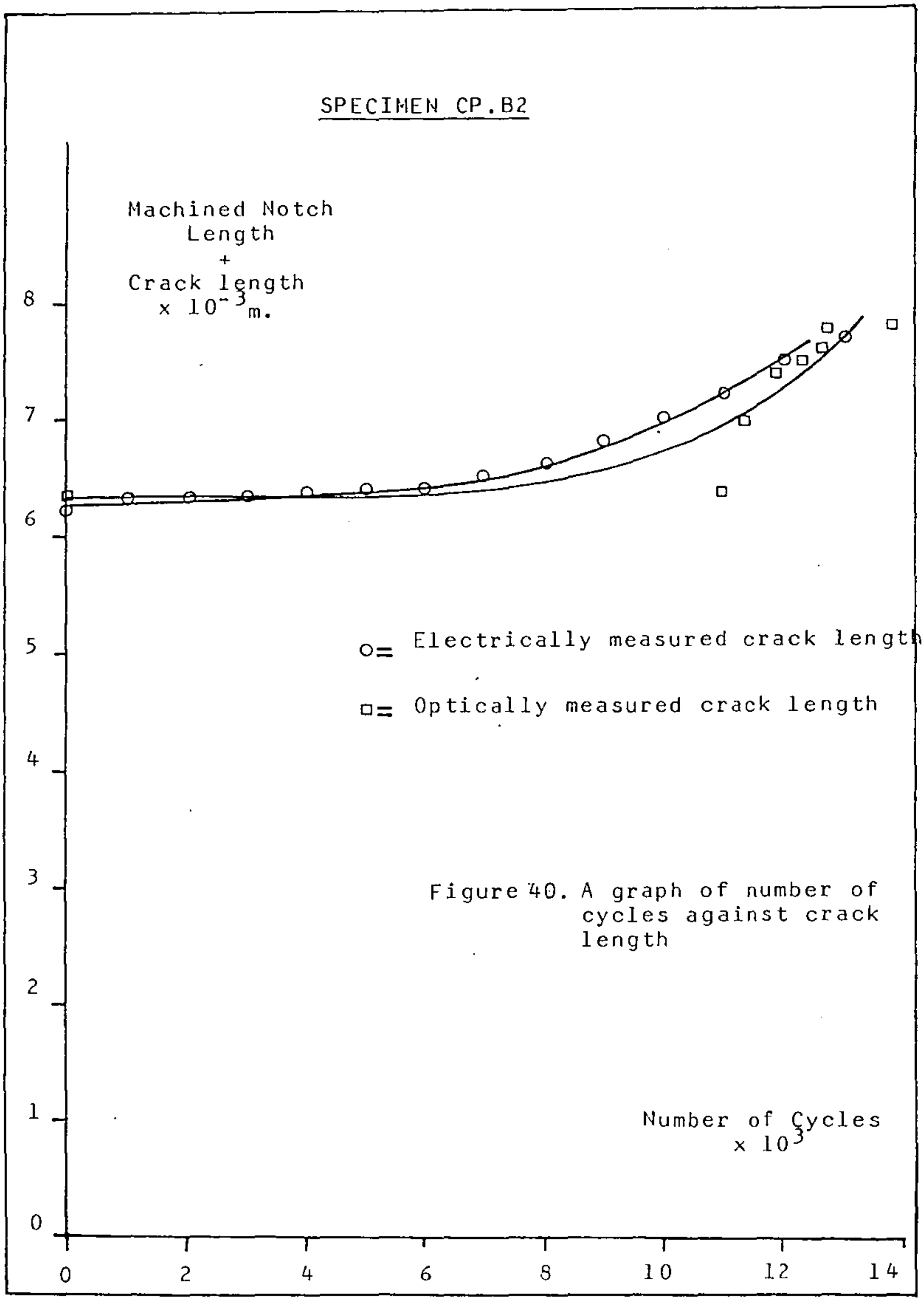

Figure 40. A graph of number of cycles against crack length

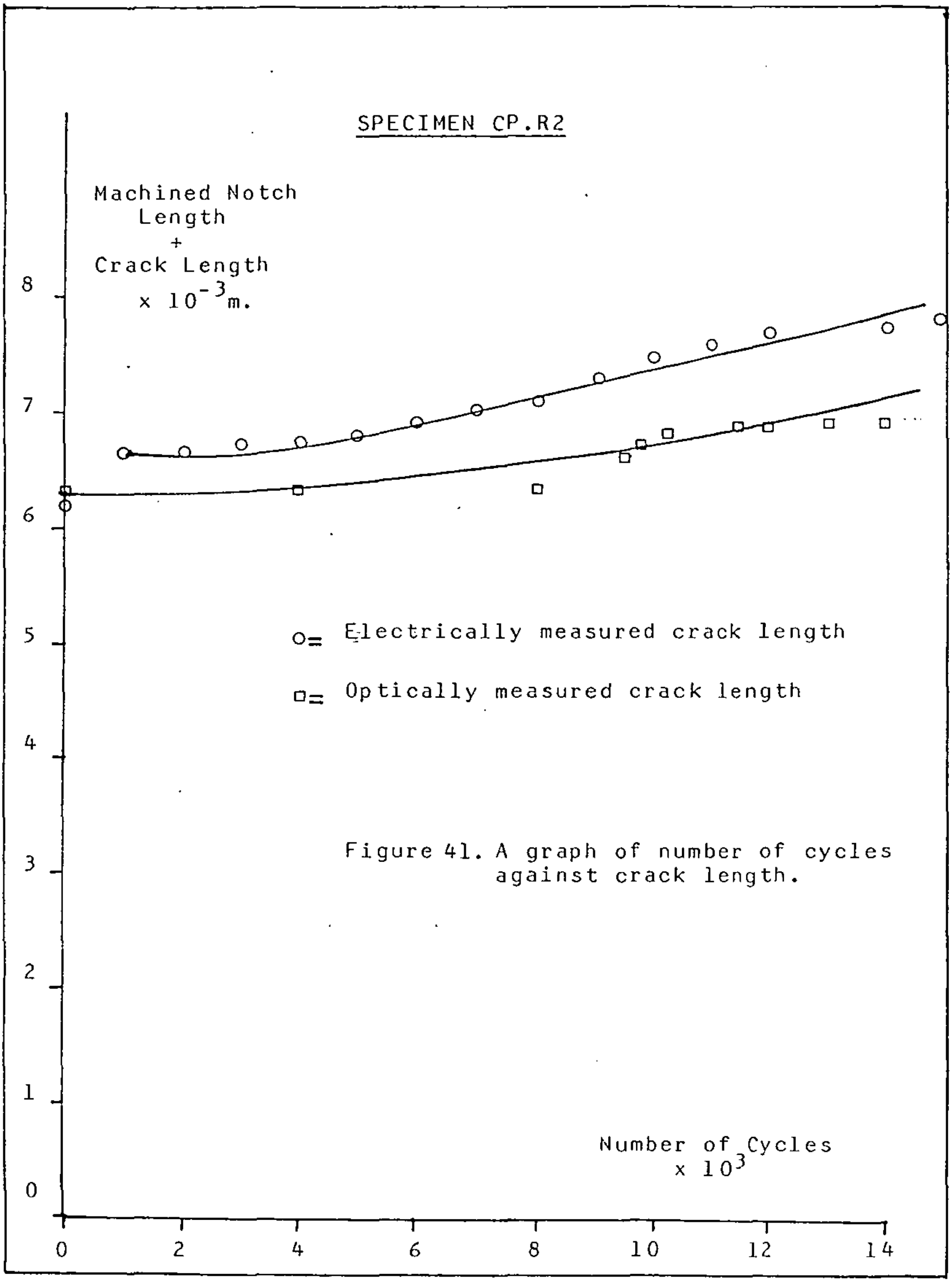

Figure 41. A graph of number of cycles against crack length.

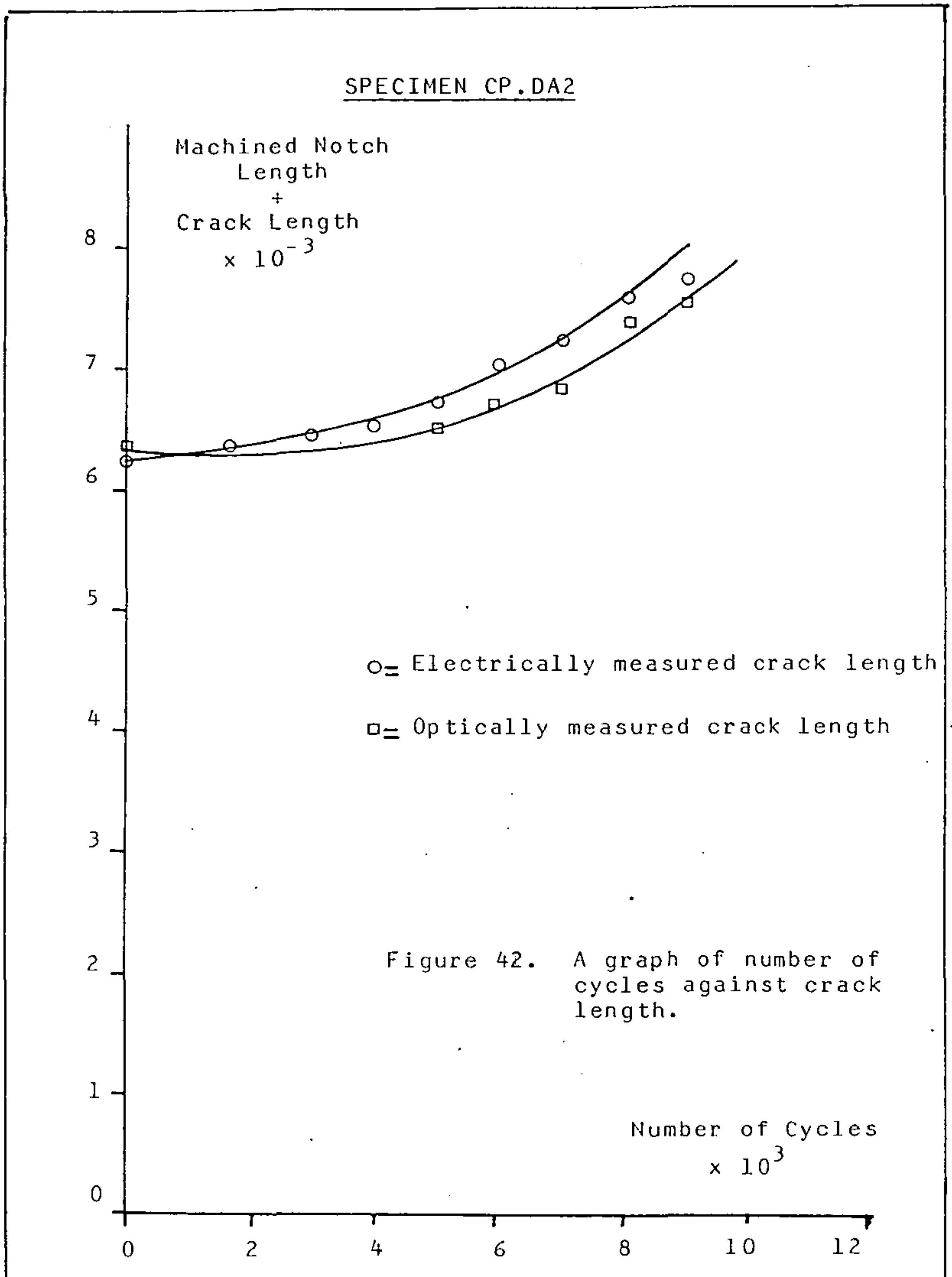

Figure 42. A graph of number of cycles against crack length.

One of the specimens (CP.DA2) was broken by immersing it in liquid nitrogen and forcing the notch apart using a cold chisel and hammer. The fatigue precrack surfaces were revealed and examined under the microscope. The method used to break this specimen ensured that the fatigue precrack front was clearly distinguishable.

Figure 43 shows a micrograph of fatigue crack front. The crack length was measured. The measurement readings were compared with electrically measured readings. Crack length measurements were made from left to right after every 10 mm. Table 6.6 shows the crack measurements. Only one of the specimens was broken because of the need to conserve the others for the high temperature crack propagation tests.

TABLE 6.6

Readings from left to right

Position in specimen	Measured crack length (mm)
1	1.125
2	1.4167
3	1.5833
4	1.6667
5	1.8333
6	2.000
7	1.8333
8	1.8333
9	1.8333
10	1.6667
11	1.5833
12	1.4583
13	1.3333

∴ Mean crack length = 1.63781 mm.

Automatically measured crack length = 1.5897 mm.

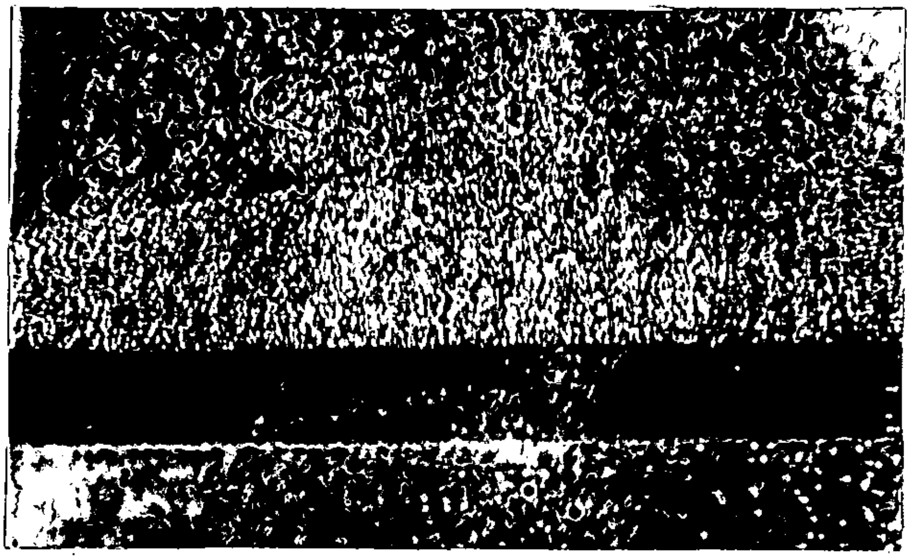

Figure 43. Micrograph of Fatigue-crack front
Magnification 12.
The crack length was measured from left to right.

Mean Crack Length = 1.63781 mm
Minimum Crack Length = 1.12500 mm
Maximum Crack Length = 2.000 mm

6.3 Microscopy

The crack surface of the one specimen broken was subjected to optical and scanning electron microscope (SEM) examination. The SEM used is a Cambridge Instruments microscope. The fracture surface was cleaned ultrasonically and carbon coated before examination. Striations were evident on the fracture surface, as shown in Figure 44.

Before the specimen was fractured, the test piece surface was polished and subjected to optical and scanning electron microscope examination in etched and unetched conditions. The polishing of the surface consisted of wet grinding on consecutively finer silicon carbide papers up to a longitudinal finish on 600 grit. The fine scratches from silicon carbide papers were removed by using alumina powder (i.e. 0.05 micron) on selvyt cloth, with ten percent oxalic acid solution as lubricant. The specimen was etched in a mixture consisting of two percent hydrofluoric acid, ten percent nitric acid and eighty-eight percent water. The specimen was etched for two to four seconds.

Figures 45 to 46 are micrographs of the etched and unetched pre-crack edge surface.

It can be seen that the crack grows in intergranular and transgranular fashion. It is intergranular when the crack grows between the grains and is transgranular when the crack grows through the β phase.

Figure 44

SEM Fractography of the Fracture Surface
Crack growth from left to right

(a)
Poorly
developed
striations
x 2200

(b)
Transgranular
and
Intergranular
fracture
x 500

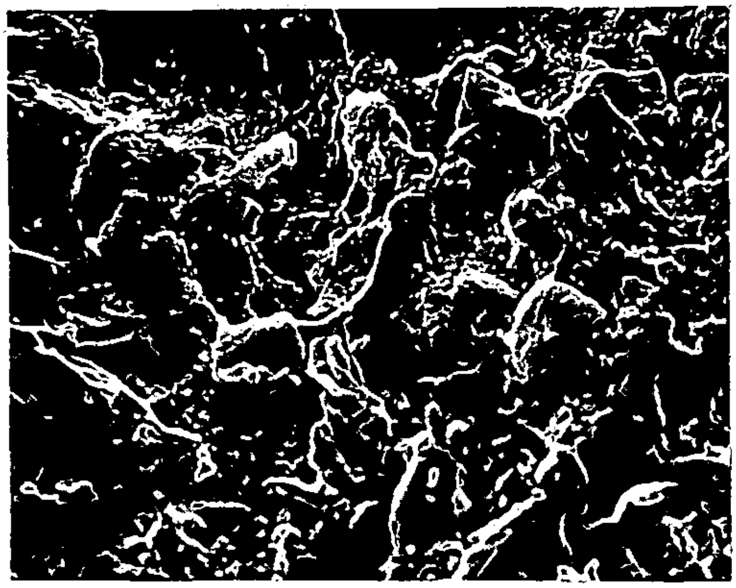

(c)
Transgranular
and
Intergranular
fracture
x 1100

Figure 45

Example of Fatigue Crack
Propagating from left to right (unetched)

(a)
Optical
micrograph
x 500

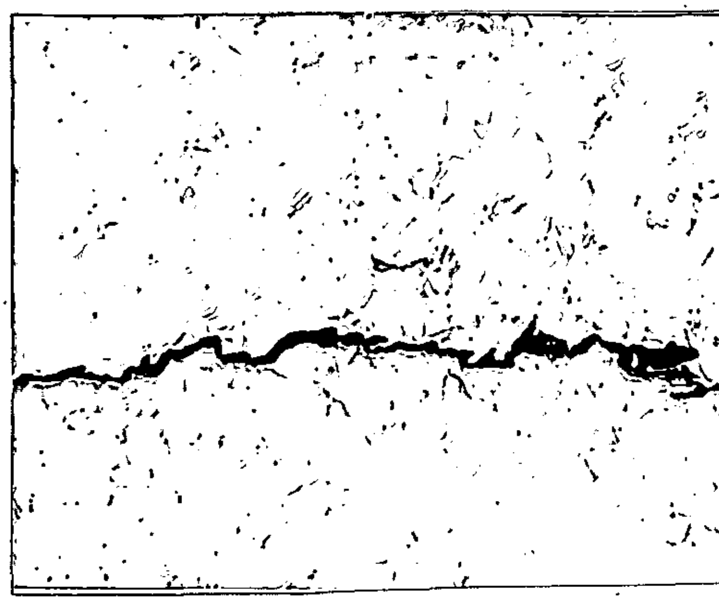

(b)
SEM
micrograph
x 1000

(c)
SEM
micrograph
x 5000

Figure 46

Illustrating Fatigue Crack Path
Crack propagating from left to right
Etched in 2% HF + 10% HNO_3 + 88% H_2O

(a)
Optical
micrograph
x 600

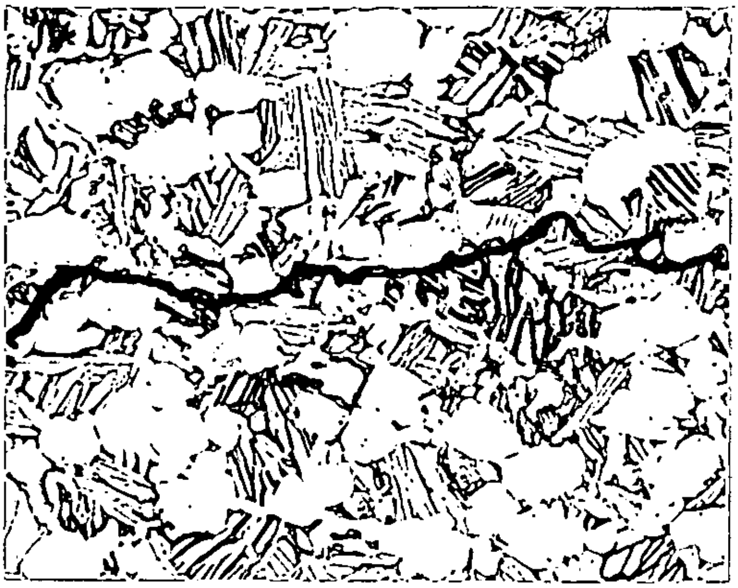

(b)
SEM
micrograph
x 1000

(c)
SEM
micrograph
x 5000

6.4 Crack Growth Rates

The crack growth rates were calculated from crack length versus cycles data obtained from pre-cracking tests with a K_I maximum of approximately 25.5MNm$^{-3/2}$ (i.e. before any stress reductions).

A computer program was used to differentiate the crack length against number of cycles curve numerically as shown in (Chapter Five). This data reduction process uses the "seven point incremental polynominal technique". Figures 47 to 49 show the print out of results for different specimens.

The crack growth measurements are presented as conventional double logarithm plots of crack growth rates (da/dN) versus stress intensity range (Δk) in Figures 50 to 52. The growth rates are about the same for each specimen.

The crack growth rates can only be measured when the crack is fully developed and growing. As can be seen from the graphs, prior to full development of the cracks, there is much scatter in the results. However, when crack is begins to grow, there is little scatter and all the points fit closely to the line drawn.

FIGURE 47

*** FATIGUE DATA ANALYSIS ***

SPECIMEN IDENTIFICATION = CP. B2

NUMBER OF DATA POINTS = 122

MAXIMUM LOAD (MN) = 9.55E-03

MINIMUM LOAD (MN) = 9.55E-04

THICKNESS (M) = .0127

WIDTH OF SPECIMEN (M) = .0254

NOTCH LENGTH (M) = 6.35E-03

TEST ENVIRONMENT = AIR

TEST TEMPERATURE (C) = 25

TEST FREQUENCY (HZ) = 8

R-RATIO (P1/P2) = .1

N(I)	A(I)	A(R)	MCC	DK(I)	DA/DN(I)
0	6.20320662E-03				
100	6.30201366E-03				
200	6.32661881E-03				
300	6.33572794E-03	6.338E-03	.86614	22.941	1.68345702E-07
400	6.33117364E-03	6.334E-03	.78038	22.937	5.7752301E-08
500	6.33117364E-03	6.334E-03	.91572	22.937	4.65087929E-08
600	6.339371E-03	6.34E-03	.83752	22.943	4.63434332E-08
700	6.34893244E-03	6.35E-03	.6617	22.954	2.71564328E-08
800	6.35849156E-03	6.353E-03	.74982	22.958	4.39090075E-09
900	6.35485026E-03	6.349E-03	.31767	22.953	-1.49596567E-08
1000	6.33436171E-03	6.34E-03	.39	22.943	1.45839814E-09
1100	6.33663874E-03	6.339E-03	.71653	22.942	1.85309091E-08
1200	6.34164775E-03	6.348E-03	.1545	22.952	2.35746211E-08
1300	6.36759333E-03	6.355E-03	.5925	22.96	4.39004596E-08
1400	6.36486302E-03	6.36E-03	.50971	22.965	2.29277287E-08
1500	6.34620084E-03	6.358E-03	.08407	22.963	8.6194489E-09
[illegible]	[illegible]	[illegible]	[illegible]	[illegible]	[illegible]

1400	6.36486302E-03	6.36E-03	.50971	22.965	2.29277287E-
1500	6.34620084E-03	6.358E-03	.08407	22.963	8.6194489E-0
1600	6.36122231E-03	6.353E-03	.62991	22.958	3.90076561E-
1700	6.35211907E-03	6.356E-03	.4554	22.961	2.11307627E-
1800	6.36122231E-03	6.364E-03	.59505	22.97	2.37331031E-0
1900	6.37168844E-03	6.364E-03	.20132	22.97	1.10528202E-0
2000	6.36759333E-03	6.365E-03	.38204	22.971	2.11294024E-0
2100	6.35758127E-03	6.366E-03	.01687	22.972	3.08788978E-0
2200	6.36577314E-03	6.365E-03	.2083	22.971	-1.33272943E-
2300	6.37350835E-03	6.366E-03	.4252	22.972	-1.46284323E-
2400	6.3634978E-03	6.363E-03	.01842	22.969	4.06192353E-0
2500	6.35667095E-03	6.358E-03	.71454	22.963	2.469374E-08
2600	6.35530545E-03	6.363E-03	.488	22.969	2.94096169E-0
2700	6.37396333E-03	6.372E-03	.44972	22.979	3.78637177E-0
2800	6.3912481E-03	6.378E-03	.64785	22.986	4.22525604E-0
2900	6.376693E-03	6.381E-03	.50684	22.989	3.47749237E-0
3000	6.37350835E-03	6.381E-03	.02554	22.989	4.55002205E-0
3100	6.38306152E-03	6.379E-03	.11825	22.987	-8.28389018E-
3200	6.38760983E-03	6.383E-03	.7007	22.991	-8.44958518E-
3300	6.37851269E-03	6.38E-03	.35526	22.988	-1.21853535E-
3400	6.37760286E-03	6.368E-03	.65886	22.974	5.87452451E-0
3500	6.36759333E-03	6.381E-03	.33568	22.989	6.16877183E-0
3600	6.37578314E-03	6.395E-03	.3011	23.005	7.04768711E-0
3700	6.44941466E-03	6.406E-03	.35348	23.017	6.07485625E-0
3800	6.39852362E-03	6.415E-03	.44174	23.027	2.3410762E-08
3900	6.40307015E-03	6.409E-03	.12617	23.021	-2.0756134E-0
4000	6.40307015E-03	6.391E-03	.77625	23	-4.21699183E-
4100	6.38670021E-03	6.398E-03	.01707	23.008	3.56955687E-0
4200	6.39670487E-03	6.398E-03	.09766	23.008	8.767365588E-0
4300	6.41670655E-03	6.4E-03	.29213	23.01	2.53297282E-0
4400	6.39488603E-03	6.405E-03	.58724	23.016	4.481277769E-0
4500	6.40670698E-03	6.408E-0	.38824	23.019	2.88986147E-0
4600	6.41397966E-03	6.411	.04963	23.023	4.059742688E-

4700	6.42034214E-03	6.414E-03	.45481	23.026	3.14924072E-0
4800	6.41488865E-03	6.414E-03	.18441	23.026	1.63928982E-0
4900	6.40261552E-03	6.413E-03	.60732	23.025	3.13182402E-0
5000	6.42670359E-03	6.418E-03	.29025	23.031	2.6776811E-08
5100	6.41943327E-03	6.423E-03	.62461	23.037	5.63065144E-0
5200	6.43987761E-03	6.431E-03	.71589	23.046	6.5229776E-08
5300	6.4230686E-03	6.437E-03	.34536	23.053	2.90408467E-0
5400	6.44941466E-03	6.44E-03	.41881	23.056	3.5205494E-08
5500	6.44714415E-03	6.438E-03	.54058	23.054	4.47608071E-0
5600	6.43215545E-03	6.445E-03	.73001	23.062	7.37845131E-0
5700	6.44941466E-03	6.452E-03	.58289	23.07	5.36681657E-0
5800	6.4698434E-03	6.461E-03	.7005	23.081	6.58297346E-0
5900	6.47755815E-03	6.47E-03	.84112	23.091	8.7055663E-08
6000	6.46666629E-03	6.474E-03	.83873	23.096	8.1348939E-08
6100	6.47619684E-03	6.48E-03	.92287	23.103	8.34297999E-0
6200	6.49661165E-03	6.492E-03	.88534	23.117	9.23320873E-0
6300	6.50794861E-03	6.508E-03	.97052	23.137	8.63416947E-08
6400	6.51746912E-03	6.512E-03	.82378	23.141	8.80874685E-08
6500	6.51928229E-03	6.517E-03	.85474	23.147	8.62703896E-08
6600	6.51157575E-03	6.525E-03	.88193	23.157	9.28859131E-08
6700	6.54465784E-03	6.537E-03	.86322	23.172	9.78892592E-08
6800	6.55462231E-03	6.55E-03	.91372	23.188	1.12108836E-07
6900	6.56141481E-03	6.564E-03	.95126	23.205	1.06433501E-07
7000	6.56639523E-03	6.569E-03	.97801	23.211	7.79306708E-08
7100	6.58178523E-03	6.574E-03	:93761	23.217	1.05205654E-07
7200	6.58223779E-03	6.588E-03	.84719	23.235	9.98631575E-08
7300	6.59219268E-03	6.599E-03	.85821	23.249	1.02590706E-07
7400	6.62701483E-03	6.606E-03	.8721	23.257	1.30311639E-07
7500	6.61073821E-03	6.623E-03	.86453	23.279	1.37394758E-07
7600	6.62791888E-03	6.636E-03	.8779	23.295	1.46053772E-07
7700	6.66677352E-03	6.649E-03	.88182	23.312	1.41479741E-07
7800	6.66045098E-03	6.67E-03	.95899	23.339	1.67098208E-07
7900	6.68754033E-03	6.685E	.95077	23.359	1.53963215E-0

8000	6.69701714E-03	6.696E-03	.9673	23.373	1.32898385E-
8100	6.71370877E-03	6.713E-03	.98989	23.396	1.60602361E-
8200	6.728139E-03	6.728E-03	.99681	23.416	1.523152655E-
8300	6.74256386E-03	6.745E-03	.9962	23.439	1.52590489E-
8400	6.76329021E-03	6.759E-03	.99418	23.457	1.542942E-07
8500	6.77590083E-03	6.774E-03	.98968	23.478	1.68689116E-
8600	6.78625649E-03	6.792E-03	.98065	23.502	1.64449695E-
8700	6.80785937E-03	6.808E-03	.98179	23.525	1.66624237E-
8800	6.83439641E-03	6.825E-03	.9851	23.548	1.77155548E-0
8900	6.83799326E-03	6.842E-03	.98092	23.572	2.01129947E-
9000	6.86136457E-03	6.864E-03	.964	23.603	1.87889218E-
9100	6.88112926E-03	6.884E-03	.95313	23.631	1.74182966E-
9200	6.91614179E-03	6.904E-03	.97673	23.66	1.67081079E-
9300	6.91434705E-03	6.915E-03	.92049	23.676	1.80248141E-
9400	6.92780557E-03	6.932E-03	.92919	23.701	1.79675521E-07
9500	6.938569E-03	6.949E-03	.91788	23.725	1.6983448E-07
9600	6.98741508E-03	6.972E-03	.95248	23.759	1.89312602E-0
9700	6.99323661E-03	6.992E-03	.95747	23.789	1.88590894E-0
9800	7.0021911E-03	7.007E-03	.93613	23.811	2.11620323E-0
9900	7.02322593E-03	7.024E-03	.97162	23.837	2.014097E-07
10000	7.04246045E-03	7.048E-03	.98024	23.873	2.41387007E-0
10100	7.08938795E-03	7.079E-03	.96466	23.921	2.31104506E-0
10200	7.09787345E-03	7.102E-03	.9604	23.957	2.2713615E-07
10300	7.13268891E-03	7.123E-03	.95269	23.989	2.10424409E-0
10400	7.12644231E-03	7.139E-03	.96333	24.015	1.87968792E-0
10500	7.1647981E-03	7.159E-03	.96753	24.046	1.98233117E-0
10600	7.17906018E-03	7.178E-03	.97	24.076	1.94303578E-0
10700	7.19999793E-03	7.2E-03	.98452	24.112	2.2855573E-07
10800	7.22047905E-03	7.219E-03	.99753	24.143	2.34570837E-0
10900	7.23961448E-03	7.245E-03	.99401	24.185	2.52712826E-0
11000	7.27607858E-03	7.274E-03	.99118	24.233	2.54164387E-0
11100	7.30584643E-03	7.298E-03	.98524	24.272	2.8234823E-07
11200	7.32582664E-03	7.328E-03	.9832	24.323	2.816927763E-0

11300	7.34490898E-03	7.356E-03	.98036	24.37	2.63434378E-
11400	7.39722504E-03	7.382E-03	.98006	24.414	2.60723019E-
11500	7.40874257E-03	7.409E-03	.98245	24.461	2.65613798E-
11600	7.42955378E-03	7.434E-03	.98031	24.504	2.70304513E-
11700	7.45875863E-03	7.457E-03	.99629	24.544	2.60587513E-
11800	7.48705685E-03	7.489E-03	.99239	24.601	2.66311072E-
11900	7.52063331E-03	7.517E-03	.99484	24.651	2.64874555E-
12000	7.54667854E-03				
12100	7.5585915E-03				
12200	7.59034088E-03				

Figure 47: Printout of Data Reduction Results

FIGURE 48

** FATIGUE DATA ANALYSIS **

SPECIMEN IDENTIFICATION		=	CP. R2
NUMBER OF DATA POINTS		=	102
MAXIMUM LOAD	(MN)	=	9.55E-0
MINIMUM LOAD	(MN)	=	9.55E-0
THICKNESS	(M)	=	.0127
WIDTH OF SPECIMEN	(M)	=	.0254
NOTCH LENGTH	(M)	=	6.35E-0
TEST ENVIRONMENT		=	AIR
TEST TEMPERATURE	(C)	=	25
TEST FREQUENCY	(HZ)	=	8
R-RATIO (P1/P2)		=	.1

N(I)	A(I)	A(R)	MCC	DK(I)	DA/DN(I)
0	6.20320662E-03				
100	6.488447E-03				
200	6.54465784E-03				
300	6.58269034E-03	6.595E-03	.8929	23.243	5.21422116E-0
400	6.58631055E-03	6.591E-03	.95359	23.238	1.80489744E-0
500	6.5944548E-03	6.598E-03	.93838	23.247	1.07633085E-0
600	6.60531116E-03	6.604E-03	.97985	23.255	7.04330029E-0
700	6.61254706E-03	6.612E-03	.99357	23.265	6.04122008E-0
800	6.61887737E-03	6.616E-03	.90247	23.27	6.2817338E-08
900	6.62068584E-03	6.621E-03	.85937	23.276	5.1344345E-08
1000	6.62068584E-03	6.625E-03	.88402	23.281	5.85977686E-0
1100	6.6401216E-03	6.632E-03	.90484	23.29	6.58524531E-0
1200	6.6342467E-03	6.641E-03	.8425	23.302	5.89108855E-0
1300	6.6505135E-03	6.647E-03	.83951	23.31	5.30955972E-0

1400	6.65593426E-03	6.649E-03	.78293	23.312	4.72721234E-
1500	6.64870641E-03	6.654E-03	.85887	23.319	6.24286363E-
1600	6.65728933E-03	6.66E-03	.77057	23.326	4.74194537E-
1700	6.66948286E-03	6.666E-03	.78602	23.334	4.98361013E-
1800	6.6794155E-03	6.672E-03	.88597	23.342	6.56326387E-
1900	6.67219202E-03	6.678E-03	.8486	23.35	5.4980664E-0
2000	6.6794155E-03	6.682E-03	.87604	23.355	5.36783994E-
2100	6.69430971E-03	6.688E-03	.73205	23.363	4.44883797E-
2200	6.69205338E-03	6.695E-03	.8921	23.372	4.54554499E-
2300	6.70378488E-03	6.698E-03	.75559	23.376	3.57782964E-
2400	6.69566345E-03	6.697E-03	.8326	23.375	4.84904987E-0
2500	6.70062675E-03	6.705E-03	.55376	23.385	4.34980335E-0
2600	6.70739386E-03	6.71E-03	.4837	23.392	3.80186235E-0
2700	6.73039323E-03	6.716E-03	.66463	23.4	4.20474018E-0
2800	6.7110025E-03	6.718E-03	.5581	23.402	4.22007484E-0
2900	6.71912073E-03	6.72E-03	.56786	23.405	3.897276685E-0
3000	6.72137549E-03	6.723E-03	.30932	23.409	2.20621171E-0
3100	6.73445053E-03	6.729E-03	.80853	23.417	4.99168843E-08
3200	6.73760592E-03	6.733E-03	.78171	23.422	4.636756607E-0
3300	6.728139E-03	6.738E-03	.77617	23.429	4.555755595E-0
3400	6.74616924E-03	6.74E-03	.84871	23.432	4.683585805E-0
3500	6.7479718E-03	6.747E-03	.83825	23.441	5.18232154E-0
3600	6.75202726E-03	6.756E-03	.92733	23.453	4.58697059E-0
3700	6.76193883E-03	6.757E-03	.78886	23.455	2.75160723E-0
3800	6.76148836E-03	6.761E-03	.69718	23.46	1.0298484E-08
3900	6.7560823E-03	6.759E-03	.09589	23.457	6.5965196E-09
4000	6.763290021E-03	6.757E-03	.606	23.455	1.30291801E-0
4100	6.75202726E-03	6.758E-03	.88599	23.456	4.03715103E-0
4200	6.76419111E-03	6.766E-03	.71033	23.467	4.79336989E-0
4300	6.77364924E-03	6.771E-03	.80237	23.474	6.224025E-08
4400	6.78715684E-03	6.78E-03	.91528	23.486	7.91202976E-0
4500	6.77770201E-03	6.786E-03	.91261	23.494	7.4920114E-08
4600	6.79660937E-03	6.795E-03	.82243	.507	5.9640297E-

4700	6.80290977E-03	6.8E-03	.79738	23.513	5.59341873E
4800	6.81145868E-03	6.806E-03	.86454	23.522	7.64916E-08
4900	6.8047097E-03	6.811E-03	.92322	23.529	7.30933803E
5000	6.81640718E-03	6.819E-03	.90849	23.54	7.77416569E
5100	6.83529565E-03	6.828E-03	.9249	23.552	8.75245529E
5200	6.84158977E-03	6.842E-03	.94441	23.572	7.45179783E
5300	6.84518594E-03	6.846E-03	.80771	23.578	6.45412099E
5400	6.85776991E-03	6.849E-03	.81235	23.582	6.09874451E
5500	6.8433879E-03	6.854E-03	.87965	23.589	7.44537089E
5600	6.86585743E-03	6.863E-03	.89862	23.602	8.69557556E
5700	6.87663818E-03	6.873E-03	.92454	23.616	1.02654196E
5800	6.8874159E-03	6.888E-03	.98728	23.637	1.16436913E
5900	6.89549722E-03	6.896E-03	.97779	23.649	1.17981265E
6000	6.91165478E-03	6.908E-03	.97563	23.666	1.22114959E
6100	6.91524443E-03	6.922E-03	.96337	23.686	1.17762023E
6200	6.94215615E-03	6.934E-03	.96549	23.704	1.22370419E
6300	6.94753623E-03	6.946E-03	.96278	23.721	1.17528319E
6400	6.95246733E-03	6.959E-03	.96222	23.74	1.10298939E
6500	6.97173732E-03	6.966E-03	.9741	23.75	1.01769992E-0
6600	6.98024883E-03	6.978E-03	.98049	23.768	1.11823766E
6700	6.98472792E-03	6.99E-03	.98305	23.786	1.16910607E
6800	7.00308643E-03	7E-03	.99231	23.801	1.17825016E
6900	7.01382881E-03	7.013E-03	.99212	23.82	1.25945166E
7000	7.02591039E-03	7.026E-03	.98941	23.84	1.45227067E
7100	7.04156604E-03	7.04E-03	.99371	23.861	1.497978E-07
7200	7.05229765E-03	7.058E-03	.96894	23.889	1.40664153E
7300	7.07821996E-03	7.073E-03	.97178	23.912	1.29452235E
7400	7.09117453E-03	7.084E-03	.95129	23.929	1.27005342E
7500	7.08938795E-03	7.096E-03	.9442	23.947	1.18350282E
7600	7.10189224E-03	7.103E-03	.97337	23.958	1.2195286E-0
7700	7.12331863E-03	7.116E-03	.98383	23.978	1.46767068E
7800	7.12911956E-03	7.136E-03	.98144	24.01	1.6123526E-0
7900	7.15543572E-03	7.153E-03	.98218	24.037	1.57992272E

8000	7.17504951E-03	7.169E-03	.9799	24.062	1.48377702E-
8100	7.18039698E-03	7.183E-03	.97032	24.084	1.63104331E-
8200	7.19598947E-03	7.197E-03	.9837	24.107	1.57293534E-
8300	7.20898413E-03	7.213E-03	.98284	24.133	1.62477465E-
8400	7.23872467E-03	7.233E-03	.98395	24.165	1.61961624E-
8500	7.25029053E-03	7.249E-03	.98413	24.191	1.55224346E-
8600	7.26585438E-03	7.262E-03	.96645	24.213	1.61966481E-
8700	7.27118909E-03	7.276E-03	.98311	24.236	1.53788111E-
8800	7.29029898E-03	7.292E-03	.98576	24.262	1.73074434E-0
8900	7.31872378E-03	7.312E-03	.98222	24.296	1.79512539E-0
9000	7.32848987E-03	7.331E-03	.98787	24.328	2.01772865E-0
9100	7.35422477E-03	7.352E-03	.98334	24.363	1.91222994E-0
9200	7.365312E-03	7.368E-03	.98252	24.39	1.99960462E-0
9300	7.39766809E-03	7.391E-03	.97922	24.43	2.02730711E-0
9400	7.40387019E-03	7.41E-03	.97872	24.463	2.09087274E-0
9500	7.44061889E-03	7.433E-03	.97912	24.502	2.11204902E-0
9600	7.44725639E-03	7.452E-03	.98042	24.536	2.08542061E-0
9700	7.48042636E-03	7.477E-03	.98284	24.58	2.05934628E-0
9800	7.49280232E-03	7.495E-03	.98248	24.612	1.88290108E-0
9900	7.5197501E-03	7.513E-03	.97772	24.644	2.10888904E-0
10000	7.52813973E-03				
10100	7.54932619E-03				
10200	7.58637368E-03				

Figure 48: Printout of Data Reduction Results

FIGURE 49

*** FATIGUE DATA ANALYSIS ***

SPECIMEN IDENTIFICATION = CP.DA2

NUMBER OF DATA POINTS = 64

MAXIMUM LOAD (MN) = 9.55E-03

MINIMUM LOAD (MN) = 9.55E-04

THICKNESS (M) = .0127

WIDTH OF SPECIMEN (M) = .0254

NOTCH LENGTH (M) = 6.35E-03

TEST ENVIRONMENT = AIR

TEST TEMPERATURE (C) = 25

TEST FREQUENCY (HZ) = 8

R-RATIO (P1/P2) = .1

N(I)	A(I)	A(R)	MCC	DK(I)	DA/DN(I)
1700	6.3074828E-03				
1800	6.31750758E-03				
1900	6.3147738E-03				
2000	6.327985532E-03	6.324E-03	.70415	22.926	4.21387105E-08
2100	6.33527254E-03	6.327E-03	.69827	22.929	4.35951773E-08
2200	6.321152333E-03	6.331E-03	.7896	22.933	5.61129498E-08
2300	6.33754952E-03	6.335E-03	.8688	22.938	5.870346642E-08
2400	6.34529027E-03	6.343E-03	.857	22.947	6.68294238E-08
2500	6.354850266E-03	6.353E-03	.97552	22.958	8.876929332E-08
2600	6.36167742E-03	6.359E-03	.97497	22.964	9.588397733E-08
2700	6.364863302E-03	6.37E-03	.96679	22.977	1.01063778E-07
2800	6.38033228E-03	6.38E-03	.97437	22.988	1.14354764E-07
2900	6.4003423E-03	6.394E-03	.97879	23.004	1.25532574E-07
3000	6.40307015E-03	6.407E-[illegible]	.98257	23.018	1.43832215E-07
31[illegible]	6.4221598E-03	6.42[illegible]	.98775	23.033	1.51720113E-07

3200	6.43306401E-03	6.436E-03	.9821	23.052	1.52316335E-0
3300	6.45667943E-03	6.455E-03	.98861	23.074	1.5147306E-07
3400	6.47438167E-03	6.47E-03	.9877	23.091	1.31808183E-0
3500	6.48345665E-03	6.481E-03	.94984	23.104	1.38388051E-0
3600	6.48980788E-03	6.492E-03	.9678	23.117	1.33948942E-0
3700	6.49842578E-03	6.504E-03	.98523	23.132	1.56063239E-0
3800	6.52925322E-03	6.523E-03	.97942	23.155	1.76406182E-0
3900	6.5401277E-03	6.543E-03	.98784	23.179	1.95269422E-07
4000	6.56911155E-03	6.564E-03	.98934	23.205	2.11336323E-07
4100	6.58133267E-03	6.583E-03	.99354	23.228	2.10076636E-07
4200	6.60350198E-03	6.608E-03	.98546	23.26	2.02733551E-07
4300	6.63243885E-03	6.627E-03	.98265	23.284	1.85196857E-07
4400	6.6523205E-03	6.646E-03	.98466	23.308	1.83499816E-07
4500	6.65683765E-03	6.663E-03	.98159	23.33	1.6679342E-07
4600	6.67535245E-03	6.675E-03	.98988	23.346	1.64757597E-07
4700	6.69656592E-03	6.692E-03	.99235	23.369	1.76285368E-07
4800	6.70874714E-03	6.711E-03	.9946	23.393	2.09213149E-07
4900	6.7353521E-03	6.733E-03	.99531	23.422	2.23101511E-07
5000	6.75337899E-03	6.757E-03	.99516	23.455	2.36811306E-07
5100	6.78715684E-03	6.783E-03	.9974	23.49	2.48747073E-07
5200	6.8083093E-03	6.808E-03	.99735	23.525	2.50191492E-07
5300	6.83394678E-03	6.835E-03	.99608	23.562	2.37538572E-07
5400	6.85687118E-03	6.856E-03	.99234	23.592	2.32386541E-07
5500	6.88427271E-03	6.878E-03	.9921	23.623	2.4121534E-07
5600	6.89415045E-03	6.901E-03	.99367	23.656	2.57061326E-07
5700	6.9300482E-03	6.929E-03	.9896	23.696	2.61714529E-07
5800	6.95694958E-03	6.957E-03	.98939	23.737	2.66514054E-07
5900	6.99189326E-03	6.987E-03	.99745	23.782	2.70367119E-07
6000	7.008458E-03	7.012E-03	.99725	23.819	2.47633393E-07
6100	7.03619911E-03	7.034E-03	.99107	23.852	2.53344269E-07
6200	7.05855636E-03	7.056E-03	.99646	23.886	2.65424611E-07
6300	7.07866674E-03	7.086E-03	.99532	23.932	2.85512218E-07
6400	7.11885579E-03	7.116E-03	.99398	23.978	2.92010071E-07

6500	7.15186849E-03	7.147E-03	.99621	24.027	3.01365566E-
6600	7.17772334E-03	7.178E-03	.99578	24.076	3.13212665E-
6700	7.20489866E-03	7.208E-03	.99635	24.125	2.96892579E-
6800	7.23605513E-03	7.237E-03	.9965	24.172	2.99986847E-
6900	7.27518963E-03	7.269E-03	.99565	24.224	2.94547645E-
7000	7.2942975E-03	7.298E-03	.99404	24.272	2.98270726E-
7100	7.33070909E-03	7.327E-03	.9939	24.321	2.89949629E-
7200	7.34934536E-03	7.354E-03	.99542	24.367	2.88593621E-
7300	7.38924931E-03	7.384E-03	.99633	24.418	3.0451846E-07
7400	7.41228571E-03	7.414E-03	.9971	24.469	3.08529618E-0
7500	7.44637146E-03	7.447E-03	.99812	24.527	3.26453053E-0
7600	7.48042636E-03	7.477E-03	.99845	24.58	3.47727025E-0
7700	7.51224201E-03	7.517E-03	.98892	24.651	3.44342079E-0
7800	7.54932619E-03				
7900	7.60047736E-03				
8000	7.60796778E-03				

Figure 49: Printout of Data Reduction Results

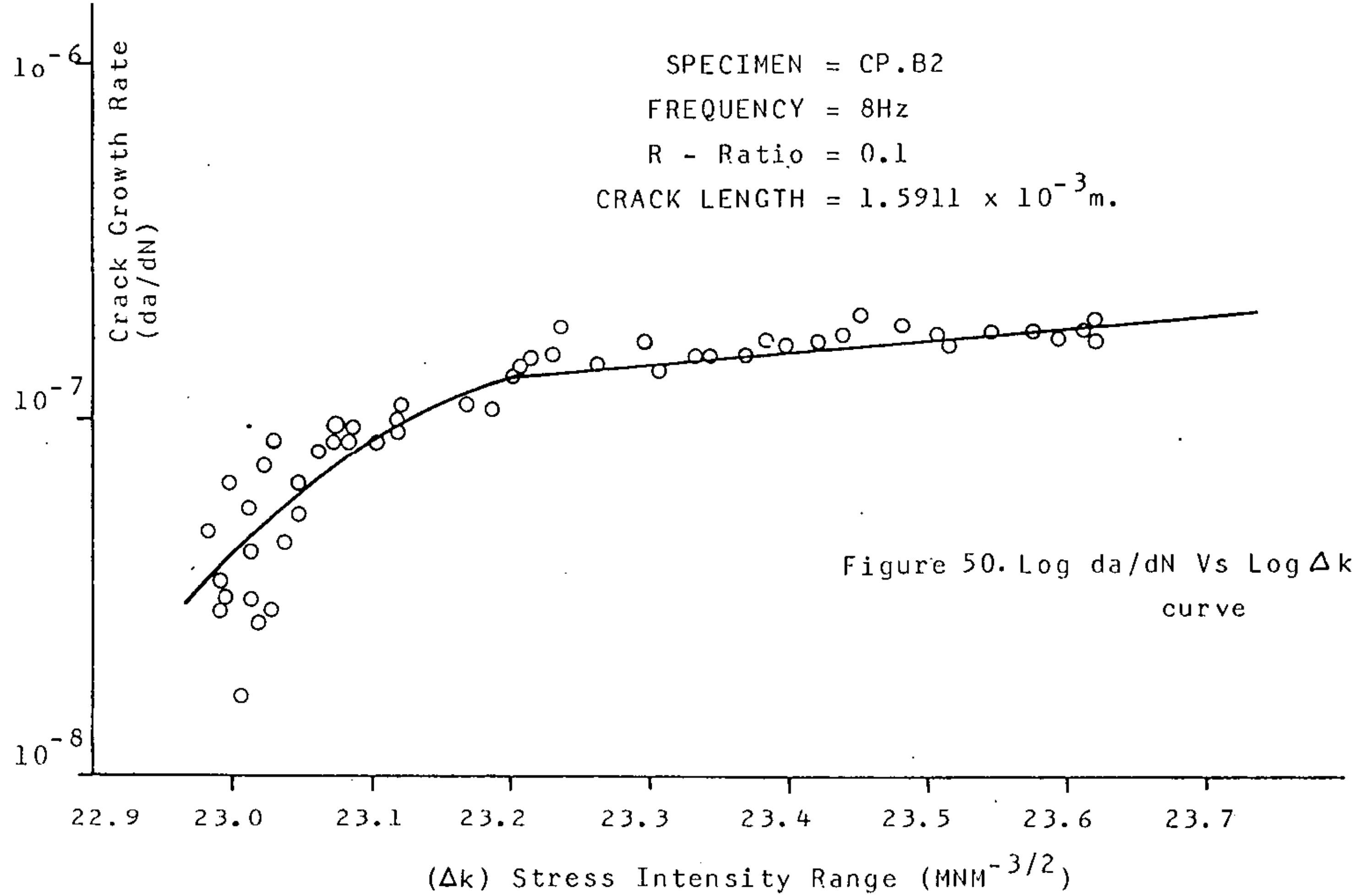

Figure 50. Log da/dN Vs Log Δk curve

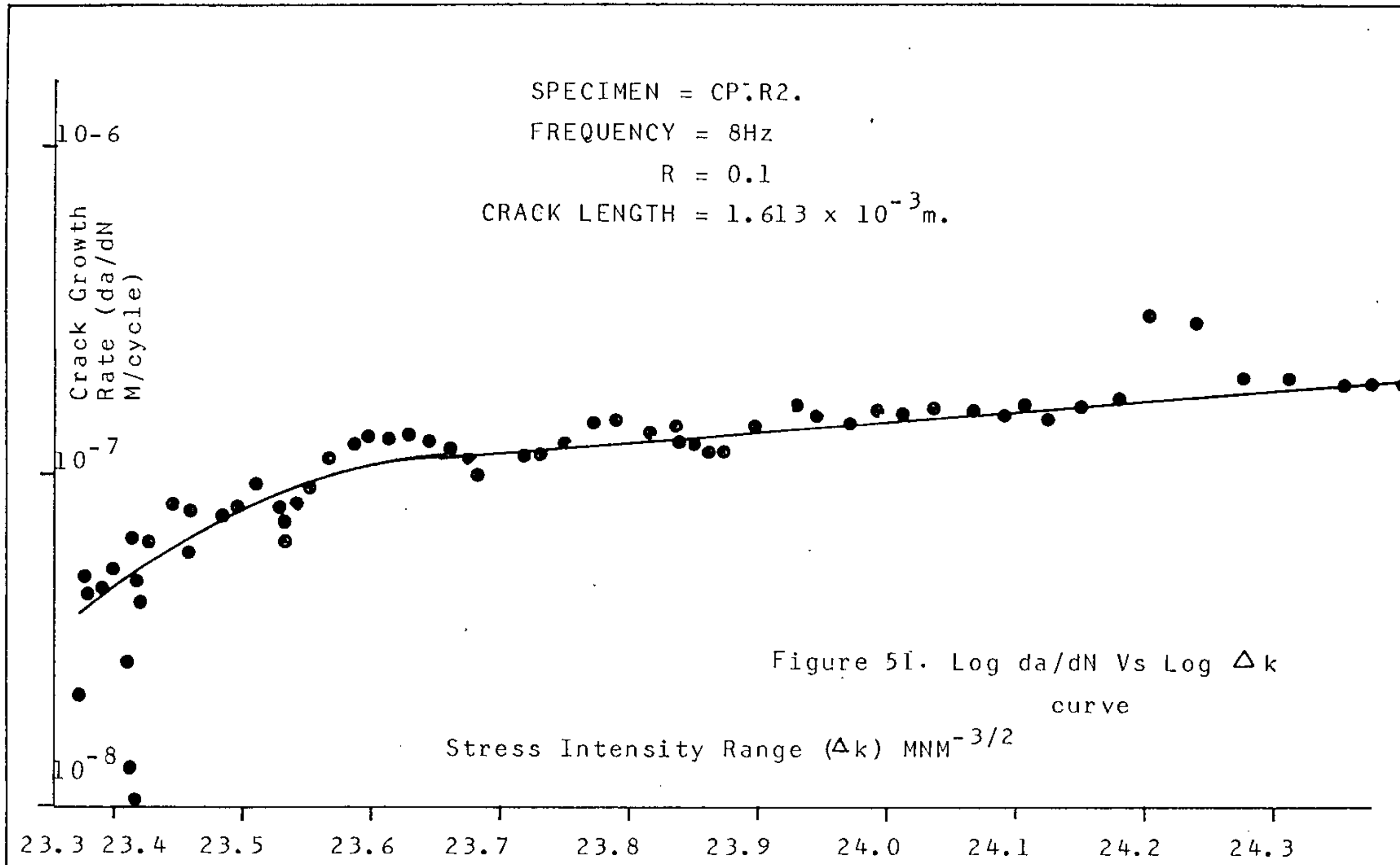

Figure 51. Log da/dN Vs Log Δk curve

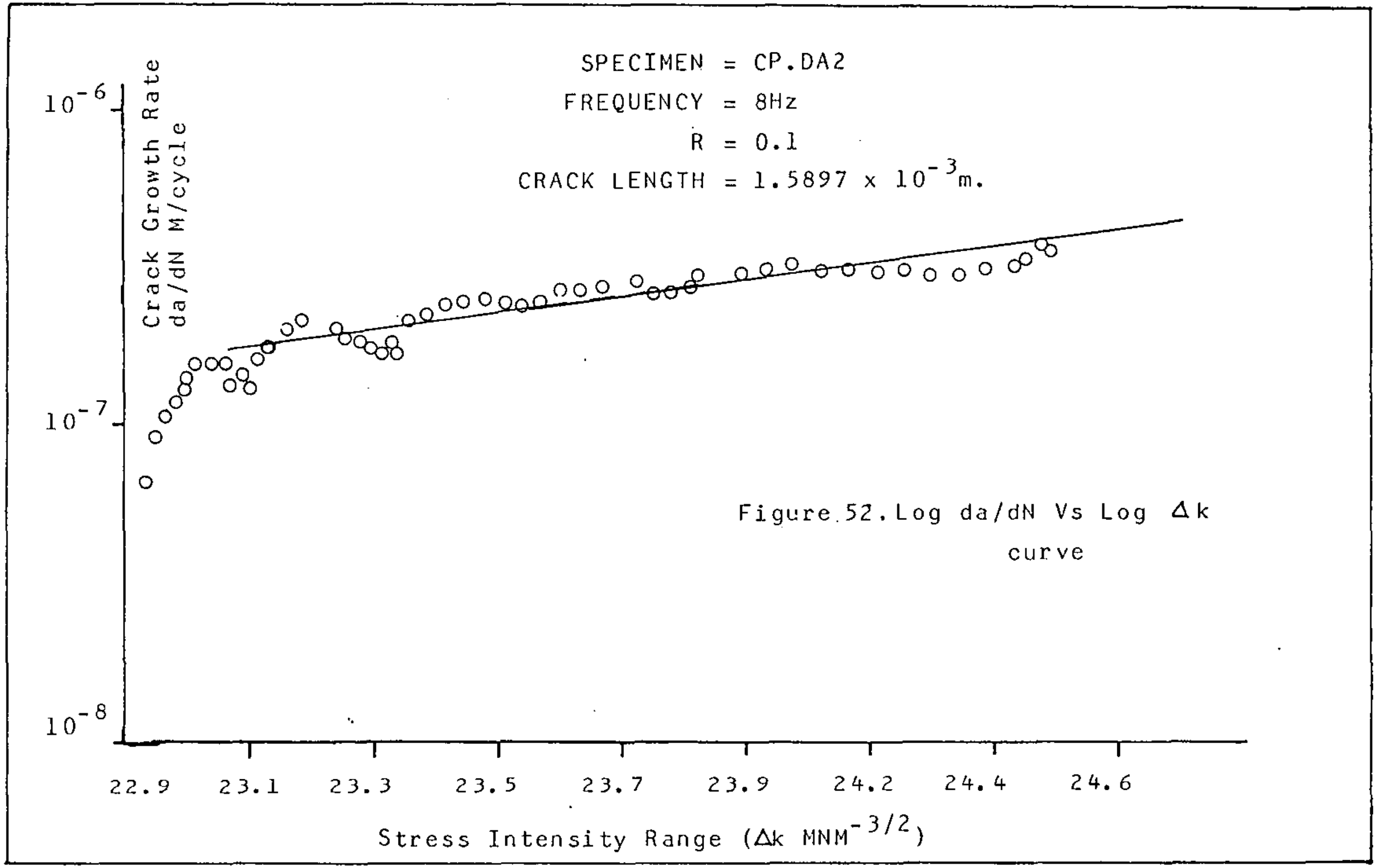

Figure 52. Log da/dN Vs Log Δk curve

CHAPTER 7.0

DISCUSSION

7.1 Fatigue Crack Growth Measurement by Optical and Electrical Potential Drop Method

The fatigue crack length was measured automatically, i.e. by the direct current potential difference method and optically by a travelling microscope. The crack growth readings were taken after every 100 cycles and compared with target values.

During the fatigue precracking the optical crack measurements are restricted to measurements of the crack length on the side surfaces of the specimens. The crack front was, however, slightly curved (as shown in Figure 53) and the optically measured crack length therefore underestimated the length of the real crack. By contrast, the direct current potential difference method measures current across the uncracked ligament. This current is proportional to the average area of the uncracked ligament, and hence this method gives an average value to the crack length. This is a more accurate and reliable method of measuring the length of the crack.

Figure 53. Fatigue Crack Front.

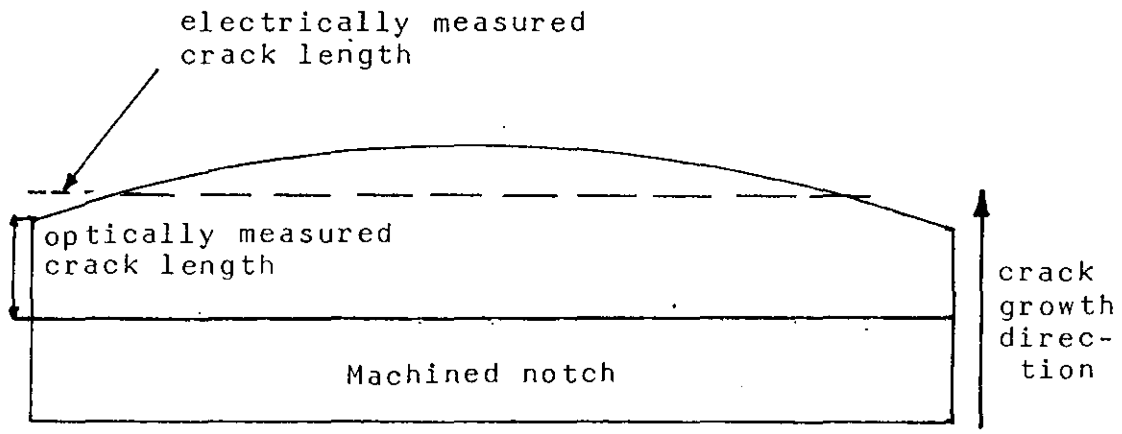

The fatigue cracks do not grow through the test specimens with crack fronts Parallel to the front and back faces of the test specimens, but are convex to the direction of the crack growth. The extent of the curvature does not usually remain constant in the test but tends to increase as the crack tip stress intensity factor increases due to the side face plasticity effect on the crack motion. In these circumstances, a calibration based on an initial crack length with a particular curvature under-estimates subsequent crack lengths if the curvature of the crack front increases. This could lead to errors in the results of the crack measurements.

In making the potential drop measurements across very small cracks a possible source of error may be present in the form of substantial plastic deformation in the material ahead of the crack tip. The change in shape of the crack tip and the change in the resistivity of the plastically deformed material ahead of the crack tip could significantly alter the potential drop values even before any true crack propagation occurs.

The crack length resolution of an electrical potential system is a function of the instrument sensitivity for a given specimen geometry, and is limited primary by the level of the noise in the system. The sensitivity, or equivalent crack growth to produce a full scale output, depends on the amplifier gain, the specimen geometry, the placement of the potential lead wires, and the applied current to the specimen.

It has been shown that the positioning of the current and potentials leads are important,[74-76] because large differences in sensitivity and reproducibility are produced by changes in the leads positions. Figure 54 shows the current lead attachments points, i.e. by the letters A and B, namely on the top surface close to the crack plane or distance from the crack plane and thirdly on the side faces. The potential probes are usually placed adjacent to the crack plane as shown by the points P. In this work the current was passed through A_3 and potential drops values were measured at points P_2.

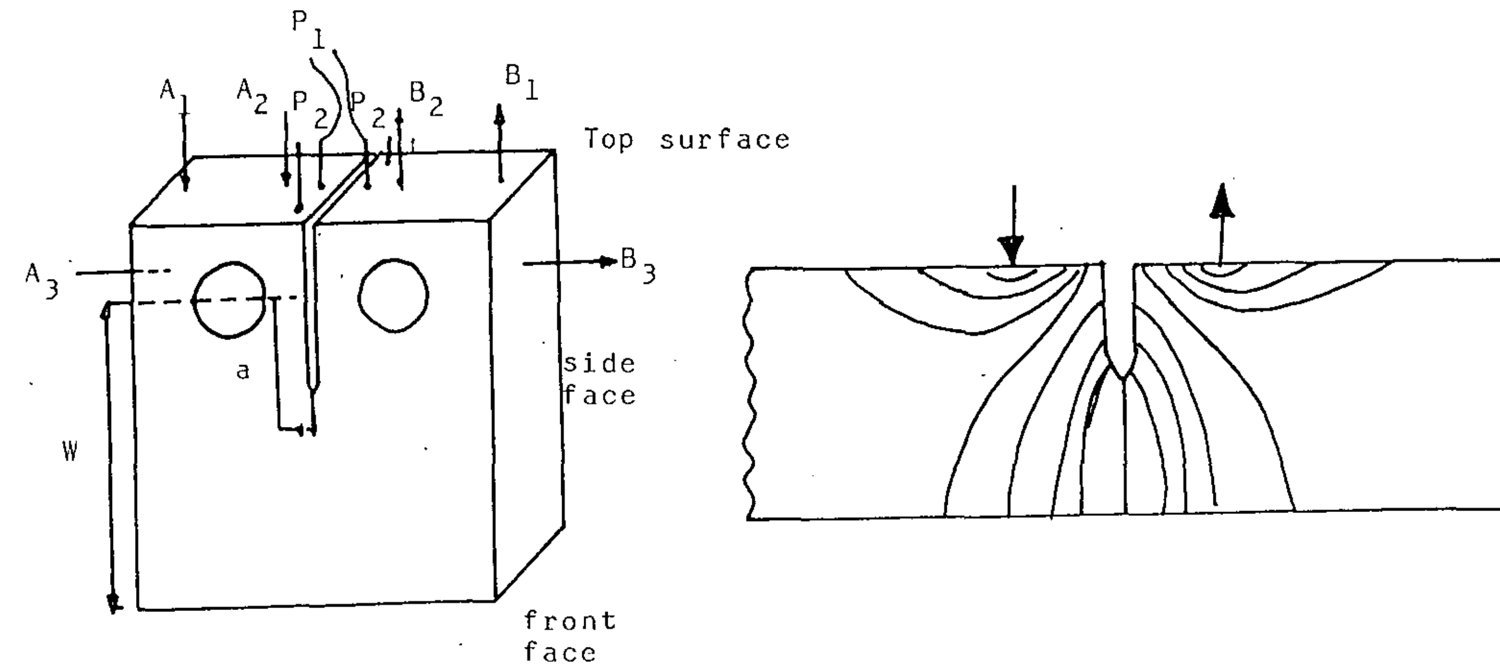

Fig. 54 (a) Compact tension specimen with alternative current lead and potential probe attachment points.

(b) non-uniform current configuration

In CTS specimens the current density is not uniform throughout the specimens and so different current lead positions will lead to different calibrations. In particular, it has been found that the potential field near the crack plane in this type of specimens is influenced by the holes for the loading pins. Care was therefore taken to ensure that the loading pins were not tight and did not result in variable electrical resistance in the region of the holes.

With careful potential drop calibration and careful attachment of the leads, reliable measurements of crack lengths should be achievable. This is seen in the results of crack growth measurements which show that the electrical potential technique does provide more reliable and accurate measurements of the fatigue crack lengths than the optical method. Furthermore the system can be readily interfaced with data acquisition devices or an automated material test system. The system provides high crack length resolution and measurement sensitivity.

7.2 Microscopy

It can be seen from the micrographs (Figure 46), that the fatigue crack propagates both through transformed (β) i.e. it is transgranular and between equi-axed grains of (α) phase and transformed (β) phase, i.e. is intergranular. Poorly developed striations were evident on the fracture surface of the specimen. The formation of regular striations requires (a) many available slip systems and easy cross slip to accommodate the (usually curved) crack front and to facilitate continuity of the crack front through adjacent grains; and (b) preferably more than one possible crystallographic plane for crack growth. If these requirements are not fulfilled slip will be irregular and fine periodic striations cannot develop. The orientation of a particular grain may be suitable for the generation of regular striations, but the limited possibilities for slip may prevent striation formation over some length along the crack front in adjacent grains of other orientation. In such cases poorly defined striations will usually be observed in a few isolated grains.

Only one of the specimens was fractured because the need to conserve the other precracked specimens for the high temperature crack propagation tests. This is the reason why very little work was carried out on the microscopy.

7.3 Fatigue Crack Growth Rates

The fatigue crack growth rates were obtained from the crack length versus cycles data (a versus N), by the incremental polynomial procedure. In this procedure a second order polynomial is fitted through seven data points at a time and the resulting polynomial differentiated and evaluated to give the gradient at the middle point.

The fatigue crack growth rates obtained were intermediate growth rates, i.e. 10^{-8} to 10^{-6} meters per cycle. The calculated crack growth rates compare favourably with other people's results, i.e. from 10^{-8} to 10^{-6} m/cycles at high stress intensity range (20 to 40 $MNm^{-3/2}$). The double logarithmic plot (Fig.50-52)of the crack growth rates (da/dN) versus the stress intensity range (Δk) shows that most of the data fall on a straight line, i.e. region B in the s-shaped curve shown in Figure 9. The region B represents the fatigue-crack propagation behaviour above the threshold value, which can be represented by the $da/dN = A(\Delta k)^m$. For the intermediate growth rates (region B), fatigue crack growth occurs predominantly by a transgranular ductile striation mechanism and is little affected by microstructure, mean stress and specimen thickness.

Although the data compares favourably with other people's work, it should be treated with caution over the reliability, and reproducibility, because of very short crack length which is not established and small range of stress intensity amplitude (Δk). But the results are encouraging and show that confidence can be placed on results produced by the system.

7.4 General Assessment of the System

From the results obtained in the precracking tests and the discussions in the previous sections, it is possible to conclude that the test system both (software and hardware) meet the objective set out in Section 4.1. The results show that it is possible to precrack different compact tension specimens to preset crack lengths. The developed software is very flexible, i.e. it can be used for different materials and for different sizes and types of specimens.

In this work, servo controls are used to provide the closely regulated testing force required for accurate, repeatable results. A servo controlled testing machine ensures that the actual load generated by the machine's power unit at any time is of the desired value programmed into the testing machine. Such control capability effectively eliminates the variability encountered in manually controlled open-loop testing systems.

7.4.1 Speed of Cycling

In the fatigue precracking tests the speed of cycling was limited to 8 to 12 Hz (depending on load amplitude). This is much slower than is often used in precracking using systems other than servo-hydraulics and is due to the following reasons:

(i) The software is written in a high level language (Basic) and is relatively slow. However, this could be speeded up but at the expense of less points per load cycle and hence is less accurate in the generation of the required load pattern.

(ii) The cycling speed is largely limited by the capacity of the hydraulic pump and servo-valve. It had been established that the practical limit for the stroke amplitude in use is about 15 Hz.

Despite the apparently low cycling speed, the specimens were fully precracked within an hour to an hour and a half. This is because a relatively high stress intensity amplitude was used to initiate and propagate the early crack.

Available evidence suggests that the speed of loading has little effect on the growth rate characteristics of material over the range 0.25 to 100 Hz although the growth rate is likely to be slightly faster at lower loading speeds.

7.4.2 Accuracy

An 8-bit convertor was used to generate the analog output command signal to the test machine. This has a theoretical accuracy of $\pm$ 0.4 percent. The servo-hydraulic machine has an overall accuracy of about $\pm$ 0.2 percent. The total system therefore possesses an accuracy of about $\pm$ 0.6 percent. This appears to be reasonable for general mechanical testing, although a higher degree of accuracy would be preferable. Unfortunately a 12-bit D-A convertor is not available for the Apple microcomputer. Twelve bit A-D convertors available and one of these was used to read in crack length signals from the specimen. This convertor has an accuracy figure of $\pm$ 0.05 percent. The error introduced by this is therefore negligible, and the total crack length reading error is governed by error in the potential drop measurement equipment and method more than by the A-D conversion devices. The possible sources of errors in the potential drop measurement across the crack plane were discussed in an earlier section.

7.4.3 Data Handling and Analysis

Data from the test are fed directly into the computer during the tests and stored into data files on flexible diskettes , at the end of the test. The file could be subsequently retrieved by another computer program, for further analysis. The output (results) from these programs could then be displayed on the video monitor or printed on paper using the printer. This process minimises data handling and speeds up the analysis of the data.

7.4.4 Effect of Load Changes

The order in which loads of varying amplitude are applied can have a profound influence on rates of crack growth.[77,78,79] In general a fatigue crack grows at the expected rate when the load is increased but is usually retarded for a time following load reductions. Basically, interactions occur because of the compressive residual stresses which arise at a crack tip when a load is removed, the wake of plastically deformed material adjacent to the crack surfaces which may cause crack closure before the minimum load is reached.

7.5 Potential for Further Development

The system can be developed to perform other related crack propagation tests. In view of the fact that the system is computer controlled, the modifications required are in the software and may be easily achieved.

A very significant advantage of an automated materials test system is the ability to conduct tests based on the control of a "calculated" variable. In most non-automated materials test systems, the parameters which may be directly controlled by the servo system are limited to load, stroke and strain. However, it is often desirable to control other parameters such as true strain or the stress intensity factor. These parameters are more closely related to the specimen material properties. Although analogue devices have been constructed to allow control of some of the more common material parameters, this procedure is considerably less versatile than the calculated variable control possible using a digital computer system.

The most commonly used calculated-variable tests are listed in Table 7.1.

TABLE 7.1 Common Calculated-Variable Tests:

Type	Test	Control Variables
Monotonic	Constant true Strain rate	$E_{true} = Ln(e_{eng} + 1)$
	Yield surface Probe	Yield condition = f(stress, strain)
Fracture Mechanics	Constant crack growth rate	$\Delta k = f(\sigma, a) = \text{constant}$
	Crack-growth theshold test	$\Delta k = f(\sigma, a)$, Δk decreasing
Fatigue	Plastic strain limit control	$e_{plastic} = e_{total} - \sigma/E$
	Transition fatigue life	$e_{plastic} = e_{elastic}$
	Thermomechanical fatigue	$e_{mechanical} = e_{total} - e_{thermal}$

The micro-computer software developed in this work can be modified slightly to perform the following tests:-

7.5.1 Fatigue-Creep-Interaction at High Temperature

Several recent papers (47,51,52) have demonstrated that dwell periods at peak stress can significantly reduce the number of cycles to failure in low cycle fatigue tests on titanium alloys and can cause enhanced growth rates in fatigue crack-propagation tests. It has been widely believed that dwell on load periods could have a significant effect only at elevated temperatures, where creep makes a large contribution to deformation behaviour. In all cases cleavage or quasi-cleavage facet formation has been intimately linked with the dwell sensitive fatigue response.

The micro-computer software can be modified to perform the crack propagation tests on the precracked compact tension specimens at high temperature (300-400°C) with hold times. This method will allow the measurement of the crack length after every 100 cycles by direct potential current method automatically at peak load (as shown in Figure 55) the storage of the crack growth data on file and the subsequent analysis of the data by the use of other computer software programs.

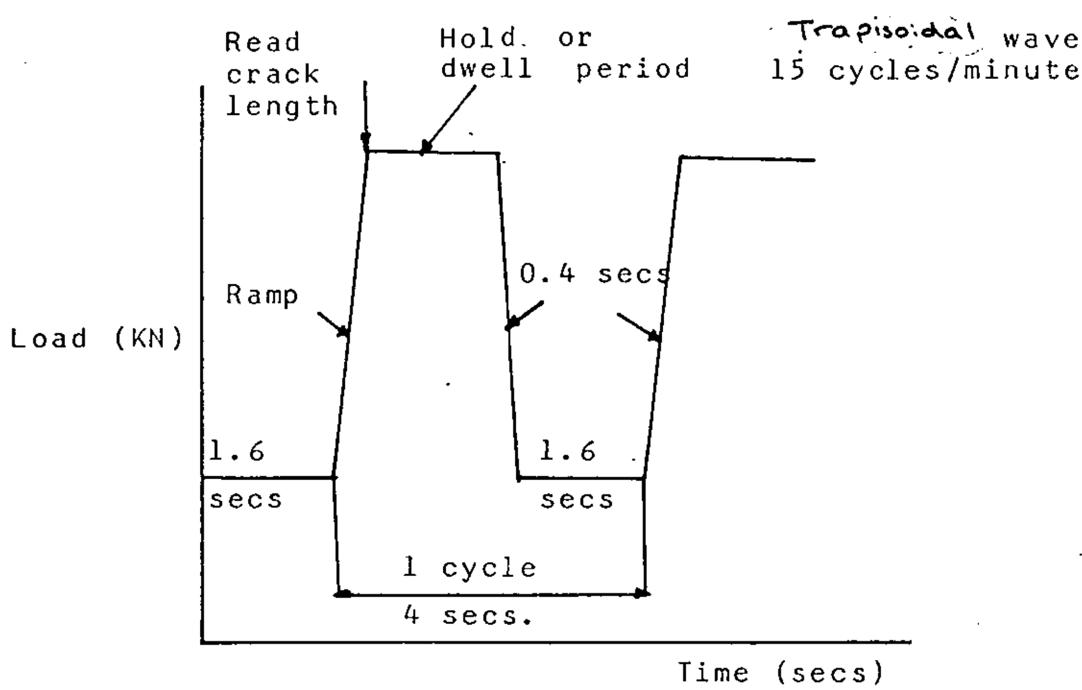

Fig. 55: Typical hold-time test

The software will carry out the following functions:-

(i) generate ramp and hold signals;

(ii) read the crack length voltage at maximum load after every 100 cycles.

7.5.2 Constant-Stress-Intensity Range Crack Growth Test

In fatigue crack growth tests, it is common to determine the crack growth rate (da/dN) as a function of the stress intensity factor (Δk). Limitations exist when constant amplitude load or displacement tests are performed. When the cyclic load amplitudes are constant, the stress intensity factor increases as the crack grows. If the displacement amplitude is constant then the stress intensity factor decreases as the crack grows. It is sometimes desirable (e.g. when studying crack growth through a weld) to perform the test with a constant stress intensity factor. To conduct such tests it is necessary to frequently update the load or displacement control amplitude as the crack length increases during the tests to maintain a constant value of Δk. Updates are typically performed on a block basis rather than cycle by cycle in order to keep interruptions to cycling at a minimum.

7.5.3 Thermomechanical Fatigue Test

Many engineering materials, e.g. turbine alloys, operate under conditions in which significant deformation is caused by both load and temperature fluctuations. For laboratory materials characterization these conditions are idealized in a thermomechanical fatigue test. In this test it is necessary to resolve and control the thermal and mechanical strains independently. Total strain is read from a high temperature extensometer. The software determines the thermal strain component by correlating temperature readings with stored values in a table previously determined and the mechanical strain then worked out as the difference between total and thermal strain.

To conduct such a test, it is necessary to integrate the automated sub-system with the temperature control loop as well as the load- and strain-control loops. Data must be acquired from the strain, load, and temperature transducers. Furthermore, temperature as well as strain on load must be programmed. The ability to select an independent or phased relationship between the two control channels is desirable.

CHAPTER 8

CONCLUSION

A system for performing controlled fatigue precracking of compact tension specimens automatically using an Apple II micro-computer, a servo-hydraulic test machine and a d.c. electrical current crack measurement device has been developed and demonstrated and found to work satisfactorily.

In a comparison between the optical and electrical method, the electrically determined fatigue precrack length is more accurate and representative of the average crack length than the optically (side-on) measured crack length. Furthermore the electrically determined fatigue precrack is more reproducible than the optically measured crack length, as the variable curvature of the fatigue crack front leads to variable visible cracks on the sides of the specimen.

Microscopic observations show that the crack length propagates both through transformed β phase, i.e. the crack path is transgranular, and between α and β phases, i.e. the crack path is intergranular. The formation of the striations were evident on the fracture surface. The crack growth rates for stress intensity range of approximately 25 MNm^{-2} are in the range 10^{-8} - 10^{-6} m/cycle. The double log plot of the crack growth rate (da/dN) versus stress intensity range (Δk) shows that the most of the data fall on a straight line.

9.0 LIST OF TABLES

10.0 LIST OF FIGURES

continued

LIST OF FIGURES

continued

LIST OF FIGURES

11.0 REFERENCES

(1) JOHNSON, H.C.; "Closed loop principle applied to material testing"; Test Engineering; Sept. (1965).

(2) RICHARDS, F.D. and WETZEL, R.M.; Materials Research and Standards; Vol. 11 No. 2; (1971); P. 19.

(3) BITTENCE, J.C.; Materials Engineering; Feb. (1979); PP 45-50.

(4) MORTON, P.H.; Phil. Trans. R. Soc.; Vol 282; (1979); P. 410.

(5) IRWIN, G.R.; Journal of Applied Mech; Vol. 25; (1957); P. 361.

(6) CONGLETON, J. and PETCH, N.J.; Acta Met; Vol. 14; (1966); P. 1179.

(7) MARSH, D.M.; Fracture of Solids; (1963).

(8) ROLF, S.T. and BARSOM, J.M.; "Fracture and Fatigue control in structures; Application of Fracture Mechanics; PRENTICE-HALL, INC. Publication; (1977); P. 16,60.

(9) HEAD, K.E.; "The Growth of Fatigue Cracks"; The Philosophical Magazine; Vol. 44; Series 7; (1953) P. 925.

(10) FROST, N.E. and DUGDALE, D.S.; "The Propagation of Fatigue cracks in sheet specimen"; Journal of the Mechanics and Physics of Solids; Vol. 6, No. 2; (1958); P. 92.

(11) MCEVILY, A.J. and ILLG, W.; "The Rate of crack propagation in Aluminium alloys"; NASA Technical Report No. 4394; Sept. (1956).

(12) LIU, H.W. "Crack Propagation in Thin Metal Sheets under Repeated Loading", The Journal of Basic Engineering; Trans ASME Series D Vol. 83, (1961) P. 23.

(13) LIU, H.W.; "Fatigue Crack Propagation and Applied Stress Range - An Energy Approach", Journal of Basic Engineering; Trans. ASME Series D, Vol. 85; (1963) P. 16.

(14) IRWIN, G.R.; "Analysis of Stress and Strains Near the End of a Crack Traversing a Plate", Journal of Applied Mechanics, Vol. 24, TRANS ASME, Vol. 79, (1957), P. 361.

(15) PARIS, P.C. and ERDOGAN, F. " A Critical Analysis of Crack Propagation Laws"; Journal of Basic Engineering; TRANS ASME, Series D Vol. 85; (1963); P. 528.

(16) RICE, J.R.; "Fatigue Crack Propagation"; ASTM STP No. 415; (1967); P. 301.

(17) MILLER, G.A.; "TRANS A.S.M. Vol. 61; (1968); P. 442.

(18) PARIS, PC. and SIH, G.C.; "Strain Analysis of Cracks"; ASTM STP No. 381; (1965).

(19) WEBER, J.H. and HERTZBERG, R.W.; "Effect of Thermo-chemical Processing on Fatigue Crack Propagation"; Met. Transaction; Vol. 4 No. 2; (1973); P. 595-601.

(20) ZWEBERS, C.; "On the strength of notched composites"; Journal of Mech. Phys. Solids; Vol. 19, No. 3; (1971); P. 103-116.

(21) GELL, M. and LEVERANT, G.R.; Acta Met; Vol. 16; (1968) P. 553.

(22) BROEK, D.; Engineering Fracture Mech; Vol. 1; (1970); P. 691.

(23) PELLOUX, R.M.; ASTM TRANS QUART; Vol. 62; (1969); P. 281.

(24) PELLOUX, R.M.; Engineering Fracture Mech; Vol. 1; (1970); P. 697.

(25) LAIRD, C.; "Fatigue Crack Propagation"; ASTM STP No. 415; (1967); P. 131.

(26) LAIRD, C. and DE LA VEAUX, R.; Met Transaction A; Vol. 8A; (1977); P. 657.

(27) NEUMANN, P., VEHOFF, H. and FUHLROTT, H.; Proc 4th Int. conf on Fracture; Waterloo; (1977).

(28) IRWIN, G.R.; "Linear Fracture Mechanics, Fracture Transition and Fracture Control"; Eng Fracture Mech; Vol. 1 No. 2; Aug. (1968).

(29) LINDLEY, T.C. and RICHARDS, C.E.; "The Relevance of Crack Closure to Fatigue Crack Propagation"; Material Science Eng.; Vol. 14 No. 3; (1974); P. 281-293.

(30) FROST, N.E., POOK, L.P. and DENTON, K.; "A Fracture Mechanics Analysis of Fatigue Crack Growth Data for Various Materials"; Eng. Fracture Mechanics, P. 281-293.

(31) COFFIN, L.F.; "Fatigue at High Temperature"; Fatigue at elevated temperatures; ASTM STP 520; (1973); PP 5-34.

(32) COFFIN, L.F.; "Fatigue at high temperature"; Proc 4th INT Conf on Fracture. Vol. 1; (1977); Waterloo Conference; P. 263.

(33) SKELTON, R.P. and BUCKLOW, J.I.; "Journal of Metal Science"; Feb (1978); P. 64.

(34) PERRY, A.J.; Journal of Material Science; Vol. 9; (1974); P. 1016.

(35) RAJ, R. and ASHBY, M.F. Acta Met; Vol. 23; (19750; P. 653.

(36) WELLS, C.H.; Acta Metallurgical, Vol. 17; (1969); PP 443-449.

(37) GELL, M. and LEVERANT, G.R.; "Fracture", (1969); P. 565; Publication Chapman and Hall.

(38) WELLS, C.H., SULLIVAN, C.P. and GELL, M.; "Metal Fatigue Damage"; Mechanisms, Detection, Avoidance and Repair; ASTM STP 495; (1971); PP 61-122.

(39) NINE, H.D. and WOOD, W.A.; Journal Institute of Metals; Vol. 95, (1967); PP 252-254.

(40) RONAY, M., REIMANN, W.H. and WOOD, W.A.; Transaction American Institute of Mining, Metallurgical and Petroleum Engineers; Vol. 223, (1965); PP 298-304.

(41) WELLS, C.H. and SULLIVAN, C.P.; Transaction Quarterly American Society for Metals; Vol. 61; (1968); PP 149-155.

(42) WELLS, C.H. and SULLIVAN, C.P. in "Fatigue at high temperature"; ASTM ST 459; (1969); PP 59-74.

(43) DUNCAN, R.M. et al; "The development of gas turbine materials"; Edited by G.W. Meetham; Publishers Applied Science; (1981); PP 72-74.

(44) YODER, G.R. et al; Met. Trans; Vol. 8a; (1977); P.1737.

(45) POLMEAR, I.; Light Alloy Metallurgy of Light Metals; Publishers Edward Arnold; (1981); P. 179.

(46) PETERS, M. et al; "Influence of Microstructure on the Fatigue behaviour of Ti-6Al-4V alloy"; (1980); Proc 4th Int Conf on Titanium; Kyoto: Japan.

(47) CHESNUTT, J.C. and PATON, N.E.; "Hold time effects on Fatigue Crack Propagation in Ti-6Al.4V and Ti-6Al"; (1980); Proc 4th Int Conf of Titanium; Kyoto: Japan.

(48) COFFIN, L.F.; Proceeding of ASME-MPC Symposium on Creep Fatigue Interaction"; (1976); P. 349.

(49) DAWSON, D. and PELLOUX, M.N.; Met Trans; Vol. 5A; (1974); P. 723.

(50) MIN, B.K. and RAJ, R.; Acta Met; Vol. 26; (1976); P. 1007.

(51) EVANS, W.J. and GOSTELOW, d.R.; "The effect of hold time on Fatigue Properties of β processed Titanium alloy"; Met Trans; Vol. 10A; (1979); P. 1837.

(52) IRVING, P.E. and BEEVERS, C.J.; "Microstructural Influences on Fatigue Crack Growth in Ti-6Al-4V"; Materials Science and Eng; Vol. 14; (1974); PP 229-238.

(53) PLUMBRIDGE, W.J.; Journal of Material Science; Vol. 7; (1972); P. 939.

(54) THOMPSON, A.W. and BACKOFEN, W.A.; Acta Met; Vol. 19; (1971); P. 597.

(55) TURNER, N.G. and ROBERTS, W.T.; Trans AIME; Vol. 242; (1968); P. 1223.

(56) MEYN, D.A.; Met. Trans; Vol. 2; (1971); P. 853.

(57) BATES, R.C. and CLARK, A.J.; Trans Am. Soc. Metals; Vol. 62; (1969); P. 380.

(58) PITTINATO, G.F.; Met Trans; Vol. 3; (1972); P. 235.

(59) BUCCI, R.J. et al; 5th Nat. Symp. on Fracture Mech; Univ of Illinois; (1971).

(60) STEIGERWALD, E.A. and HANNA, G.L.; Proceeding ASTM. Vol. 62; (1962); P. 885.

(61) JOHNSON, H.H.; Materials Research and Standards; Vol. 5; (1965); P. 442.

(62) LI-CHE-YU and WEI, R.P.; Materials Research and Standards; Vol. 6; (1966); P. 392.

(63) WEI, R.P. et al; "Fatigue Crack Propagation"; ASTM STP 415; (1967); P. 460.

(64) GANGLOFF, R.P. and WEI, R.P.; Met. Trans; Vol. 8A; (1977); P. 1043).

(65) RITCHIE, R.O. et al; International Journal of Fracture Mechanics; Vol. 7; (1971); P. 462.

(66) UNANGST, K.D. et al; Eng. Fracture Mechanics; Vol. 9; (1977); P. 725.

(67) WEI, R.P. and BRAZILL, R.L.; "An A.C. Potential System for Crack Length Measurement"; The measurement of crack length and shape during fracture and fatigue; C.J. Beevers et al Eds; conf; (1980); P. 190.

(68) SMITH, R.A.; "Calibrations for the Electrical Potential Methods of Crack Growth Measurement by a Direct Electrical Analogy"; Strain, Vol. 10; (1974); PP 183-187.

(69) CLARK, G. and KNOTT, J.F.; Journal of the Mechanics and Physics of Solids; Vol. 23; (1975); P. 47.

(70) RITCHIE, R.O. and BATHE, K.J.; International Journal of Fracture Mechanics; Vol. 15; No. 1; (1979); P. 47.

(71) ARONSON, G.H. and RITCHIE, K.J.; Journal of Testing and Evaluation; Vol. 7; (1975); P. 208.

(72) HEAS, T. and KREISKONTE, H.; "Symposium on development in material testing machine design"; Proc. Inst. Mech. Engrs; Vol. 180 No. 3A; (1965-66); P. 155.

(73) FONG, J.T. and DOWLING, N.E.; "Analysis of Fatigue Crack Growth Rate Data from Different Laboratories"; ASTMSTP 738; (1981); PP 171-193 and 333-337.

(74) BARNETT, W.J. and TROIANO, A.R.; "Crack Propagation in the Hydrogen-Induced Brittle Fracture of Steel"; Journal of Metal, Vol. 9; (1957); PP 486-494.

(75) SMITH, R.A.; "Calibration of the Electrical Potential Method of Crack Growth Measurement by Direct Electrical Analogy"; Strain; Vol. 10; (1974); PP 183-187.

(76) RITCHIE, R.O., GARRETT, G.G. and KNOTT, J.F.; "Crack Growth Monitoring; Optimisation of the Electrical Potential Technique using an Analogue Method"; Int. Journal of Fracture Mech.; Vol. 7; (1971); PP 462-467.

(77) SCHIJVE, J.; "Fatigue damage accumulation and incompatible crack front orientation"; Eng. Fracture Mech.; Vol.6; (1974); PP 245-252.

(78) WHEELER, O.E.; "Spectrum loading and crack growth"; Journal of Basic Eng.; Vol. 94D; 1972; PP 181-186.

(79) BRUSSAT, T.R.; "An approach to predicting the growth to failure of fatigue cracks subjected to arbitrary uniaxial cycling loading", ASTM STP 486; (1971); PP 122-147.

APPENDIX A

APPENDIX B

APPENDIX A

COMPUTERS

A.1 The Conceptual Computer

There are two main aspects of computer systems: hardware and software. The hardware refers to the electronic, mechanical and magnetic elements from which the computer is fabricated. Software refers to the totality of programs and programming systems used by a computer. These programs are all initially written on paper (software) before being transferred to some storage media (hardware), and completely control the computer's operation from start-up to shut-down.

Every computer contains five essential elements or units; the arithmetic logic unit (ALU), the memory unit, the control unit, the input unit and the output unit. The basic interconnection of these units is shown in Fig. 1. The arrows in this diagram indicate the direction in which data, information, or control signals are flowing. Two different size arrows are used; the larger arrows represent data or information that actually consist of a relatively large number of parallel lines, and the smaller arrows represent control signals that are normally only one or a few lines.

A.1.1 Arithmetic/Logic Unit

The ALU is the area of the computer in which arithmetic and logic operations are performed on data. The type of operation to be performed is determined by signals from the control unit (arrow 1). The data that are to be operated on by the ALU can come from either the memory unit (arrow 2) or the input unit (arrow 3). Results of operations performed in the ALU can be transferred to either the memory unit for storage (arrow 4) or to the output unit (arrow 5).

A.1.2 Memory Unit

The memory unit stores groups of binary digits (words) that can represent instructions (Program) which the computer

Fig. 1 Basic computer organization

EIG. 1

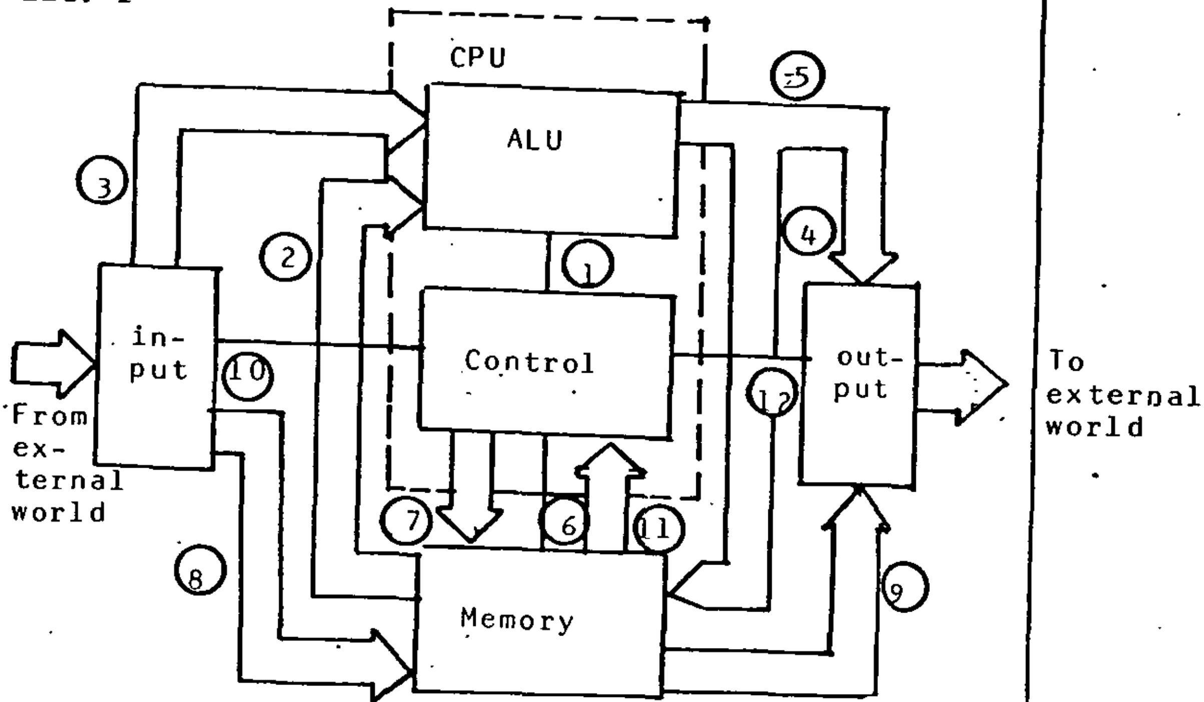

FIG. 2

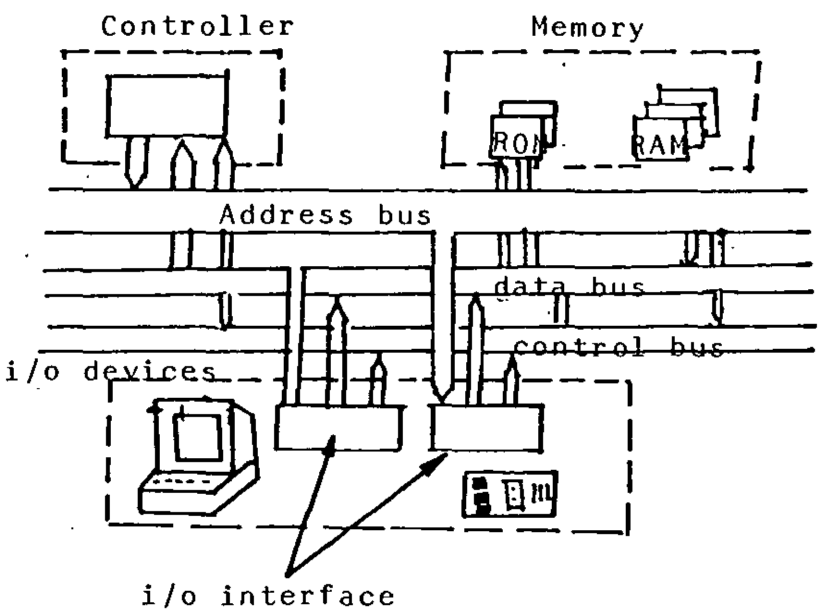

Fig. 2 The various component parts communicate through busses.

is to perform and the data that are to be operated on by the program. The memory also serves as storage for intermediate and final results of arithmetic operations (arrow 4). Operation of the memory is controlled by the control unit (arrow 6) which signals for either a read or a write operation. A given location in memory is accessed by the control unit, providing the appropriate address code (arrow 7). There are two different types of memory (ROM and RAM). ROM is random access read only memory: RAM is random access read write memory. (Random access means that any location in memory can be accessed in the same amount of time, an example of a memory device which is not random access is cassette tape in which values are accessed sequentially). Information can be read from memory into the ALU (arrow 2) or into the output unit (arrow a).

A.1.3 Input Unit

The input unit consists of all the devices used to take information and data that are external to the computer and put it into the memory unit (arrow 8) or the ALU (arrow 3). The control unit determines where the input information is sent (arrow 10). The input unit is used to enter the program and data into the memory unit prior to starting the computer. This unit is also used to enter data into ALU from an external device during the execution of a program. Some of the common input devices are keyboards, switches, teletypewriters, punch cards and punched paper-tape readers, magnetic-tape readers and analog-to-digital conventors (ADC).

A.1.4 Output Unit

The output unit consists of the devices used to transfer data and information from the computer to the "outside world". The output devices are directed by the control unit (arrow 12) and can receive data from memory (arrow 9), or the ALU (arrow 5), which are then put into appropriate forms for external use. Examples of common output devices are LED readouts, indicator lights, teletypewriters, printers, cathode ray tube displays and digital-to-analog conventers (DAC).

A.1.5 Control Unit

The function of the control unit should now be obvious. It directs the operation of all the other units by providing timing and control signals. In a sense, the control unit is like the conductor of an orchestra, who is responsible for keeping each of the orchestra members in proper synchronization. The unit contains logic and timing circuits that generate the signals necessary to execute each instruction in a program.

The control unit fetches an instruction from memory by sending an address (arrow 7) and a read command (arrow 6) to the memory unit. The instruction word stored at the memory location is then transferred to the control unit (arrow 11). The instruction word, which is in some form of binary code, is then decoded by logic circuitry in the control unit to determine which instruction is being called for. The control unit uses this information to generate the necessary signals for executing the instruction.

A.1.6 Central Processing Unit (CPU)

In Fig. 1 the ALU and control units are shown combined into one unit called the CPU. This is commonly done to separate the actual 'brains' of the computer from the other units.

A.2 The Bus System[1]

The three major components of the computer shown in Fig. 2 are interconnected by groups of wires called busses. The address bus communicates 16-bit values from the controller to memory and I/O. The data bus communicates 8-bit values from any component to the others. The control bus is used to communicate control and synchronization singles among the components. For example, if the controller is carrying out an instruction which says to store a value in a specific spot in memory, place the address of the desired memory location on the address bus. All devices on the address bus receive the signal, and it is up to circuitry on each device to determine if it should respond. Thus only the block of memory which the other busses to affect it. The controller places the value which is to be stored on the data bus and it too in course, the block of memory previously mentioned. In addition, the controller places a signal on the control bus which specifies that a memory write (as opposed to memory read) operation is to take place, and this causes the specified memory location to store the value appearing on the data bus in the memory location whose address appears on the address bus. Since most microprocessors use synchronous busses, no further communication is necessary (i.e. in an asynchronous bus, the controller would wait until it received a signal informing it that the memory operation had taken place).

A.3 Read and Write Operations[2]

During the execution of a program the control processing unit (CPU) constantly READING or WRITING into memory. The program may also call the CPU to read from one of the input devices or write into one of the output devices.

A.3.1 The READ Operation

The following steps take place during a READ operation:

(1) The CPU generates the proper logic level on its R/W line for initiating a READ operation. Normally, R/W = 1 for READ. The R/W line is part of the control bus and goes to all the memory and I/O elements.

(2) Simultaneously, the CPU places the 16-bit address code onto the address bus to select the particular memory location or I/O device which the CPU wants to receive data from.

(3) The selected memory or I/O element places an 8-bit word on the data bus. All nonselected memory and I/O elements will not affect the data bus, because their tristate outputs will be in the disabled (high-Z) condition.

(4) The CPU receives the 8-bit word from the data bus on its data pins, D_0 through D_7. These data pins act as inputs whenever R/W = 1. This 8-bit word is then latched into one of the CPU's internal registers, such as the Accumulator.

This sequence can be better understood with the help of a timing diagram showing the interrelationship between the signals on the barious buses, see Fig. 3. Everything is referenced to the Ø1 and Ø2 clock signals. The complete READ operation occurs in one clock cycle. The leading edge of Ø1 initates the CPU's generation of the proper R/W and

Fig. 3 Typical micro-computer timing for a READ operation

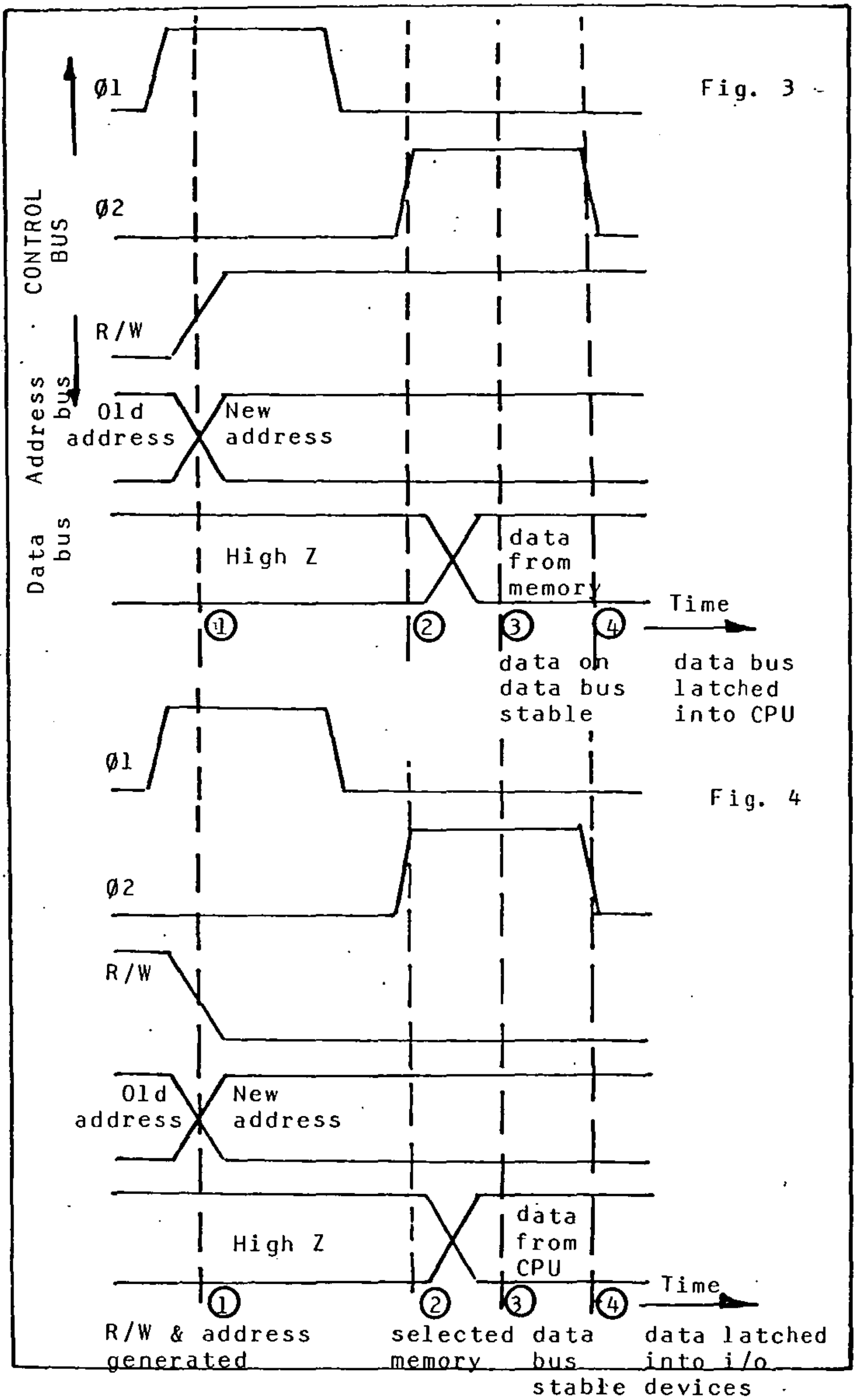

Fig. 4 Typical micro-computer timing for a WRITE operation

address signals. After a short delay, the R/W line goes High and the address bus holds the new address code (Point 1 on timing diagram). During the Ø2 pulse, the selected memory or I/O device is enabled (Point 2) and it proceeds to put its data word on the data bus, is in its high Z state, since no device connected to it has been enabled. At some point during the Ø2 pulse, the data on the data bus becomes stable (Point 3). The delay between the start of the Ø2, pulse and the data bus stabilizing depends on the speed of the memory and I/O elements. For memory this delay would be its access time. On the falling edge of Ø2, the data on the data bus are latched into the CPU (Point 4).

A.3.2 The WRITE Operation

The following steps occur during a WRITE operation:

(1) The CPU generates the proper logic level on the R/W line for initiating a WRITE operation. Normally R/W = 0 for WRITE.

(2) Simultaneously, the CPU issues the 16-bit address code onto the address bus.

(3) The CPU then places an 8-bit word on the data bus via its data pins D_0 through D_7, which are now acting as outputs. This 8-bit word typically comes from an internal CPU register, such as the Accumulator. All other devices connected to the data bus have their outputs disabled.

(4) The selected memory or I/O element takes the data from the data bus. All nonselected memory and I/O elements will not have their inputs enabled.

This sequence has the timing diagram shown in Fig. 4. Once again the loading edge of Ø initiates the R/W and address bus signals (Point 1). During the Ø2 Pulse the selected memory or I/O device is enabled (Point 2) and the CPU places its data on the data bus. The data bus levels become stabilized a short time into the Ø2 pulse. These data are then written into the selected memory location while Ø2 is high. If an I/O device has been selected, it usually latches the data from the data bus on the falling edge of Ø2 (Point 4).

A.4. Interfacing with the Analog World

Digital systems, e.g. computers, perform all their internal operations in binary or some type of binary code, owing to the increased accuracy possible, and the simplicity of the design. Any information that is to be input to a digital system must be put into binary form before it can be processed by the digital circuits. On the other hand, the outputs of a digital system are in some type of binary code and very often must be converted to a different form depending on how the outputs are to be used. Many devices are used on the input and/or output sides of digital systems to serve as the communications link to the outside world. (Fig. 5) Process-related I/O devices provide the means by which a digital system (i.e. computer) monitors and controls a physical process. On the input side, measurements of process parameters that are analog in nature are usually transduced (changed to a proportional electronic voltage or current) and sent to an analog-to digital converter, ADC, which converts the analog quantity to a corresponding digital representation.

A.4.1 Digital-to-Analog Conversion

Essentially, D/A conversion is the process of taking a value represented in digital binary code and converting it to a voltage or current which is proportional to the digital value. This voltage or current is an Analog quantity, since it can take on many different values over a given range. In order to explain the concept, the diagram of a 4-bit D/A converter is shown in Fig. 6. The same idea would hold true for the 8-bit D/A converter which is used for this project.

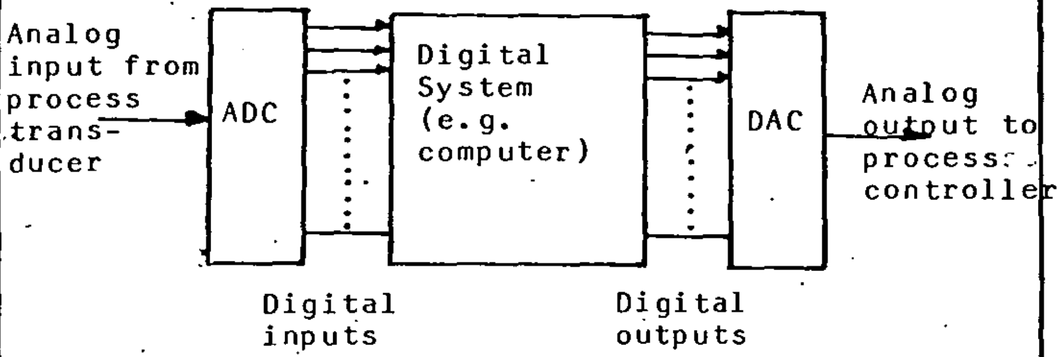

Fig. 5 ADC and DAC are used to interface a purely digital system with the Analog outside world[2]

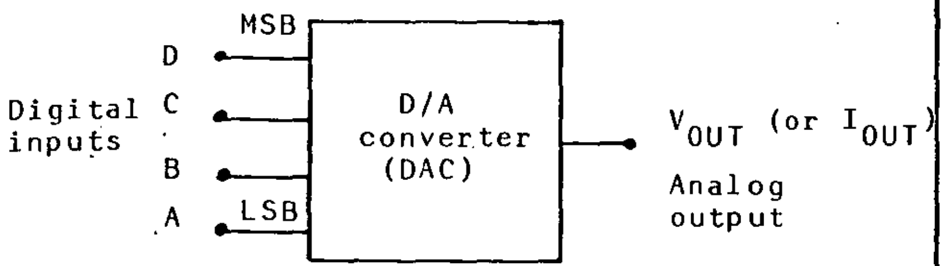

Fig. 6 Schematic representation of a 4-bit D/A converter[2]

D	C	B	A	V_{OUT}	
0	0	0	0	0	volts
0	0	0	1	1	
0	0	1	0	2	
0	0	1	1	3	
0	1	0	0	4	
0	1	0	1	5	
0	1	1	0	6	
0	1	1	1	7	
1	0	0	0	8	
1	0	0	1	9	
1	0	1	0	10	
1	0	1	1	11	
1	1	0	0	12	
1	1	0	1	13	
1	1	1	0	14	
1	1	1	1	15	volts

Fig. 7 4-bit D/A converter with voltage output[2]

The digital input D,C,B and A are usually derived from the output register of a digital system. The $2^4 = 16$ different binary numbers represented by these 4 bits are listed in Fig. 7. For each input number, the D/A converter output voltage is a different value. In fact, for this case, the analog output voltage V_{OUT} is equal in voltage to the binary number. For the DAC of Fig. 7, it should be noted that each digital output contributes a different amount to the analog output. This is easily seen if we examine the cases where only one input is high. The contributions of each digital input are weighted according to their position in the binary number. Thus A, which is the LSB (least significant bit), has a weight if Iv, B has weight of 2v, C has a weight of 4v and D, the MSB (most significant bit) has the largest weight, 8v. The weights are successively doubled for each bit, beginning with LSB. Thus, we can consider V_{OUT} to be weighed sum of the digital outputs. For instance, to find V_{OUT} for the digital input 0111 we can add the weight of C, B and A bits to obtain 4v + 2v + 1v = 7v.

A.4.2 Resolution (step size)

Resolution of a D/A converter is defined as the smallest change that can occur in the analog output as a result of a change in the digital input. Referring to table in Fig. 7, we can see that the resolution is 1v, since V_{OUT} can change by no less than 1v when the input code is changed. The resolution is always equal to the weight of the LSB and is also referred to as the step size, since it is the amount V_{OUT} will change as the input code goes from one step to the next. This is illustrated graphically in Fig. 8, where the digital inputs are being derived from the outputs of a 4-bit binary counter. The counter is being continuously cycled through its 16 states by the clock input. The wave form at the D/A output is a repetitive staircase which goes up 1v per step as the counter advances from 0000 to 1111. When the counter returns to 0000, the D/A output returns to 0.v. The resolution or step size is the size of the jumps in the staircase wave form. In this example each step is 1v.

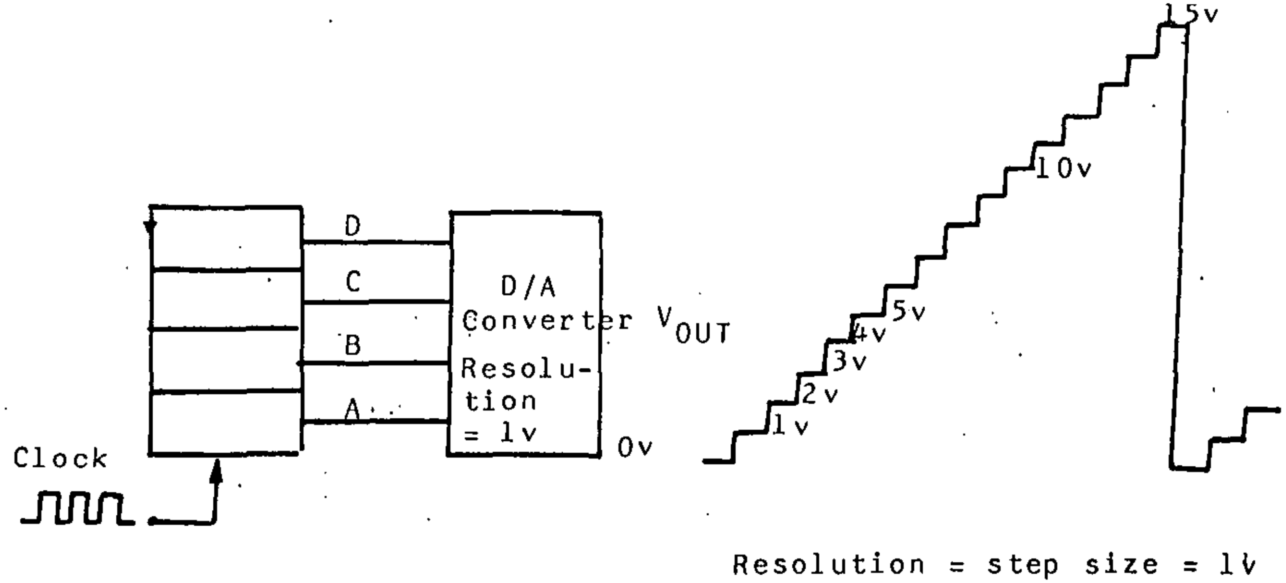

Fig. 8 Output waveform of D/A converter as inputs are provided by a binary counter.

Although resolution can be expressed as the amount of voltage or current per step, it is more useful to express it as a percentage of the full-scale output. To illustrate, the D/A converter of the (Fig. 8) has maximum full scale output of 15v (when the digital input is 1111). The step size is 1v which gives a percentage resolution of

$$\% \text{ resolution} = \frac{\text{step size}}{\text{full scale (f.s)}} \times 100\%$$

$$= \frac{1v}{15v} \times 100\% = \underline{\underline{6.67\%}}$$

A.4.3 The Successive-Approximation A/D Converter

For process control applications, many types of transducers are available that will change a physical quantity, such as temperature or light intensity, into a linearly proportional voltage. This voltage is an analog quantity that can have any value within a given range, such as 0v to 10v. To interface this analog voltage to a digital controller r requires that the voltage be converted to its digital representation by an A/D converter. Fig. 9 shows one type of A/D converter, which is easily interfaced to a system.

This type of converter changes to the analog voltage input V_A to an 8-bit digital output (D_7 through D_0) which can be straight binary. The conversion process is initiated by a pulse applied to the A/D converter's START input. The complete conversion process will take an amount of time that depends on the A/D conversion method which the particular converter uses. This time, called conversion time, tc, can be high as 100 s for some A/D converters. During this tc interval, as the conversion process is taking place the A/D convertor's BUSY output will go LOW. The BUSY output returns HIGH when the conversion is complete.

The digital output lines D_7 through D_0 come from tri-state latches which are part of the converter. A HIGH on the ENABLE input will enable these outputs so that the digital

Fig. 9 Typical A/D Converter used in μp based process control systems.

μp = microprocessor

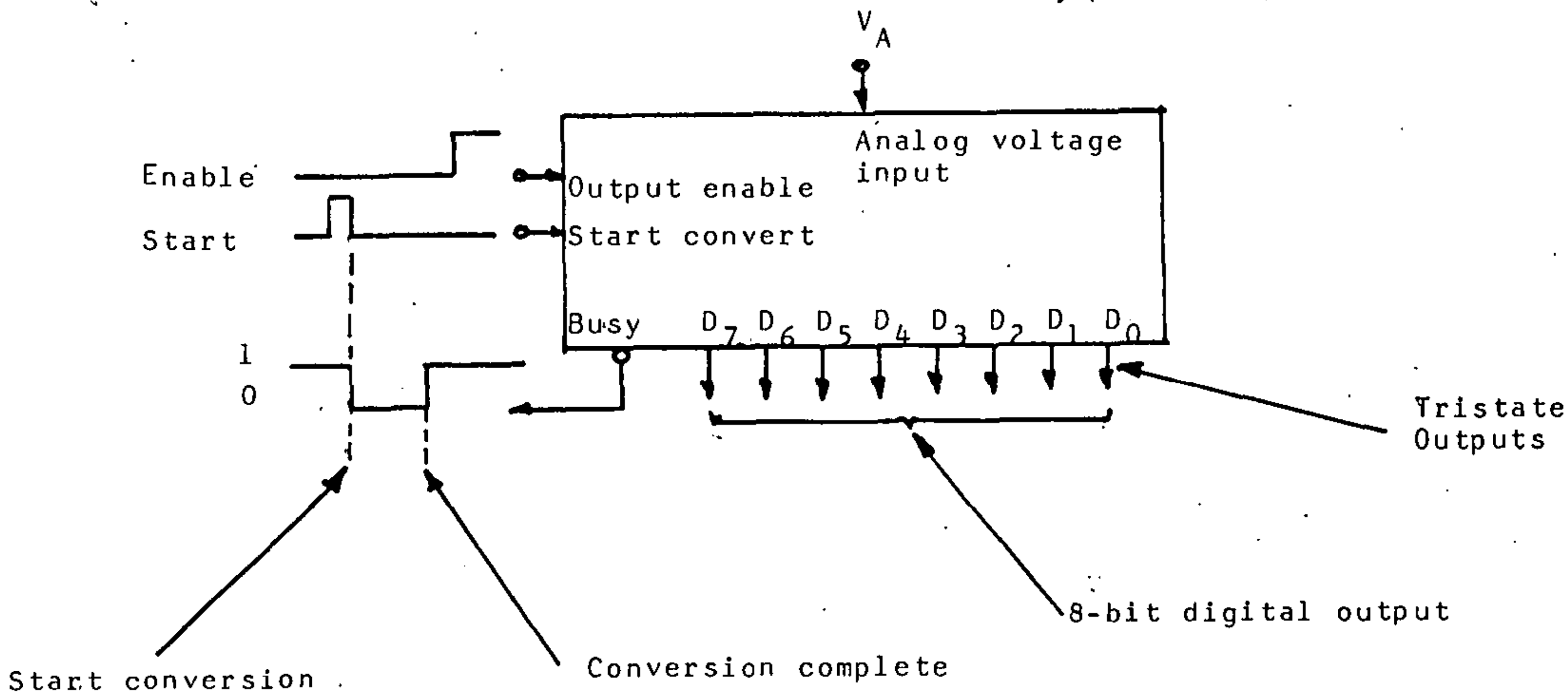

representations of V_A is present on these lines. A LOW on the ENABLE inputs these output lines in their high-Z-state. In most situations, the ENABLE input will be pulsed HIGH only after the BUSY output has indicated that the conversion is complete. If the ENABLE input is made HIGH during the tc interval, the output lines will indicate the results of the previous A/D conversion.

REFERENCES:

(1) Rich Didday, Home Computers 2^{10} Questions and Answers Vol. 1: Hardware, Vol 2: software. Publications: Dilithinium Press., P.O. Box 92, Forest Grove, Oregon 97116.

(2) TOCCI. Digital Systems, Principles and Applications, Publication: Prentice/Hall International.

APPENDIX B

Microcomputer Control

B.1 Introduction

In a closed-loop hydraulic materials test system a specific variable is controlled by comparing the actual value of this variable achieved (output) with the desired value (command) and using the difference (error signal) to drive the system in a direction such that the error is reduced. For the computerized materials test system diagrammed in (Figure 1) a transducer signal (load, strain or stroke) is selected as the feedback signal to the servo-controller where it is compared with the command signal. In this case, the command signal (usually a sinusoidal wave form) is supplied by the digital computer using Digital-to-Analog converter. The difference between the command and the selected feedback signal is applied to the servovalve which in turn causes the hydraulic system to load the specimen in the appropriate direction to minimize the error between command and feedback. In this manner a specimen may be subjected to a load, strain, or stroke history generated by the digital computer. Also, transducer feedback signals are connected to the Analog-to-Digital converter. In this way, analog data from the test system can be read and reduced by the digital computer and if desired, results printed out on the printer. The digital computer serves two major functions in the test: generation of the command input to the test system, and recording and reduction of analog data from the test system. These functions are performed by the software described in Chapter 5.

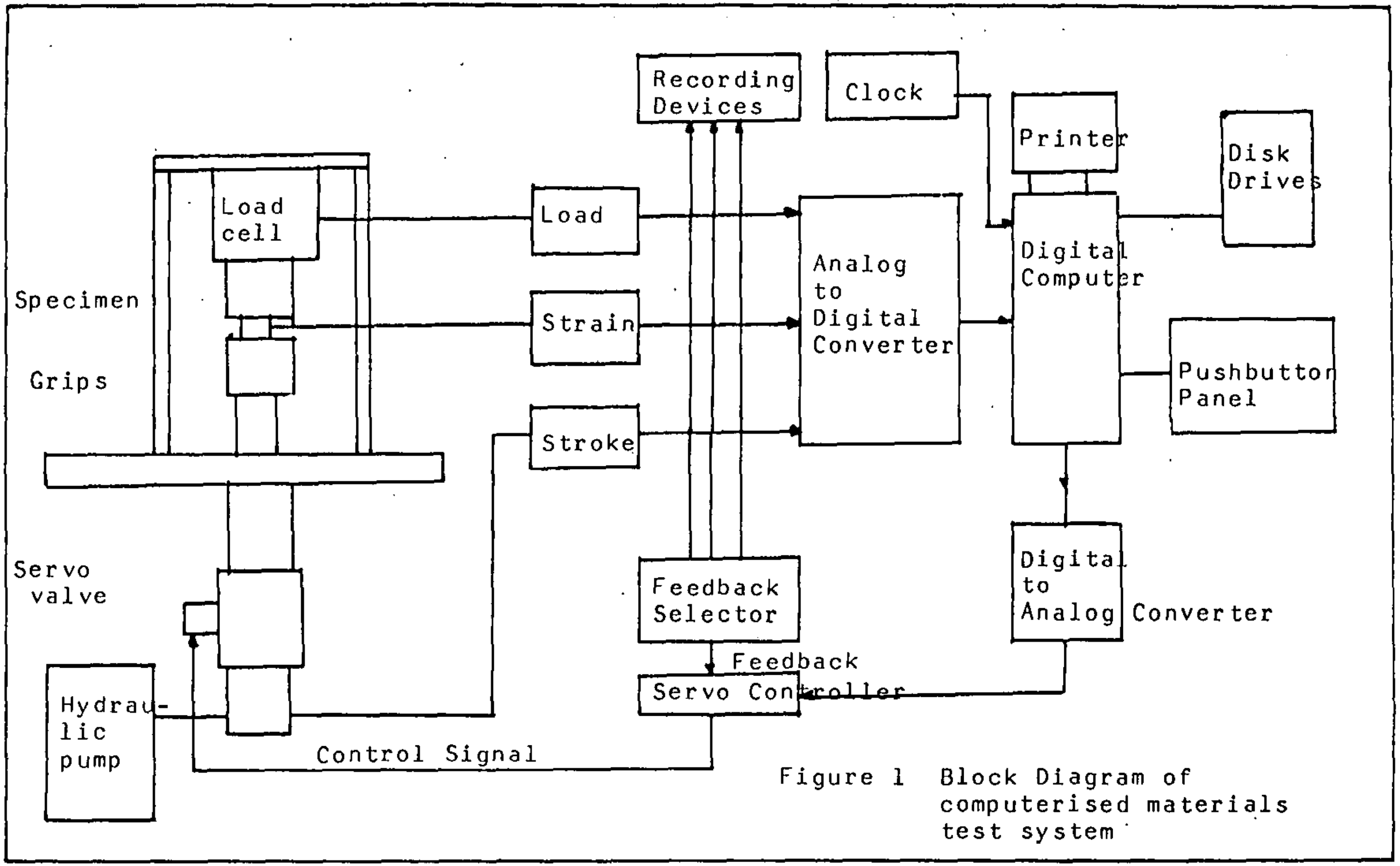

Figure 1 Block Diagram of computerised materials test system

B.2 The APPLE II Micro-Computer[1]

The Apple II is a self-contained single board micro-computer system with a built-in Asc II type keyboard. Asc II keyboards are laid out similar to a conventional typewriter keyboards for easy two-hand operation. Each key is a switch which, when depressed, connects two points together in the same manner as for the hex keyboard. Asc II keyboards normally operate into a keyboard encoder circuit which generates the 7-bit Asc II code bit pattern for the key being depressed. This bit pattern is transferred to the micro-processor over the data bus. Again, a key ACTUATION output allows either polled operation or interrupt operation to be used. Asc II keyboard encoders are more complex than hex keyboard encoders because of the greater number of keys and codes.

The single board concept features an 8-slot motherboard with full connectors, and uses the 6502 type micro-processor. A 6 k-byte BASIC and a 2 k-byte system monitor are in Read-Only-Memory (ROM) plus an additional 4 k which can be added to give a total of 12 k-bytes. For user work space 16 k-bytes of Random-Access-Memory (RAM) are available. Sockets are in place for future expansion of up to 48 k bytes of RAM, which is the configuration used for the purposes of this research project.

Peripheral devices include a printer for hard copy and a pair of disc drives for floppy discs.

B.3 The Interfacing Devices (2,3,4)

The Interfacing devices between the analog control system and the computer provides the hardware needed for data acquisition, function generation and test-machine control monitoring. Interface hardware characteristics coupled with the software device driver determines the overall capability of the automated system. Speed, precision and accuracy are the most important parameters of the interfaces. The interfacing devices for this set-up consist of the Interactive structures AO-Ø3 analog output and AI-13 analog input cards.

B4 AO-Ø3 Analog Output Card (3)

The AO-Ø3 output system of the APPLE II micro-computer to be used to control the ESH testing machine by providing analog voltage signals in the range of 0-10 volts.

The output voltage can be specified by the software (program) by sending a number from 0 to 255. The AO-Ø3 converts this into the desired voltage value within 3 micro-seconds, then latches or holds the voltage level until it is next changed by the program. The output voltage will drive the machine to apply a load until the specimen is extended a fixed amount. This is illustrated as follows:

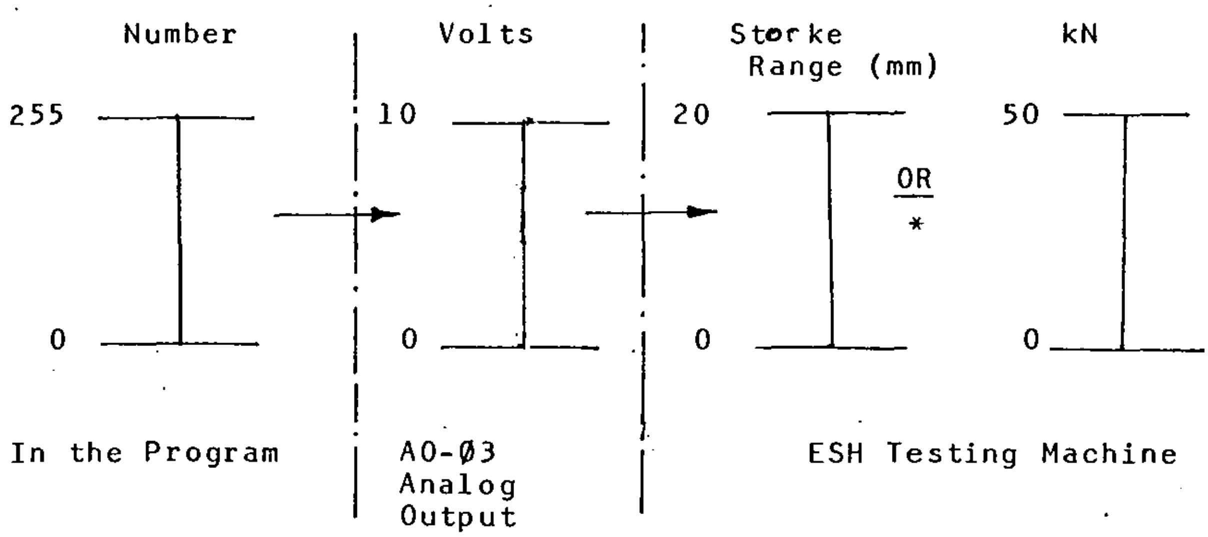

* (depending on mode of machine control selected)

Because the computer is a digital device, the analog output voltage changes in descrete steps when numbers are sent to the converter. For example, if a series of numbers from 1 to 255 were sent to the converter the output signal will appear as shown in Figure 2.

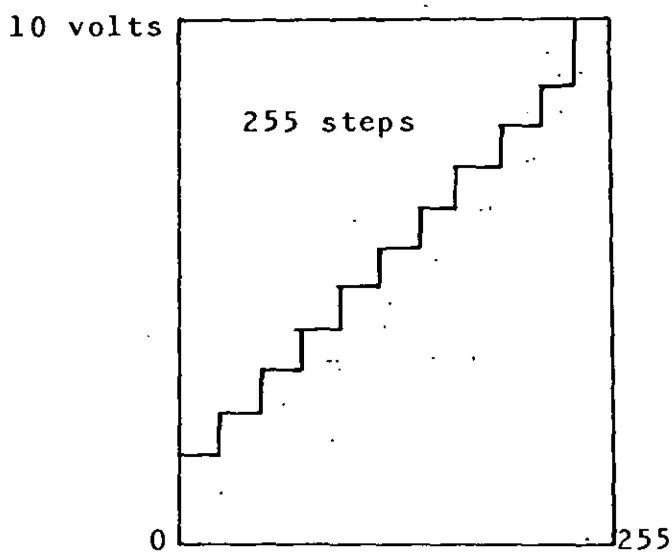

Figure 2
Output voltage from the AO-13 Converter.

Each step projected on the ordinate corresponds to (1/255 x 10) volts which is the resolution of this analog output system.

The AO-Ø3 is connected to the computer and the E.S.H. testing machine in the manner shown in Figure 3. Sixteen channels are available in the output-system. These may be connected to the testing machine (in this case only 1 channel is used), which up to 8 slots are available on the Apple II mother board. Any combination of which may be connected to AO-Ø3. Each channel is addressed through a memory address. To address Channel M and Slot N, the output address code is given by

$$- 16384 + (256 \times N) + M$$

In the set-up used the card was inserted into Slot 3 and the test machine was connected to Channel 1; hence

$$N = 3 \quad \text{and} \quad M = 1.$$

Therefore the write address is

$$- 16384 + (256 \times 3) + 1$$
$$= - 15615$$

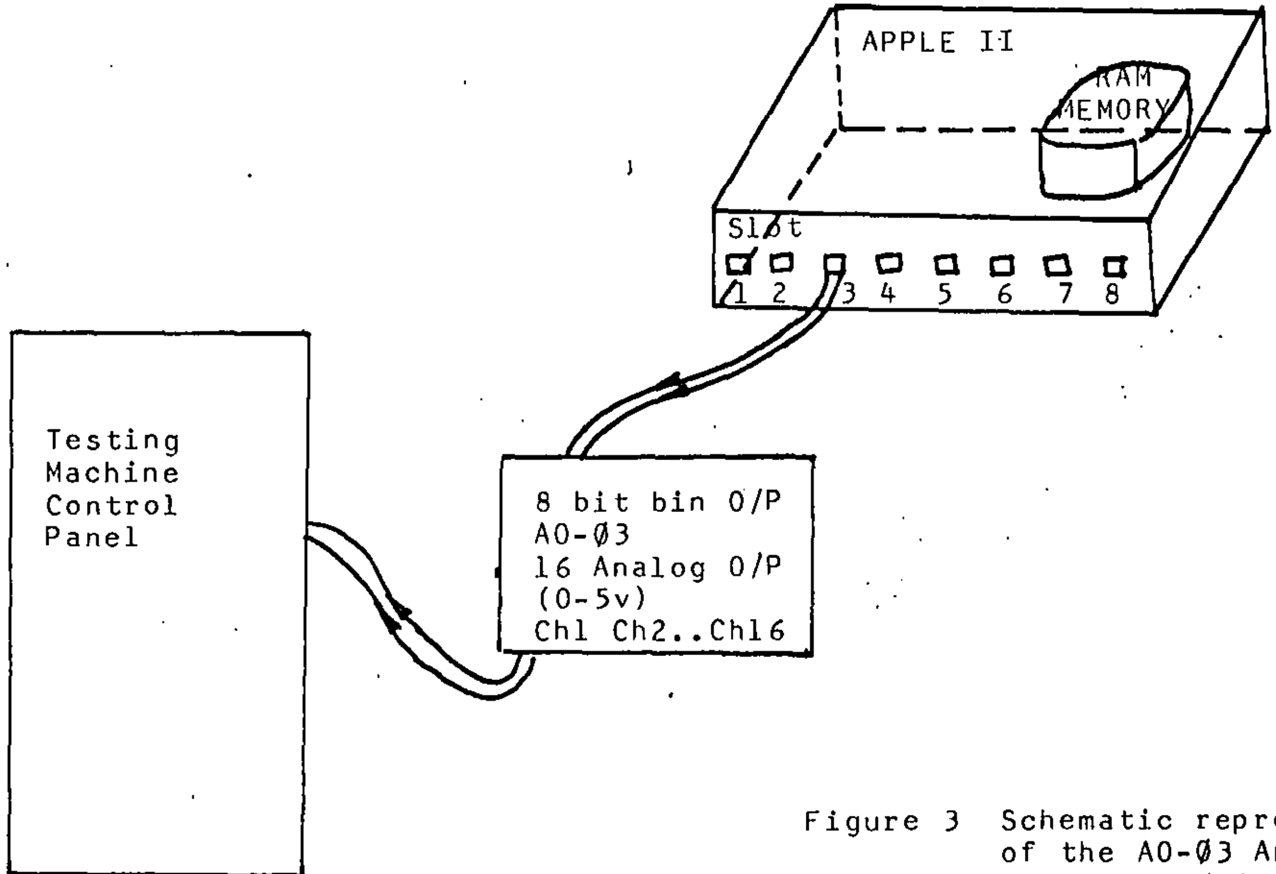

Figure 3 Schematic representation of the AO-Ø3 Analog Output System used in this work.

B.5 AI-13 Analog Input System [4] (Fig. 4)

The AI-13 is designed to take analog voltage readings and return a number proportional to the actual result for analysis by the program. It can select any one of the 16 input channels and scale the input according to any of 8-full scale ranges.

The AI-13 appears to a program as a block of locations in memory whose address is determined by the slot number the input system is connected to. To refer to a particular slot number, the input address code would be

- 16256 + SLOT x 16

In this case the SLOT number is 5, hence the computer would 'read' from address (A)

- 16256 + 5 x 16

However, the result of the AI-13 conversion is a 12-bit quantity, hence the 8-bit APPLE II micro-computer has to retrieve the 12-bit quantity with two read operations. The most significant 4 bits are read from the location A + 1 and the least significant 8 bits are read from A which is based on successive approximation method. The command address for this is given as

PEEK (A + 1) x 256 + PEEK (A)

For a standard conversion, this will produce a number between 0 and 4095.

e.g. consider the 12-bit binary code in Table B.1.

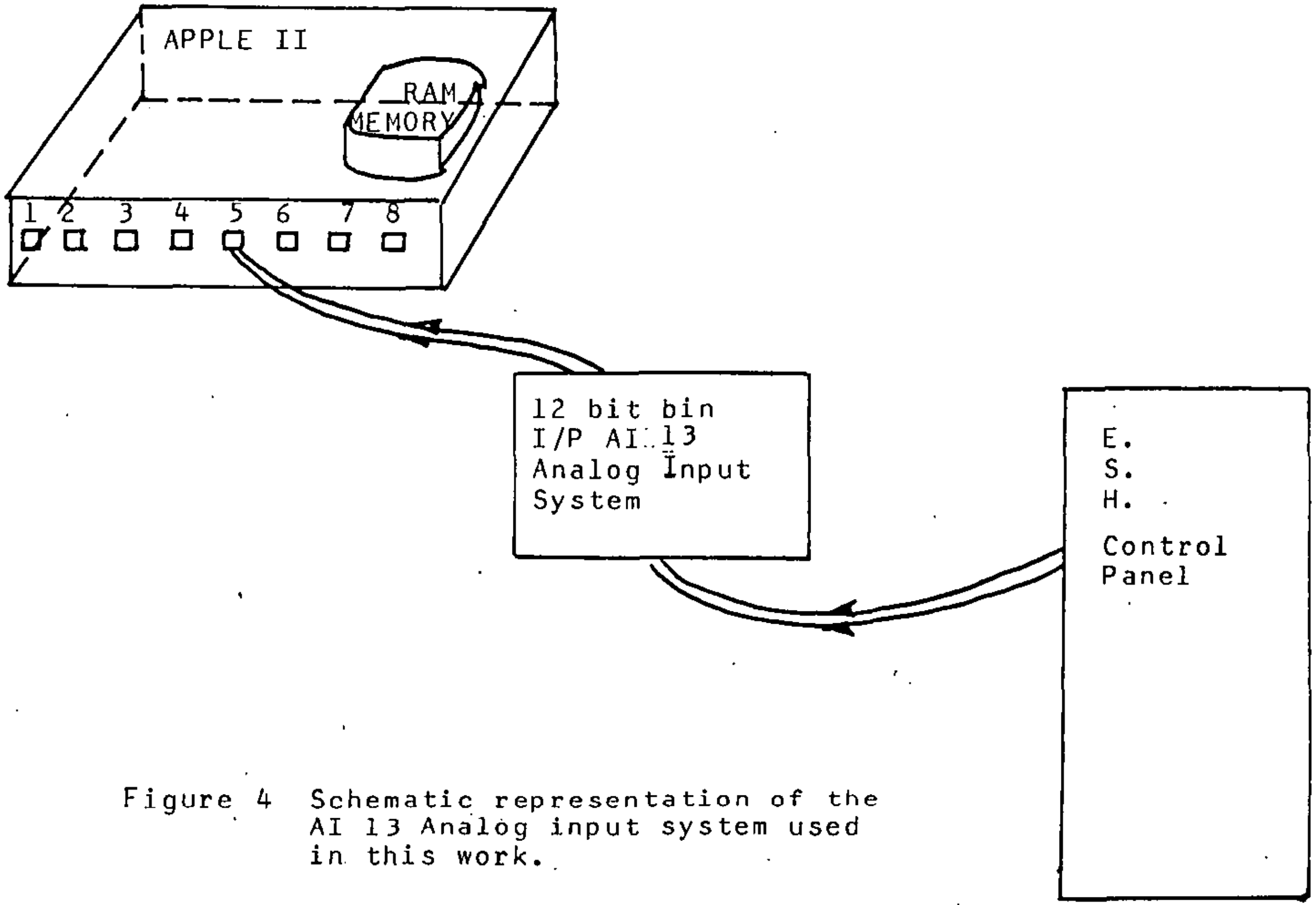

Figure 4 Schematic representation of the AI 13 Analog input system used in this work.

TABLE B.1

BINARY CODE	0	0	0	1	0	1	0	1	0	0	1	0
BINARY WEIGHTING	2^{11}	2^{10}	2^9	2^8	2^7	2^6	2^5	2^4	2^3	2^2	2^1	2^0

i.e. 000101010010

$$= 2^8 + 2^6 + 2^4 + 2^1 = 256 + 64 + 16 + 2$$
$$= 338$$

The APPLE II works in 8 bits per byte, the above to be represented by 2 bytes. Say at location A + 1 and A. Hence the required numbers (338 in this case) can be represented as:-

TABLE B.2

Memory location A + 1								Memory location A							
0	0	0	0	0	0	0	1	0	1	0	1	0	0	1	0
2^7	2^6	2^5	2^4	2^3	2^2	2^1	2^0	2^7	2^6	2^5	2^4	2^3	2^2	2^1	2^0

The Table B.2 shows contents of memory locations at the end of conversion of number 338.

A second command is necessary to initiate the conversion of the appropriate channel.

References

(1) FRIEBERGER, S. and CHEW, J. Jnr., "A Consumer's Guide to Personal Computing and Microcomputer"; Publication: Hayden Brok Company Inc.

(2) Interfacing Microcomputers to Analogue Signals; Design Engineering; Nov (1979).

(3) AO-Ø3 Analog output system for Apple II users Manual.

(4) AI-13 Analog Input System. 16 Input Channels, 12 bit precision Data Acquisition Modules by Interactive Structural Inc.